ENTEROVIRUS A71 SQUAMOUS EPITHELIOTROPISM AND INFECTION IN A HAMSTER MODEL AND HUMAN ORGANOTYPIC AND PRIMARY SQUAMOUS CELL CULTURE SYSTEMS

PHYU WIN KYAW

THESIS SUBMITTED IN FULFILMENT OF THE REQUIREMENTS FOR THE DEGREE OF DOCTOR OF PHILOSOPHY

FACULTY OF MEDICINE
UNIVERSITY OF MALAYA
KUALA LUMPUR

2017

ABSTRACT

Enterovirus A71 (EV-A71) (Family: *Picornaviridae*, Genus: *Enterovirus*) is the one of most common and important causes of hand-foot-and-mouth disease (HFMD) in young children. Typical HFMD lesions in and around the oral cavity, palms, soles, and buttocks may be associated with severe neurological complications such as acute flaccid paralysis and acute encephalomyelitis.

To study viral replication sites in the oral cavity, skin and other tissues, and to gain further insights into virus shedding, neuropathogenesis and person-to-person transmission, a novel, orally-infected, 2-week-old hamster model of HFMD and EV-A71 encephalomyelitis was developed. Hamsters developed the disease and died after 4-8 days post-infection (dpi); the LD_{50} was 25 $CCID_{50}$. Macroscopic cutaneous lesions around the oral cavity and paws were observed. Squamous epithelium in the lip, oral cavity, paw, skin, and esophagus showed multiple small inflammatory foci and demonstrated viral antigens/RNA. Virus was isolated from oral washes, feces, brain, spinal cord, skeletal muscle, serum, and other tissues.

To study viral spread and distribution, the hamster model was orally infected with 10^5 $CCID_{50}$ viral dose and sacrificed at 1, 2, 3 and 4 dpi, respectively. Infected animals at 1 dpi remained healthy, all tissues were negative for viral antigens/RNA, and virus was not isolated, including in oral washes and feces. Although spinal cord was negative at 2 dpi, focal viral antigens in sensory ganglia and brainstem neurons were detected. The degree of infection in the CNS including spinal cord, gradually increased at 3 and 4 dpi, consistent with virus titration results.

To model person-to-person transmission, animals (index cases) were orally-infected with 10^4 $CCID_{50}$ virus dose. Index animals developed severe disease after 4-5 dpi, while

littermates (contact cases) developed severe disease after 6-7 days post-exposure. Viruses in oral wash and feces were detected at 3-4 dpi in index animals and 3-8 days post-exposure in contact animals. Seroconversion in exposed, healthy mother hamsters was also detected. Based on the results, orally-shed virus was most likely from infected oral mucosa and salivary glands, while fecal virus could be from these sites as well as from oesophageal and gastric epithelia.

The cellular target/s of EV-A71 in human skin and oral mucosa were investigated using human skin and mucosa organotypic cultures from the prepuce and lip, and primary prepuce squamous cells. Focal viral antigens/RNA were localized to cytoplasm of squamous keratinocytes or mucosal squamous cells in organotypic cultures as early as 2 dpi, and were associated with cytoplasmic vacuolation and cellular necrosis. Infected primary epidermal keratinocyte cultures showed cytopathic effects from 2 dpi, with concomitant detection of viral antigens/RNA in the cytoplasm corresponding to increasing viral titres over time. Thus, EV-A71 demonstrated squamous epitheliotropism in the prepuce and lip skin, and oral mucosa organotypic tissues. All other skin structures such as blood vessels, fibrous tissue, etc. showed no evidence viral infection.

Neuroinvasion is likely via retrograde motor nerve transmission but intriguingly, our results show that sensory nerves may also play a role in neuroinvasion. In addition, the results from human organotypic and primary squamous cell culture systems strongly support EV-A71 squamous epitheliotropism both in the human skin and oral mucosa, and suggest that these organs are important primary or secondary viral replication sites that contribute significantly to viremia, oral and cutaneous viral shedding, and perhaps also cutaneous-oral transmission.

ABSTRAK

Enterovirus A71 (EV-A71) (Keluarga: Picornaviridae, Genus: Enterovirus) merupakan salah satu sebab utama dan terpenting penyakit kaki tangan dan mulut dalam kalangan kanak-kanak. Lepuhan di mulut, tapak tangan, tapak kaki dan punggung boleh dikaitkan dengan komplikasi neurologi yang parah seperti lumpuh layu akut dan encephalomyelitis akut.

Bagi menyiasat tentang tapak membiak virus ini di kawasan mulut, kulit dan tisu-tisu lain juga bagi mengetahui lebih lanjut tentang perlepasan virus, neuropatogenesis dan jangkitan dari manusia ke manusia, seekor hamster berusia 2 minggu dijangkiti secara oral telah dijadikan model untuk penyakit kaki tangan dan mulut serta EV-A71 encephalomyelitis. Hamster yang dijangkiti penyakit itu mati setelah 4-8 hari selepas jangkitan dengan dos maut, LD_{50}, 25 $CCID_{50}$. Secara makroskopinya, lepuhan kulit di sekeliling kawasan oral dan tapak kaki dapat kelihatan. Skuamus epitelium di bahagian bibir, kawasan oral, kaki, kulit dan esofagus menunjukkan beberapa keradangan bertumpu yang kecil dan mempamerkan viral antigen/RNA. Virus diasingkan darpada kumuhan oral, najis,otak saraf tunjang otot skeletal dan tisu-tisu yang lain.

Bagi menyiasat tentang penyebaran dan pengedaran virus, model tikus belanda dijangkiti dengan 10^5 $CCID_{50}$ dos virus and dikorbankan pada 1, 2, 3 and 4 dpi. Manakala untuk tisu yang dijangkiti dengan 2dpi, viral antigen/RNA dapat dikenalpasti tertumpu di kawasan oral, kaki , kulit dan otot skeletal dan makin bertambah pada 3 dan 4 dpi. Tahap jangkitan di kawasan CNS termasuk saraf tunjang beransur-ansur meningkat pada 3 dan 4 dpi, konsisten dengan keputusan titrasi virus.

Untuk model jangkitan manusia ke manusia, haiwan-haiwan (kes indeks) dijangkitkan secara oral dengan 10^4 CCID$_{50}$ dos virus. Indeks haiwan mula menjadi parah selepas 4-5 dpi, manakala kes kontak menjadi parah selepas 6-7 hari selepas pendedahan. Virus-virus pada kumuhan dan najis dapat dikenalpasti pada 3-4 dpi dalam indeks haiwan dan 3-8 hari setelah pededahan pada haiwan kontak. Haiwan kontak bukan littermate yang terdedah selama 8 jam akan dijangkiti penyakit selepas 6 hari manakala yang terdedah selama 12 jam pula dijangkiti penyakit selepas 4 hari. Berdasarkan keputusan yang diperolehi, virus yang disebarkan secara oral besar kemungkinan datang daripada oral mukosa dan kelenjar air liur yang telah dijangkiti manakala virus fekal juga mungkin daripada tempat yang sama selain esofegul dan epitelium gastrik.

Target sel untuk EV-A71 pada kulit manusia dan mukosa oral telah disiasat menggunakan kulit manusia dan kultur organotipik mukosa daripada bibir dan kulup dan sel skuamus utama kulup. Kultur epidermal keratinosit utama yang telah dijangkiti menunjukkan kesan sitopatik dari 2 dpi, seiring dengan pengenalpastian viral antigen/RNA di dalam sitoplasma dan sepadan dengan peningkatan titer virus/masa. Oleh itu, EV-A71 menunjukkan skuamus epitheliotropisma pada kulup dan kulit bibir, dan tisu organotipik oral mukosa. Kawasan struktur kulit yang lain seperti pembuluh darah, tisu fibrous dan sebagainya tidak menunjukkan bukti jangkitan virus.

Tambahan pula, keputasan yang diperoleh daripada organotipik manusia dan system kultur sel skuamus utama menyokong kuat skuamus epitheliotropisma EV-A71 pada kedua-dua kulit manusia dan mukosa oral dan mencadangkan bahawa organ-organ tersebut adalah tapak replikasi virus yang penting dan secara signifikannya menyumbang kepada viremia, perlepasan pada oral dan kutanus serta transmisi kutanus-oral.

ACKNOWLEDGEMENTS

Thanks also go to grants: High Impact Research (HIR) UM.C/625/1/HIR-MOHE, RG141/09HTM and FP038/2015A FRGS from Ministry of Higher Education, Malaysia for research fund.

Finally, I am extremely grateful and also like to say a heartfelt "Thank You" to my parents for their infinity love, encouragement and personal support for studying in PhD degree and for believing in me. I wish to express my deepest gratitude to my sisters and brother for their love, understanding and encouragement throughout my study in PhD degree.

Last, but not least, to those who are not mentioned here, you are never forgotten, thank you all.

TABLE OF CONTENTS

CHAPTER 3: MATERIALS AND METHODS

LIST OF FIGURES

LIST OF TABLES

LISTS OF SYMBOLS AND BBREVIATIONS

%	percent
ºC	degree Celsius
dpi	days post-infection
g	gram
mg	milligram
μg	microgram
L	liter
ml	millilitre
μl	microliter
M	molar
mm	millimolar
nm	nanometer
rpm	rotation per minute
min	minute
kDa	kilodaltons
nt	nucleotide
bp	base pair
kb	kilo base
RT-PCR	reverse transcriptase-polymerase chain reaction
dH$_2$O	distilled water
IHC	immunohistochemistry
ISH	*in situ* hybridization

HE	hematoxylin and eosin
IEM	immunoelectron microscopy
EV-A71	Enterovirus A71
HFMD	hand-foot-and-mouth disease
LD_{50}	median lethal dose
$CCID_{50}$	50% cell culture infectious dose
CNS	central nervous system
DMEM	Dulbecco's modified Eagle's growth medium
GM	growth medium
MM	maintenance medium
MAV	mouse-adapted virus
PBS	phosphate buffered saline
TBS	tris buffered saline
SCARB2	Scavenger Receptor Class B member 2

CHAPTER 1

INTRODUCTION

1.1   Introduction

Enterovirus A71 (EV-A71) is a non-enveloped, single-stranded, positive-sense RNA virus which belongs to the human Enterovirus A species group within the *Picornaviridae* family. The EV-A71 genome is approximately 7.4 kb and encodes for 4 capsid proteins and other non-structural proteins (Brown & Pallansch, 1995; Knipe & Howley, 2001). It is one of the enteroviruses most often associated with large outbreaks of pediatric hand-foot-and-mouth disease (HFMD) (Brown et al., 1999; Ong et al., 2008b). Most cases of EV-A71 associated HFMD infection are mild and self-limited, and typically characterized by ulcerating vesicles and lesions in the mouth, hands, feet, and occasionally on the buttocks and knees (Brown & Pallansch, 1995; Ho et al., 1999; Hsiung & Wang, 2000). Although most patients recover uneventfully, EV-A71 infection may sometimes be complicated by aseptic meningitis, acute flaccid paralysis and encephalomyelitis (Brown et al., 1999; Hsiung & Wang, 2000; Lum et al., 1998; Mcminn, 2003). Patients had pulmonary oedema and extensive damage to the medulla and pons strongly suggesting an etiologic link between EV-A71 and brainstem encephalomyelitis as the cause of death (Lum et al., 1998).

In complicated HFMD, neuroinvasion most probably follows viremia (Liu et al., 2011a; Nagata et al., 2004a). Fatal cases of EV-A71 encephalomyelitis showed stereotyped distribution of inflammation in the spinal cord, brainstem, hypothalamus, cerebellar dentate nucleus and the cerebrum (Wong et al., 2008b; Wong et al., 2012). Virus could be isolated from CNS tissues, and viral antigens/RNA and virions were localized to infected neurons,

confirming viral cytolysis as an important cause of neuronal injury (Shieh et al., 2001; Wong et al., 2008b; Wong et al., 2012).

Viral predilection for neurons or neuronotropism has also been demonstrated in monkey and mouse models of EV-A71 infection (Fujii et al., 2013a; Lin et al., 2013b; Liu et al., 2011a; Nagata et al., 2002a; Ong et al., 2008b; Wang et al., 2004a). Furthermore, retrograde axonal viral transport up peripheral and cranial motor nerves to infect the CNS has also been shown in the mouse model (Ong et al., 2008b; Tan et al., 2014b). However, in most of these models, the routes of infection were mostly parenteral, via intraspinal, intracerebral, intratracheal, intraperitoneal (i.p), intramuscular (i.m), and subcutaneous routes (s.c) (Liu et al., 2011a; Nagata et al., 2002a; Ong et al., 2008b; Tan et al., 2014b). Although infection by the natural oral route in animal models is desirable, it is rare and consistently successful infections have never been described (Chen et al., 2004a; Khong et al., 2012a; Ong et al., 2008b; Wang et al., 2004a). Preliminary observations in a new hamster model used to test the protective efficacy of an EV-A71 candidate vaccine against infection by a mouse-adapted virus (MAV), suggested that it may be useful as an alternative small animal model for EV-A71 infection (Ch'ng et al., 2012b). We hypothesize that this orally-infected hamster model could be used to validate the infectious disease pathology and pathogenesis of EV-A71 infection. Currently, there is no consistent orally-infected animal model to demonstrate EV-A71 HFMD and encephalomyelitis. A viral spread study of hamster model may also extend the existing knowledge on the viral cellular targets and pathogenesis of EV-A71 infection.

There are only a few published reports on person-to-person transmission of EV-A71. In one study, it was found that intra-family transmission usually occurred after contact with infected siblings (Chen et al., 2008). In a previous study, orally EV-A71 infected one

day-old ICR mice developed skin lesions and hind limb paralysis, and transmitted the infection to their littermate controls. However, orally-infected animal models of EV-A71 infection with demonstrable oral shedding and faecal excretion of virus have not been used to systematically investigate person-to-person transmission. This may be because most existing animal models such as monkey and mouse models including the AG129 (alpha/beta, interferon and IFN-ϒ receptor knock-out) and human SCARB2 transgenic mouse models, cannot be consistently infected orally (Chen et al., 2004a; Fujii et al., 2013a; Khong et al., 2012a; Ong et al., 2008b; Zhang et al., 2011). Although person-to-person transmission of EV-A71 via oral and fecal viral shedding is well-known, this unique hamster model could be used to further investigate some of the relatively unknown factors that might influence transmission. We hypothesize that the oral cavity and orodigestive tracts as an important replication sites play crucial roles in viral shedding and transmission leading to viremia, spread to other distant organs and neuroinvasion.

Palatine tonsillar crypt squamous epithelium infection (He et al., 2014) strongly suggests that EV-A71 is squamoepitheliotropic i.e. has a predilection for squamous cells or keratinocytes. Although virus can be readily isolated from mouth ulcers and skin lesions (Brown & Pallansch, 1995; Chatproedprai S et al., 2010; Chong et al., 2003; He et al., 2014; Liu et al., 2011a; Nagata et al., 2004a), there have been very few pathological studies on infected human skin and oral cavity tissues, and hence no available evidence other than the palatine tonsil that squamous cells lining these organs are susceptible to infection (He et al., 2014). We hypothesize that human squamous cells/keratinocytes in the epidermis and oral cavity as important viral replication sites that contribute significantly to oral and cutaneous virus shedding.

1.2   Objectives of the study

The general aim of this project is to establish an orally-infected EV-A71 animal model and *in vitro* culture systems infection to study, viral cellular targets, neuroinvasion and viral transmission.

The specific objectives of this study are:

1.   To develop a consistent orally-infected hamster model of EV-A71 HFMD and encephalomyelitis.

2.   To characterise the pathology of the orally-infected hamster model.

3.   To investigate the viral spread in the hamster model.

4.   To study viral shedding and person-to-person EV-A71 transmission in the hamster model.

5.   To study viral epitheliotropism and replication in human squamous organotypic and primary squamous cell culture systems.

CHAPTER 2

LITERATURE REVIEW

2.1   Literature review

Enterovirus A71 (EVA-71) is first isolated in California, USA, in 1969, although an analysis showed that EV-A71 was circulating in the Netherlands as early as 1963. EV-A71 epidemic has become a major public health issue across the Asia-Pacific region (Ho et al., 1999). The reasons for large outbreaks in the Asia-Pacific region are not well understood. Large outbreaks of HFMD are most frequently caused by a few serotypes of enteroviruses including, EV-A71 and coxsackievirus A16 (CAV-16) (Brown et al., 1999; Chan et al., 2003b). EV-A71 in particular had caused major outbreaks of HFMD and encephalomyelitis and emerged as the most important fatal neurotropic enterovirus since a global campaign has almost eradicated poliomyelitis from many regions worldwide (Huang & Shih, 2014).

2.2   Classification of human enteroviruses

Human enteroviruses were traditionally separated into four subgroups, according to virion morphology, the nature of the genomic nucleic acid, replication strategy and their pathogenicity in human beings, experimental animals, and cytopathic effects in tissue culture. These subgroups include polioviruses (three serotypes), coxsackievirus A (23 serotypes), coxsackievirus B (six serotypes), and echoviruses (28 serotypes). More recently, human enterovirus are classified into 4 species groups (A-D) (Table 2.1). Grouping of individual virus types and strains within the families using biological, physicochemical, antigenic and genomic properties are important for identification (Hsiung & Wang, 2000; Knipe & Howley, 2001; Solomon et al., 2010).

The *Picornaviridae* (*Enterovirus* genus) family consists of 6 genera; *Enterovirus* (eg. polio virus)*, Rhinovirus* (eg, human rhinovirus 1A), *Hepatovirus* (eg, human hepatitis A virus), *Parechovirus* (eg, human parechovirus 1 and 2), and two important animal virus genera, *Cardiovirus* (eg, encephalomyocarditis virus) and *Aphthovirus* (eg, foot and mouth disease virus) (Knipe & Howley, 2001). However, phylogenetic analysis of genomic nucleic acid sequences are likely to be the most useful basis for classification. In 1970, serologically distinct human enteroviruses were isolated and because of the limitations of this system, serotype numbers were designated beginning with EV68. As one of the largest virus families *Picornaviridae*, is classified into 29 genera (Figure 2.1). Polioviruses were designated as members of the human enterovirus C species (Linden et al., 2015).

Table. 2.1 Human enterovirus serotypes.

Species	Serotype
A	CV-A2–8, CV-A10, CV-A12, CV-A14, CV-A16 EV71, EV76, EV89–92
B	CV-A9, CV-B1–6 E1–7, E9, E11–21, E24–27, E29–33 EV69, EV73, EV74–75, EV77–88, EV93, EV97, EV98, EV100, EV101, EV106, EV107
C	CV-A1, CV-A11, CV-A13, CV-A17, CV-A19–A22, CV-A24 EV95, EV96, EV99, EV102, EV104, EV105, EV109 PV1–3
D	EV68, EV70, EV94

CV-A=coxsackievirus A,
CV-B=coxsackievirus B,
EV=enterovirus,
E=echovirus,
PV=poliovirus.
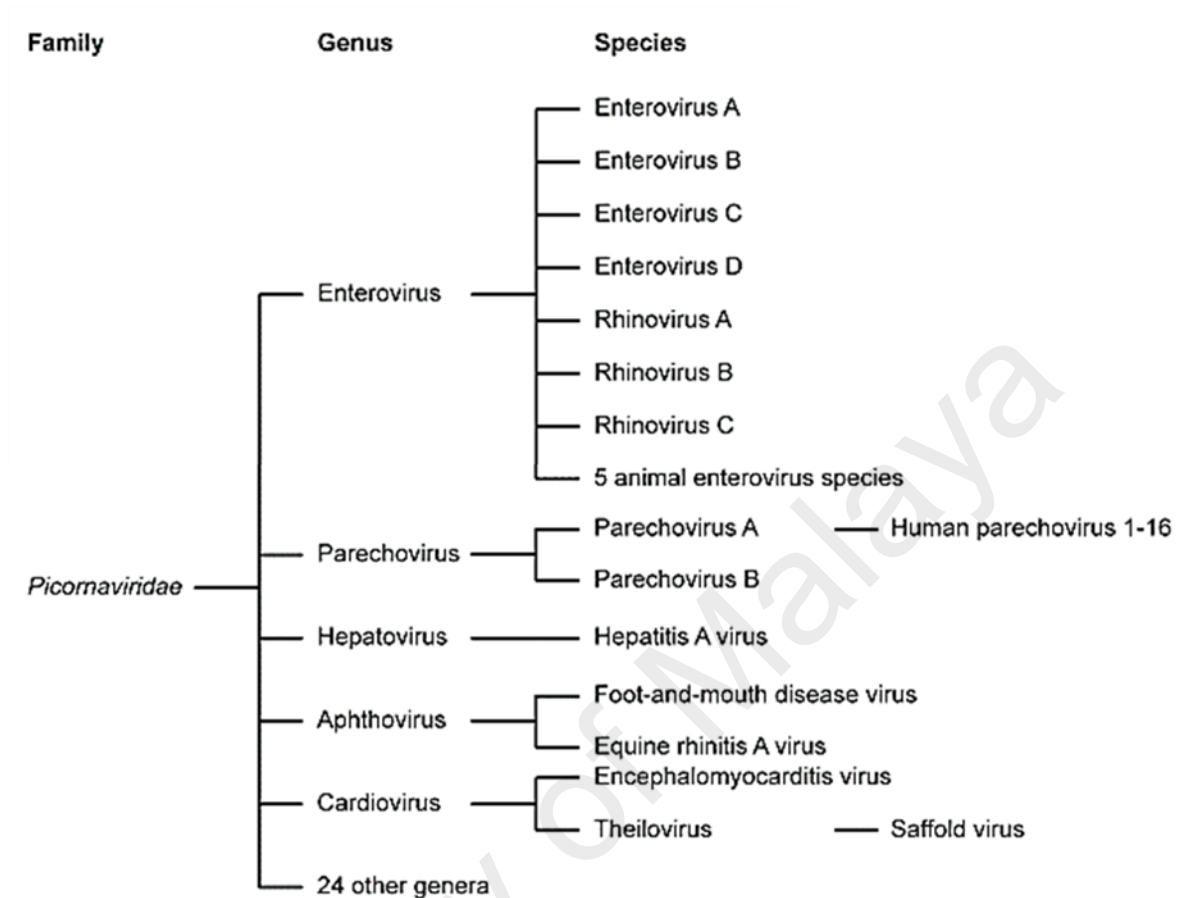
Figure 2.1. Classification of the family *Picornaviridae*. Adapted from Linden, 2015.

2.3 Structural biology of EV-A71

2.3.1 EV-A71 virion and genome organization

EV-A71 is a small non-enveloped single-stranded, positive-sense RNA virus (Chen et al., 2007c; Knipe & Howley, 2001; Mcminn, 2003). EV-A71 is closely related to coxsackievirus A16, most frequently affecting children and causes HFMD (Knipe & Howley, 2001). The virion is about 30 nm in size and consists of 60 copies of each of 4 capsid proteins (VP1, VP2, VP3 and VP4). The genome is encapsulated within the icosahedral capsid composed of these proteins (Figure 2.2). The capsid proteins VP1, VP2 and VP3 are exposed on the virus surface whereas the smallest VP4 capsid is arranged inside (Huang et al., 2011; Solomon et al., 2010). The viral genome contains a single open reading frame with highly structured untranslated regions (UTR) at the 5' and 3' end and a 3' poly (A) tail (Figure 2.2).
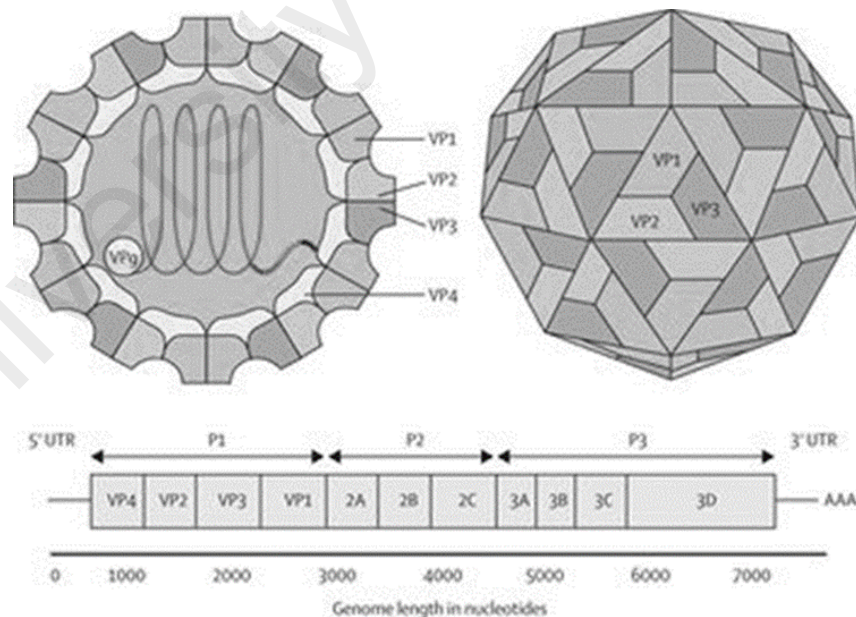
Figure 2.2. EV-A71 and the virion genome structures. Adapted from Solomon, 2010.

VPg (viral protein genome-linked) is termed as viral genome uncapped and the 5' end is covalently coupled to the viral protein 3B. The 5' UTR consists of an internal ribosomal entry site (IRES) which mediates cap-independent translation. The organization of the open reading frame is generally similar in all picornaviruses, but there are some differences between genera. The open reading frame of EV-A71 encodes a polyprotein that contains structural proteins VP0 (VP4 + VP2), VP1 and VP3 in the P1 region and the nonstructural proteins (2A – 2C and 3A – 3D) in the P2 and P3 regions (Figure 2.3) (Huang & Shih, 2014; Huang et al., 2011; Linden et al., 2015; Solomon et al., 2010; Wong et al., 2010; Yamayoshi et al., 2014; Yang et al., 2011).
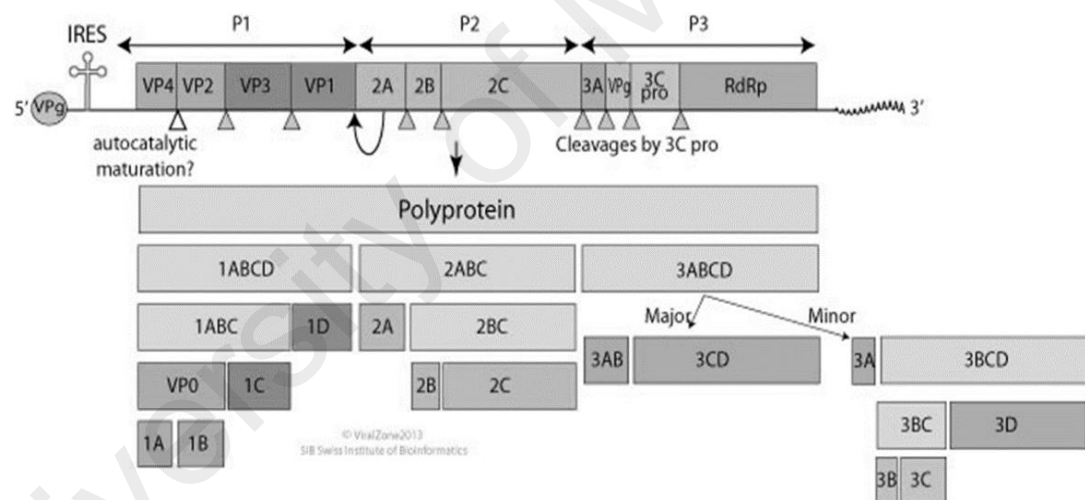
Figure 2.3. Genome structure of EV-A71. Adapted from viralzone, 2013. http://viralzone.expasy.org/all_by_species/33.html

2.3.2   Viral entry receptors

Humans are the only known natural hosts of human enteroviruses (Zaoutis & Klein, 1998). The replication cycle of EV-A71 is similar to most other enteroviruses. Viral entry into the host cells is dependent on specific EV-A71 receptors. Generally, viral entry receptors for this virus are found on white blood cells, cells in the respiratory and gastrointestinal tract, and dendritic cells. A ubiquitously expressed cellular receptor; scavenger receptor class B member 2 (SCARB2), and a functional receptor; human P-selectin glycoprotein ligand-1, found on white blood cells, specific for EV-A71 have been identified among several others as viral entry receptors for EV-A71.

Member of the annexin family, Anx2, a calcium and phospholipid binding protein, which serves as a profibrinolytic co-receptor for tissue plasminogen activator and plasminogen on endothelial cells, was also identified as one of the cellular receptors for EV-A71. However, Anx2 is thought to be an attachment receptor since viral entry and uncoating via Anx2 have not been reported (Hajjar & Acharya, 2000; Yang et al., 2011). Heparan sulfate has also been reported to contribute to the binding of EV-A71 to the cell surface (Tan et al., 2013). In the respiratory and gastrointestinal tracts, sialic-acid-linked glycan expressed in abundance and dendritic-cell-specific intercellular adhesion-molecule-3-grabbing non-integrin, which is found exclusively in dendritic cells in lymphoid tissues, have also been identified as receptors for EV-A71 (Chen et al., 2012; Huang & Shih, 2014; Li et al., 2011; Yang et al., 2011).

Among all EV-A71 receptors, SCARB2 has been reported as most important viral entry receptor. SCARB2 is a type III double-transmembrane protein which comprises 478 amino acids. It is also known as lysosomal integral membrane protein II, LGP85, or CD36b like-2 and belongs to the CD36 family which includes CD36 and scavenger receptor B

member 1 (SR-BI and its splice variant SR-BII) (Yamayoshi et al., 2014). SCARB2 participates in membrane transportation and reorganization of the endosomal/lysosomal compartment. It is expressed ubiquitously in variety of human tissues. After binding EV-A71 is internalized, conformationally changed leading to uncoating of the viral genome at low pH (Yamayoshi et al., 2014; Yamayoshi et al., 2009). It is also reported that SCARB2 may be involved in systemic EV-A71 infections since SCARB2 serves as a receptor for EV-A71 strains isolated from patients with HFMD and encephalitis (Yamayoshi et al., 2009).

2.3.3 Viral replication cycle

The attachment of the virus to its host surface cellular receptor is the first step of virus replication. A series of structural changes occur in the virus capsid after an enterovirus binds with a specific receptor on the cell surface and pores are formed in the cell membrane. The extruded VP4s form a channel through the membrane after the externalized N-termini of VP1 anchors the cell membrane. Upon viral attachment, the internal VP4 polypeptide is released by the interaction with the cellular receptor (s), followed by the RNA genome. The viral RNA is then released from a hole near the two-fold axis and the virion becomes an empty capsid. RNA-dependent RNA polymerase (3D) carries out the replication of the genome with the aid of other viral and host factors. The parent genomic RNA of approximately 7.5 kb with positive polarity, acts as a messenger RNA. A negative-strand copy is initially synthesized which is then used as a template for new genomic RNA-strands. The error-prone RNA-dependent RNA polymerase 3Dpol is present in a vesicle membrane structure (viral replication complex) when the replication of the virus genome occurs. It is estimated that the polymerase misincorporate or nucleotide

substitutions occur per site per year of one or two bases in every genome copying event within VP1 gene, which explains why the virus mutation evolves rapidly. The number of mutation is similar to the poliovirus, and it is higher than influenza viruses (Hyypia et al., 1997; Linden et al., 2015; Solomon et al., 2010).

In the replication and assembly process, the 5' end of the genome associated with a small polypeptide VPg where the genomic RNA is packed inside the capsid may participate. Cellular protein synthesis is inhibited (host-cell shut off) by the action of the 2A protease during infection, which leads the cleavage of one of the translation initiation factors. Translation results in a large polypeptide (200 kDa) which is promptly cleaved by two viral proteases: 2A and 3C, into 11 mature structural and non-structural proteins. The activity responsible for the final maturation cleavage between VP4 and VP2, which occurs after assembly of virus particles is still unknown (Hyypia et al., 1997; Lai et al., 2016; Linden et al., 2015; Solomon et al., 2010). However, viral protein synthesis is not inhibited since picornaviruses use cap-independent initiation in their own protein synthesis.

In one infected cell, approximately 10^4 - 10^5 of infectious virus particles are produced and the host cell is destroyed allowing the viruses to release to infect new target cells or neighbouring cells (Hyypia et al., 1997; Solomon et al., 2010). After packaging of a progeny viral RNA into a virus capsid in the cytoplasm of the infected cells, an infectious virus particle is formed and then mature infectious virus particles are released when an infected cell is lysed (Figure 2.4) (Solomon et al., 2010; Yamayoshi et al., 2014).
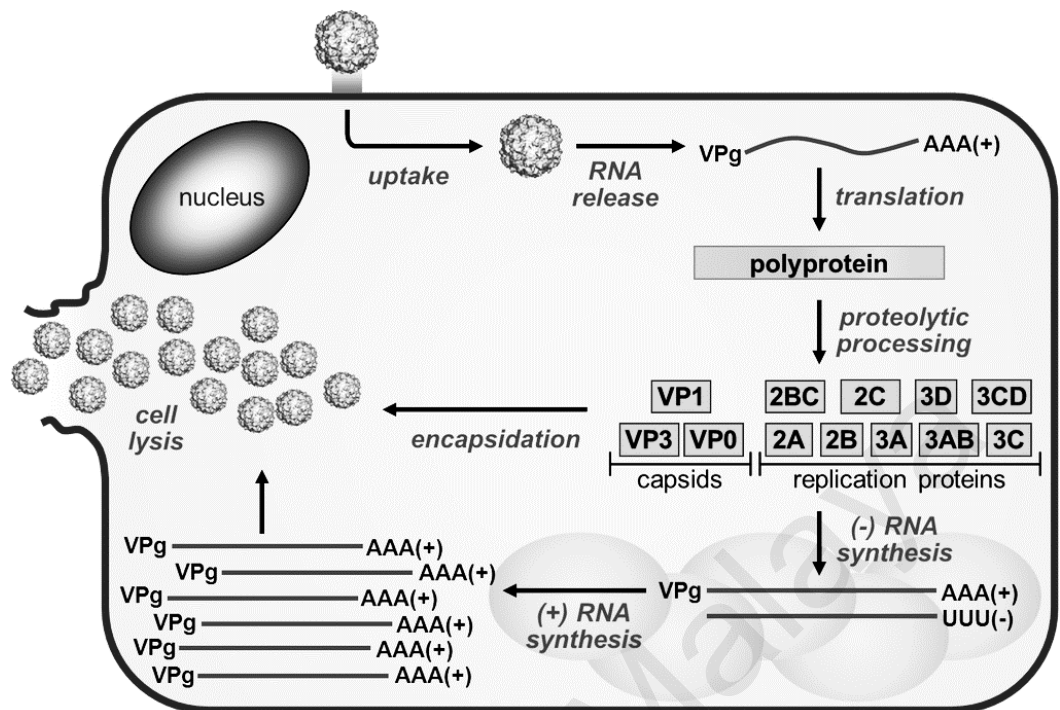
Figure 2.4 Enterovirus replication cycle. Binding of the virus to the receptor initiates the replication cycle and internalization into the cell. The viral RNA genome is released from the virion and translated into a single polyprotein which is then processed by the viral proteases to release the viral proteins. Next, the nonstructural proteins mediate the replication of the RNA genome via a negative-stranded intermediate. Newly synthesized positive-stranded RNA molecules can either enter another round of replication or they can be packaged into the viral capsid proteins to form new infectious virus particles which are released upon cell lysis and through several non-lytic mechanisms. Adapted from Linden, 2015.

2.4   Clinical epidemiology of EV-A71

In 1969, EV-A71 infection was first recognised and isolated from the stool of a child aged 9 months with encephalitis in California. HFMD is recognized as a common childhood illness, most typically noted in children younger than 10 years old. Adult cases are uncommon, possibly because of cross-immunity from other enteroviruses and immunologic memory from childhood infections. HFMD epidemics are common across Asia, occurring in China, Taiwan, Hong Kong, Japan, Vietnam, South Korea, and Malaysia. In one series of 157,707 cases of HFMD it was reported that 97% of patients were 0 to 9 years of age (with the highest cases of 0 to 4 years of age range). Other studies indicated that boys were reported to be affected more commonly than girls, with an average male-to-female ratio of 1.52 (Hubiche et al., 2014; Ventarola et al., 2015; Wang et al., 2014; Wong et al., 2010).

Although HFMD is usually considered a benign disease, neurologic complications only occur. In two outbreaks in Japan of over 1000 cases with frequent involvement of the central nervous system was reported, which included acute flaccid paralysis or poliomyelitis, brainstem encephalitis, the Guillain–Barré syndrome, rapidly fatal pulmonary edema and haemorrhage (Ho et al., 1999; Mcminn, 2003; Yip et al., 2010).

Besides the Asia-Pacific regions, several large outbreaks of HFMD associated with EV-A71 have also been reported in Europe, Australia, and the United States (Yang et al., 2009). Fatal EV-A71 infection outbreaks caused more than 44 deaths in Bulgaria in 1978, 45 deaths in Hungary in 1978, 30 deaths in Malaysia in 1997, 78 deaths in Taiwan in 1998, and 40 deaths in China in 2008 (Hsiung & Wang, 2000; Lin et al., 2003; Yang et al., 2009). In the United States alone, it was estimated around 10-15 million symptomatic enterovirus infections occur annually. In Asia-Pacific regions, most of the patients in Malaysia and Taiwan, had HFMD or herpangina and died of pulmonary edema, hemorrhage and/or after

the onset of brain-stem encephalitis. It is also reported, various types of enterovirus infection occur sporadically almost every year, however, EV-A71 epidemic before 1998 is unknown due to a lack of appropriate data collection (Chen et al., 2007a). In China, several millions of HFMD cases have been reported, and the data showed that enteroviruses were the main pathogens of HFMD, most of these were EV-A71 and CVA-16. It is speculated that a relatively poor sanitary condition and contaminated sources of water, may cause a high incidence of EV-A71 infection (Knipe & Howley, 2001; Yan et al., 2015).

In addition, enteroviruses are stable in the host environment because the lack of lipid envelopes, enable it to resist human gastric acid, and they can survive at room temperature for several days (Knipe & Howley, 2001). Other enteroviruses and EV-A71 could also be detected in surface, ground water and in hot spas as well. Enteroviruses can be inactivated by higher temperatures (>56°C), chlorination, formaldehyde, and ultraviolet irradiation, or can be destroyed by virucidal disinfectants. However, they are resistant to various solvents (ether, chloroform etc.), alcohol, freezing and detergents at ambient temperatures (Muehlenbachs et al., 2015; Solomon et al., 2010).

2.4.1 Clinical features

The typical clinical manifestations of HFMD is usually benign, and includes fever accompanied by vesicles, rashes or erosions most commonly occurs in the oral mucosa, hands, feet and sometimes the buttocks. Other dermatological manifestations such as perioral rash and onychomadesis have also been reported (Hubiche et al., 2014). Patients with mild HFMD manifestation usually recover after treatment without any sequela (Yan et al., 2015).

Atypical HFMD patients usually presented with fever, poor appetite, salivation, with skin distributed not only in typical sites such as hands, feet, mouth and frequently buttocks but also on other sites such as face, upper limbs, lower limbs, trunk and genitalia as well. Rashes on face were mainly noted in perioral area and in lower limbs mainly found in the thigh. Morphologically, papular rashes were found in majority of the patients. Vesicular rashes or both papules and vesicles in some patients. Large vesicles, erosive lesions with itching, and scabs in late phase were also found in some atypical HFMD patients. Oral lesions were often ulcerated (Chen et al., 2007a; Ho et al., 1999; Yan et al., 2015). Furthermore, atypical HFMD manifestation could also be mistaken for other infections such as coxsackieviruses and the infection may be occasionally associated with neurological and systemic complications (Hubiche et al., 2014).

Patients with complicated HFMD have manifestations that include high fever (temperature of at least 38°C), startle response, vomiting, tachypnea, and convulsions but headache, limb trembling, unconsciousness and unsteady gait were shown inconsistently in some patients. In severe infections, neurologic complications such as encephalitis, aseptic meningitis, or acute flaccid paralysis or cardiopulmonary complications such as pulmonary edema, pulmonary hemorrhage, or myocarditis were reported. Patients with any of these complications were considered to have neurologic involvement.

Late complications include limb weakness, dysphagia requiring tube-feeding, cerebellar dysfunction, delayed neurodevelopment, and impaired cognitive functions (Wong et al., 2010). Encephalitis is characterized by a disturbance in the level of consciousness (lethargy, drowsiness, or coma). Aseptic meningitis was characterized by headache, meningeal signs and mononuclear pleocytosis. Pulmonary edema is characterized by respiratory distress such as tachypnea, tachycardia, pink frothy sputum,

17

and rapidly progressing patchy, diffuse pulmonary infiltrates and congestion on a chest film. Acute flaccid paralysis is defined as the acute onset of paresis or paralysis of one or more skeletal-muscle groups, usually of one or more limbs. Cardiopulmonary collapse is defined as the development of hypoxemia and hypotension, despite the administration of inotropic drugs. Myocarditis is characterized by evidence of decreased contractility on echocardiography, arrhythmia, an enlarged heart, and elevations in cardiac enzymes that are markers for cardiac damage. EV-A71 infected children were hospitalized due to brainstem encephalitis and/or cardiopulmonary failure. Significant higher rates of neurological complications, long-term sequelae and fatalities in children than adults was previously reported (Chen et al., 2007a; Ho et al., 1999).

Virus shedding from upper respiratory tracts and feces are observed in survivors who had more serious CNS disease and cardiopulmonary failure (Han et al., 2010). Interestingly, it is also reported that the clinical outcome of secondary cases was not significantly different from that of primary cases (Chang et al., 2004).

2.5   Transmission and epidemic potential

Enterovirus infections are usually more common in poor sanitary conditions and low socioeconomic status resulting in high household transmission rates among family members (Knipe & Howley, 2001). Chang et al., 2004 reported that the overall rate of household transmission of EV-A71 infection was 52%, particularly in children which may be as high as 84%. These data suggested that the most important factor in EV-A71 transmission was intra-family transmission, especially the presence of seropositive adult/older sibling (s) (Chen et al., 2008). EVA-71 transmission intervals ranged from 1-15 days and the average transmission interval was 3 days (Chang et al., 2004). In addition,

most severe infection cases had a history of close contact with an infected sibling, and the role of viral exposure with the infected sibling may also increase infective dose of EV-A71 as well (Mcminn, 2003).

Person-to-person transmission occurs through direct contact with respiratory secretion, saliva, vesicle fluids, and feces from infected individuals (Knipe & Howley, 2001; Linsuwanon et al., 2015). The palatine tonsil and oropharyngeal mucosa were thought to be important primary viral replication sites, contributing significantly to oral shedding. Since virus is very likely to undergo primary replication and propagation in these sites, there could also be direct shedding into the orodigestive tract and feces (He et al., 2014). Consistent with the relative importance of the upper orodigestive tract, throat swabs have been reported to have a higher viral diagnostic yield than rectal swabs (Ooi et al., 2007a; Podin et al., 2006b). So far, there is no evidence that other parts of the human orodigestive tract support viral replication. EV-A71-related sequences persisted in the HFMD children for weeks after recovery, and virus shed in the feces may continuously persist for up to 6 weeks and up to 24 days in throat swabs (Han et al., 2010).

EV-A71 was previously isolated from vesicular fluid or swabs from both fatal and non-fatal EV-A71 cases and the morphology of skin rashes did not significantly differ from fatal and non-fatal EV-A71 cases (Chatproedprai S et al., 2010; Chong et al., 2003; Podin Y et al., 2006). Virus may possibly shed from infected skin vesicles to the environment when the vesicles were physically ruptured and thus may contribute to the person-to-person or cutaneous-to-oral transmission. EV-A71 may be able to enter the skin through direct contact with EV-A71 infected skin vesicles or fluid. The hypothesis of cutaneous-to-cutaneous viral spread/transmission through direct or indirect contact with vesicular fluid which contains infectious virus was previously suggested (Knipe DM & Howley, 2001).

Several countries in the Asia-Pacific region have established surveillance systems for EV-A71 mainly to monitor viral transmission and spread, and have provided information on virus evolution during outbreaks. It is reported that the pattern of viral activity increased every 3 years in Sarawak, Malaysia since 1997, and it is closely associated with increases in community incidence of HFMD. Similar epidemics was also seen in Fukushima Prefecture, Japan (Chen et al., 2007a). Regular cyclical activity is assumed to be related to births of children who have not been exposed to the virus. Since the virulence is different, it is difficult to predict the epidemic potential of particular genotypic subgroups. Subgroup dominance shifts have been reported widely such as Malaysia, Vietnam, Japan, Taiwan and Netherlands since a few decades ago. Low levels of disease have been occurred in many years by circulating older subgroups of EV-A71, whereas newly described subgroups such as B5, possess antigenicity distinct from other viruses and therefore, may have the potential to cause large outbreaks (Huang et al., 2011; Ooi et al., 2007b; Solomon et al., 2010).

Since late 1990s, EV-A71 is an emerging pathogen that has caused several outbreaks worldwide, but mostly in the Asia-Pacific region (Linden et al., 2015). Based on the structural VP1 gene, the first complete phylogenetic analysis of EV-A71 was identified. Three independent lineages were designated A, B, and C with at least 15% divergence between groups. Group A consists of one member, the prototype BrCr strain, which was first identified in California, in 1970, but similar reports were not received from other countries. BrCr strain was then isolated from 5 of 22 children presenting with HFMD in Anhui province of central China in 2008. Sequencing of the complete VP1 gene showed very little divergence between the two isolates (Yang et al., 2009).

To provide accurate and relevant information about EV-A71 transmission and evolution, and to confirm whether group A viruses have re-emerged, reliable and good surveillance programmes are needed in many different regions. Initially, group B viruses were separated into subgroups B1 and B2, with 12% divergence at the nucleotide level, were the predominant circulating strains in the 1970 - 1980s. In the mid-1980s, group C viruses were separated into C1 and C2 subgroups. According to findings in the Asia-Pacific region in the past 12 years, several subgroups have been added to groups B and C. Since 1997, viruses in subgroups B3 and B4 are thought to have circulated in the region (Yip et al., 2010). Subgroup C5 was reported in southern Vietnam and Taiwan. In India, a genetically distinct EV-A71 strain (R13223, Genbank accession number AY179600 to AY179602), with no genetic relationship to other EV-A71 strains was isolated from one child with acute flaccid paralysis in 2001 (Deshpande et al., 2003; Hyypia et al., 1997; Knipe & Howley, 2001; Linden et al., 2015; Saxena et al., 2015; Solomon et al., 2010).

Genogroup B (B3, B4, B5) have emerged in southeast Asia in the past few years. In peninsular Malaysia, Singapore, and Australia, group B (B3 and B4) has been predominant in 1997-1999, 2000-2002, and B5 in Malaysia in 2003. In 2003, subgroup B5 was first isolated in Japan and Malaysia, later caused epidemics in Brunei, Malaysia, and Taiwan in 2006. Genogroup C has been circulating in east Asia especially in mainland China (C4), Vietnam in 1998 and again in 2000 and was subsequently reported in Japan, and Taiwan whereas genogroup C2, circulated widely in Japan and Taiwan between 1998 and 2000 and an outbreak in Australia, in 1999. Subgroup C1 viruses isolated in the mid-1980s suggesting low-level circulation worldwide. Genogroup C3 have been identified in northern Asia, it was isolated in Japan in 1994, and was first identified in Korea during a HFMD

epidemic in 2000 but appears to have circulated in mainland China as early as 1997 (Mcminn, 2003; Ryu et al., 2010).

2.6   Autopsy finding in human EV-A71 encephalomyelitis

Neuropathologic evidence of EV-A71 infection in spinal cord and brain was previously reported in 7 cases of fatal EV-A71 encephalomyelitis (Wong et al., 2008). Viral antigen/RNA was localized in the anterior horn cells of spinal cords in all cord levels with the same intensity of inflammation. In addition, the distribution of inflammation in the brainstem was also consistent and viral antigen/RNA was detected in the neuronal cell bodies and processes but not in glial or other cells (He et al., 2014; Wong et al., 2008b; Yang et al., 2009). The inflammation in the brainstem which includes pons, medulla, and diencephalon was also previously reported by light microscopy analysis (Lum et al., 1998).

Another autopsy finding in an 8-year-old patient also reported extensive inflammation in hypothalamus, gray matter of cerebrum, dentate nuclei of cerebellum, brainstem and spinal cord by light microscopy. The most severe degrees of inflammation were reported in brainstem and spinal cord (Hsueh et al., 2000). In addition, the autopsy findings of another 2 patients with fatal HFMD cases reported that the brain tissues showed evidence of encephalitis, lymphocytic leptomeningitis with widespread perivascular cuffing by lymphocytes and plasma cells within the cortex and white matter and, localized perivascular hemorrhage, focal neuronal necrosis, and microglial reaction in the pons (Chan et al., 2003b). Two possible routes for EV-A71 have been suggested by which the virus reaches CNS either via blood across the blood-brain barrier (BBB), or transmission into the CNS through peripheral nerves via retrograde axonal transport (Chen et al., 2008; Lum et al., 1998; Wong et al., 2008b).

In the orodigestive tract, EV-A71 viral antigens were localized in the squamous epithelium lining tonsillar crypts of palatine tonsil and desquamated cells within the crypts. However, no viral antigens in the lymphoid cells or squamous epithelium covering external surface of tonsil were reported (He et al., 2014). In other non-CNS tissues, features of myocarditis such as mild biventricular hypertrophy interstitial infiltrates of lymphocytes, mononuclear cell infiltration in the myocardium and plasma cells associated with focal myonecrosis were reported (Chan et al., 2003b; Hsueh et al., 2000). However, no accompanying myocyte damage or viral inclusions was reported. In lung tissues, pulmonary congestion, acute pulmonary edema, multifocal haemorrhage, acute intra-alveolar hemorrhage, diffuse alveolar damage associated with interstitial lymphocytic infiltrates, extensive hyaline membrane formation, patchy atelectasis, and focal pneumocyte desquamation and hypertrophy were reported. Mild microvesicular fatty change was found in the liver (Hsueh et al., 2000). The other internal organs showed no remarkable pathological changes (Chan et al., 2003b; He et al., 2014; Hsueh et al., 2000).

2.7   Apoptosis

EV-A71 infection has been reported to trigger apoptosis and induced infected cell death in many different cell types including lymphocytes, endothelial cells, muscle cells and neural cells (Chen et al., 2007c; Too et al., 2016). EV-A71-induced apoptosis can be either caspase-dependent intrinsic apoptosis or calpain-induced caspase-independent apoptosis that is morphologically characterized by internucleosomal DNA cleavage, and apoptotic body formation. Apoptosis is also a defensive pathway for the host to prevent the generation and spread of viral progeny during infection. In EV-A71 infected neural cells, the hallmark event of early apoptosis, phosphatidylserine translocated from the inner to the

outer leaflet of the plasma membrane was observed. The mitochondrial pathway of apoptosis was identified as a main apoptosis pathway for EV-A71 inducing neural apoptotic cell death, which is mediated by activation and cleavage of caspase-9 (Weng et al., 2010). However, neural apoptosis that could significantly contribute to EV-A71 associated neural pathogenesis has not been reported.

2.8   Squamous epitheliotropism in humans and animal models

The typical clinical manifestations of HFMD is characterized by vesicles or rashes confined mainly to the hands, feet and perioral areas (Muehlenbachs et al., 2015). Recently, it has been reported that HFMD related to CVA-6 has more intense and widespread rashes than EV-A71. However, clinical studies of HFMD describing dermatological manifestations are limited and rare (Hubiche et al., 2014).

Vesicular maculopapular rashes are transient and typically associated with clinical symptoms of a mild viral infection. Biopsies are generally not obtained in EV-A71 infected children, but can be taken from older individuals or those with an atypical infection. The only one available skin biopsy of EV-A71 encephalomyelitis patient showed no viral antigens (He et al., 2014). The skin biopsy of CVA-6 case, skin epidermis showed keratinocyte necrosis most prominently in the upper layers, intraepidermal oedema, vesicle formation and neutrophilic infiltrates were also observed. The papillary dermis showed oedema and perivascular lymphohistiocytic infiltration. Viral antigens were only detected predominantly in the upper half of the epidermis, are localized to the cytoplasm of keratinocytes by immunohistochemistry and associated with areas of epidermal necrosis but no multinucleated giant cells or viral inclusions were reported (Muehlenbachs et al., 2015).

Orally-infected 1-day-old ICR mice developed skin lesions characterized by desquamation or skin rash and the hairless lesions persisted throughout the period until the animals developed limb paralysis. Viral antigens were also detected in the skin by IHC analysis, however, the author did not discuss localization of the viral antigens in the skin (Chen et al., 2004a). In 1-day-old transgenic mice, viral antigens were detected in oral mucosal epithelium cells in the lip and skin epidermal cells on terminal parts of limbs. Viral antigens were convincingly demonstrated within the squamous epithelial cells in these regions (Fujii et al., 2013a). In another 7-day-old transgenic mice showed HFMD-like hair loss or lesions but the viral antigens were only demonstrated in the dermis of the lower back skin (Lin et al., 2013b). In a hSCARB2 knock-in mice, epithelial cell necrosis and edema in the subcutaneous connective tissue were observed on footpads and the histological analysis showed the viral antigens in the epidermis of the footpads (Zhou et al., 2016). In the neonatal pig model, although the authors did not detect the viral antigens in the skin, vesicular lesions on the snouts were observed (Yang et al., 2014).

2.9   EV-A71 vaccine development

Vaccines against EV-A71 infection are urgently needed to control and prevent epidemics of EV-A71 transmission. However, no vaccines against EV-A71 has been developed until recently. In an EV-A71 vaccine study, Kuo et al., 2013 suggested that blocking virus entry may be an ideal antiviral strategy since neutralizing epitopes were located on the VP1 protein which is also identified as the major receptor binding protein among viral capsid proteins. Thus, the author speculated that the development of specific antibodies against neutralizing epitope on the VP1 viral capsid protein could be a successful antiviral strategy (Kuo & Shih, 2013).

In addition, EV-A71 has been divided into four genotypes (A, B, C and D genotypes) followed by further 12 sub-genotypes. Recently, C4 and B5 were reported the two pandemic strains. It has also been speculated that the major factor affecting vaccine efficacy may be protection against the other prevalent viruses when the particular vaccine derived from a specific strain with single genotype. However, people vaccinated with C4 vaccine showed good cross-neutralization and protection effect against various sub-genotypes of EV71 virus (B4, B5, C2, C5) in their serum (Liang & Wang, 2014). Other research groups have also generated the inactivated alum-adjuvant EV-A71 vaccine, which had completed phase 3 trials and proved to provide high efficacy, safety, and sustained immunogenicity (Huang & Shih, 2014; Huang et al., 2011; Li et al., 2012; Liang & Wang, 2014). Another potential vaccine candidate against EV-A71 infection, virus-like particle based vaccines have also been investigated and resulting highly immunogenic in mice and monkeys, and has a protection against lethal EV-A71 challenge in neonatal mice (Huang & Shih, 2014).

Ch'ng et al., have previously developed the NPt-VP11-100 candidate vaccine and validated in a hamster system with a 4-week susceptibility period to EV-A71 infection. Their results showed that the NPt-VP11-100 candidate vaccine stimulated humoral immune response in the hamsters however; they failed to neutralize EV-A71 viruses or protect vaccinated hamsters in viral challenge studies (Ch'ng et al., 2012b). In 1-day-old mice, passive immunization with adjuvant carrying formaldehyde inactivated MAV vaccine at 1 and 7 days of age were effectively protected from lethal virus challenge and disease at 14 days of age (Ong et al., 2010). In recent passive immunization with EV-A71-specific mouse MAb in 2-week-old ICR mice study showed its effectiveness to prevent CNS infection and spreading in mice (Tan et al., 2016). In humans, EV-A71 seroconversion rates

in adults for the general population were >50% and among the family members were about 93%. However, infection in adults is usually mild or asymptomatic and seroprotective (Chang et al., 2004).

Although recently licenced two EV-A71 vaccines are available to prevent the disease in children in China by WHO reports (Giersing et al., 2017), re-emergence of EV-A71 infection has become another challenge for public health, especially in the Asia-Pacific region. Successful production of anti-EV-A71 vaccine/drug has become an urgent issue to relieve distress in epidemic areas. However, to develop products beyond well-established vaccine, technological improvement is much needed. The future of EV-A71 vaccine development depends on global collaboration, technology, appropriate animal model to evaluate the vaccine and public support (Huang & Shih, 2014; Lu, 2014).

2.10   EV-A71 infection in animal models

Histopathological and clinical analyses in human and animal studies have suggested that the major cellular targets of EV-A71 infection in the CNS are neuronal cell bodies and processes (Li et al., 2011; Wong et al., 2008b). Previous animal infection models are summarised in Table 2.2. EV-A71 infection in rhesus monkey models demonstrated that CNS could be infected by various routes including intraspinal (i.p), intracerebral (i.c), intravenous (i.v) or intratracheal routes (Liu et al., 2011a; Nagata et al., 2004a; Nagata et al., 2002a; Zhang et al., 2011) (Table 2.2). In neonatal rhesus monkey model, virus inoculated via the respiratory tract, showed signs of HFMD such as some papules, vesicles or petechiae manifested on limbs or mouths and viral RNA was also detected in brown adipose tissue and skeletal muscle (Liu et al., 2011a).

Orally-infected 7-day-old mouse model showed consistent limb paralysis, CNS infection and viral shedding in feces (Wang et al., 2004a). In 1-day-old mouse model, infected via the oral and intraperitoneal routes, respectively, CNS and skin lesions, characterized as desquamation followed by cicatrisation were reported (Chen et al., 2004a). Persistence of hairless lesions at the early stages with positive virus isolation from skin was also reported (Chen et al., 2004a). In a 2-week-old mouse model, infection via various routes including i.c, i.p, intramuscular (i.m), and subcutaneous (s.c) developed consistent CNS infection, hindlimb paralysis and the animals succumbed to death (Ong et al., 2008b). In another 2-week-old EV-A71 infected mice via i.p., i.m., and i.c. infection, necrotizing myositis of respiratory-related muscles caused severe restrictive hypoventilation and subsequent hypoxia (Xiu et al., 2013). In a 10-day-old mouse model, massive necrotic myositis, varying degrees of infection in CNS, and extensive interstitial pneumonia were observed (Yu et al., 2014b).

In orally-infected AG129 (type 1 and 2 interferon receptors knock-out) mouse model, signs of CNS infections such as neuropil vacuolation and neuronal loss in the spinal cord anterior horn area and brainstem reticular formation and viral antigens in brainstem were reported, but other parts of the brain were negative (Khong et al., 2012a). In an hSCARB2 transgenic mouse model, the animals developed HFMD-like syndromes such as hair loss, skin rash and viral antigens localized in dermis of the skin, and neurological syndromes upon infection and caused fatal disease (Lin et al., 2013b). Another human SCARB2 expressing transgenic mouse model has been recently developed and demonstrated CNS and squamous epithelial cells infection in 3-week-old and neonatal mice (Fujii et al., 2013a). In a 4-week-old human SCARB2 knock-in mice infected with EV-A71 via i.v route, demonstrated epidermal involvement such as epithelial cell necrosis and

edema in the subcutaneous connective tissue, paralysis, and death. Viral antigens were detected in the brain and footpads (Zhou et al., 2016).

In human P-selectin glycoprotein ligand-1 (PSGL-1) transgenic mice, hindlimb paralysis and viral RNA was detected in skeletal muscle but no viral replication increment and no CNS infection were detected (Liu et al., 2012). In an orally or oral-nasally infected neonatal gnotobiotic pig model, signs of infection such as fever and vesicles on the snouts were observed but no lesions in the CNS and obvious pathological changes except for lung tissues (Yang et al., 2014).

In general, although the monkey models are susceptible to EV-A71 infection and developed skin lesions, the monkey models may have ethical and economic problems. Mouse models did not show consistent susceptibility to oral infection and the most consistent infections were obtained from 1-day-old or younger mice, older mice lose their susceptibility to EV-A71. EV-A71 infection using mouse adapted viral strains via intraperitoneal route in the 6-day-old mice showed clinical signs of neurogenic pulmonary oedema (Victorio et al., 2016). In the immunodeficient mouse model, although animals developed hind limb paralysis and CNS infection, viral antigens were not detected by histological analysis (Liao et al., 2014).

In addition, the transgenic mouse models showed similar pathological features to those of EV-A71 encephalomyelitis in humans, however, expression of human PSGL-1 in transgenic mice failed to increase the infectivity of EV-A71 which indicated that PSGL-1 alone may not be sufficient for EV-A71 infection. Most of the mouse studies including human SCARB2 transgenic mouse models showed infection in skeletal muscle tissues, causing severe necrotizing myositis and controversial results in CNS involvement (Chen et al., 2004a; Khong et al., 2012a; Lin et al., 2013b; Liou et al., 2016; Wang et al., 2004a).

Although, SCARB2 transgenic mice may be useful to evaluate the neurovirulence of EV-A71, an ideal model system has yet to achieve because the ideal animal model for EV-A71 infection is supposed to reproduce the important features of HFMD, including neurological symptoms (Huang & Shih, 2014).

Vaccine studies in animal models are urgently required to verify the effectiveness of antivirals against EV-A71. Neonatal mice and cynomolgus monkeys have been widely used for *in vivo* studies to evaluate the protection of neutralizing antibodies against EV-A71 and to investigate CNS involvement after infection. However, there are technical difficulties in handling 1-day-old mice and monkeys for evaluating antiviral efficacy and toxicity. However, other researchers have suggested that mouse models with the mouse-adapted strain may be a relatively low-cost and effective solution for evaluating new antivirals (Kuo & Shih, 2013).

Table 2.2 EV-A71 infections in animal models.

Animal type	Age	Route of infection	Findings	Virus shedding	References
Monkey, cynomolgus	Adult	Intravenous, Intraspinal	CNS infection, Limb paralysis, death	NA	Nagata et al., 2004
Monkey, rhesus	Neonatal	Respiratory tract	CNS infection, vesicular lesions, no death	Throat swabs, feces	Liu et al., 2011
Mouse, ICR	7-day-old	Oral	CNS infection, hind limb paralysis, death	Feces	Wang et al., 2004
Mouse, ICR	1-day-old	Oral	CNS and skin infections, hind limb paralysis, death	NA	Chen et al., 2004
Mouse, ICR	2-week-old	Intracerebral, Intramuscular, Intraperitoneal, Subcutaneous	CNS infection, hind limb paralysis, death	NA	Ong et al., 2008
Mouse, ICR	2-week-old	Oral	CNS infection, hind limb	NA	Ong et al., 2008

Animal type	Age	Route of infection	Findings	Virus shedding	References
			paralysis, no death		
Mouse, ICR	2-week-old	Intraperitoneal, Intramuscular, or Intracerebral	CNS infection, hind limb paralysis, death	NA	Xiu et al., 2013
Mouse, BALB/c	10-day-old	Intraperitoneal	CNS infection, limb paralysis	NA	Yu et al., 2014
Mouse, BALB/c	1-week-old	Intraperitoneal	CNS infection, skin lesions, limb paralysis, neurogenic pulmonary oedema, death	NA	Victorio et al., 2016
Mouse, AG129	2-week-old or younger	Intraperitoneal, Oral	CNS infection, hind limb paralysis, death	NA	Khong et al., 2012
Mouse, hSCARB2 transgenic	3-week-old or adults	Intravenous	CNS infection, hind limb paralysis, death	NA	Fujii et al., 2013

Animal type	Age	Route of infection	Findings	Virus shedding	References
Mouse, hSCARB2 transgenic	1-day-old	Subcutaneous	CNS, oral mucosa and skin infection, hind limb paralysis, death	NA	Fujii et al., 2013
Mouse, hSCARB2 transgenic	1-3-week-old	Intraperitoneal	CNS, limb paralysis, death	NA	Liou et al., 2016
Mouse, hSCARB2 knock-in	4-week-old	Intravenous	CNS and skin infections, limb paralysis, death	NA	Zhou et al., 2016
Mouse, human PSGL-1 transgenic	10-day-old	Intraperitoneal	CNS infection, hind limb paralysis, no death	NA	Liu et al., 2012
Mouse, immunodeficient	1-week-old	Intraperitoneal, Subcutaneous, Oral	CNS, hind limb paralysis, death	NA	Liao et al., 2014
Pig, gnotobiotic	Neonatal	Oral Oral-nasal	Vesicles on the snouts, lung lesions, fever, limb paralysis, no death	Feces/rectal swabs	Yang et al., 2014

CHAPTER 3

MATERIALS AND METHODS

3.1   MATERIALS AND METHODS

3.1.1   Cell lines

African monkey kidney (Vero) cell lines were previously obtained from Department of Medical Microbiology, Faculty of Medicine, University of Malaya and were used for virus isolation and titration throughout this study. Primary epidermal keratinocytes were cultured from human prepuce skin and used for EV-A71 infection (see sections: 3.6.1 and 3.6.2).

Dulbecco's modified Eagle's growth medium (DMEM) (Sigma-aldrich, USA) supplemented with 5% fetal bovine serum (FBS) (Hyclone, USA), 20mM HEPES buffer (pH 7.4) (Sigma, USA), 0.08% sodium hydrogen bicarbonate (NaHCO$_3$), 1 mM sodium pyruvate (Sigma, USA) and 50 µg/ml gentamycin (Alantic Laboratories, Thailand) was used to grow cells. DMEM maintenance medium (MM) containing 2% FBS, 20 mM HEPES buffer (pH 7.4), 0.19% NaHCO$_3$, 1 mM sodium pyruvate, 50 µg/ml gentamycin was prepared and used for maintaining the Vero cells infection and viral titration experiments.

Cell cultures were examined for percentage of confluency, morphology and presence of microbial contamination using an inverted microscope (Zeiss, Germany). When the culture was found to be free of contamination, growth medium (GM) was discarded from the cell culture flask and the cell monolayer gently washed twice with PBS (phosphate buffered saline). Trypsin-EDTA (Sigma-aldrich, USA) was added into the cell monolayer and incubated for 5–10 min at 36ºC until all cells were detached from the flask as confirmed using the inverted microscope. Cells were then re-suspended in 5 ml of GM and

gently aspirated a few times to break the cell clumps. Cells suspension was then diluted in 1: 4 ratio with GM and approximately 1×10^6 per ml of cell suspensions were added into a new flask. The flask was slightly shaken to distribute the cells evenly, tightly capped and placed in a 37ºC incubator.

3.1.2 Viruses

All experiments using live viruses were conducted in a biosafety level 2 cabinet. A EV-A71 mouse-adapted virus (MAV) (See Appendix G) was used in the all animal experiments. The unadapted parental EV-A71 strain (Genotype B3; GenBank accession number AY207648) was previously produced by serially passaging in infected brains of 1-day-old ICR mice as described previously (Ong et al., 2008b). Briefly, after one-day-old ICR mice were initiated by i.c inoculation of 10^5 $CCID_{50}$ of the parental strain, virus from infected mice' brains were isolated and serial passages were done by i.c inoculation into the new mice' brains. The MAV from the fifth passage was further propagated in Vero cell monolayers using T25 flasks (Corning, USA) at a multiplicity of infection of 0.01 per cell and incubated at 36℃ until complete cytopathic effect was achieved in order to increase the volume of the virus stock. Another human EV-A71 strain isolated from a child with HMFD and designated as A104 (Genotype B4; Genbank No: AF376067), obtained from Dr. Ong Kien Chai, Department of Pathology, Faculty of Medicine, University of Malaya, was used for all human tissues and epidermal keratinocytes infection studies.

3.1.3 Virus stock preparation

Both MAV and A104 were propagated and maintained in 2 % FBS DMEM MM in 25 cm² flasks (Nunc, Denmark) of confluent Vero cells. Briefly, virus suspension (1 ml) was

inoculated into the Vero cells with a multiplicity of infection (MOI) of 0.01 and incubated for 60 min at 36ºC with gentle shaking of the flask every 15 min. After that, 4 ml of MM was added and cells were incubated at 36ºC until 90% or more of the cells showed cytopathic effect (CPE). An uninfected control flask was also prepared in the same way without infection. The culture flasks were then subjected to three freeze-thaw cycles, followed by centrifugation at 4,500 rpm for 10 min at 4ºC. The supernatant was harvested and stored at -80ºC until use.

3.1.4 Virus titration

Virus stock titer was determined by a standard micro-titration assay. First, 10-fold diluted virus suspensions in DMEM MM were prepared (10^{-1} – 10^{-8}), 4 replicates for each dilution. GM from confluent Vero cell monolayers grown in 96-well plate (Falcon, USA) was removed, a volume of 50 µl per well (10^{-1} – 10^{-8}) was inoculated into 4 replicate wells (a total of 32 wells) of Vero cells. The plate was incubated for 1 hour at 36ºC. After that, 100 µl of DMEM MM was added to each well and the plate was returned to the 36ºC incubator and further incubated for 7 days. Four negative control wells were also prepared without infection. After 7 days post-infection (dpi), all the wells were examined for CPE and the number of infected and uninfected wells at each virus dilution were recorded accordingly. The virus titer was determined using the Karber method (Karber, 1931).

3.1.5 Antibodies used for immunohistochemistry (IHC) and immunofluorescence (IF)

All the primary antibodies used in this study are shown in Table 3.1.

Table 3.1 Primary antibodies for IHC and double IF.

No.	Antibody	Type	Specificity	Dilution & incubation	Antigen retrieval	Positive control tissues	Source
1	Enterovirus A71	Monoclonal	EV-A71	1:50, 2 h*, RT**	Steamed in citrate buffer****	EV-A71 infected mouse	Light Diagnostics, UK
2	Human cytokeratin	Monoclonal	Human cytokeratins	1:100, O/N***	Steamed in citrate buffer	Human skin	Dako, Denmark
3	LIMPII/lgp85	Polyclonal	Human SCARB2	1:2000, O/N	Steamed in citrate buffer	Human skin, rhabdomyosarcoma cells	GeneTex, USA
4	S100	Polyclonal	Dendritic cells	1:500, O/N	Steamed in citrate buffer	Human skin	Abcam, UK

*h: hour

**RT: room temperature

***O/N: slides were incubated overnight (~16 h) at 4ºC

****citrate buffer (See appendix C)

3.2 Experimental animals

The protocols for all animal experiments were approved by the Faculty of Medicine Institutional Animal Care and Use Committee, University of Malaya (Ethics Reference No: 2014-02-14/PATHO/R/WKT). New-born hamsters were raised up to 2-week-old for our experiments from pregnant Syrian golden hamsters purchased from Monash University, Sunway Campus, Malaysia. Unless otherwise stated, each group of new-born hamsters was housed together with their mothers until the end of the experiments, and provided with adequate autoclaved food and water in an air-conditioned room with 12 hours light/dark cycles. Two-week-old hamsters were used throughout the studies.

Three separate sets of animal studies were performed in this project, 1) to develop a new orally-infected hamster model, 2) to study the viral spread within the CNS and non-CNS tissues, and 3) to model person-to-person transmission (see sections 3.3, 3.4 and 3.5).

3.3 Animal Infection Experiments

3.3.1 Determining the susceptibility of 2-week-old hamsters to MAV by oral infection

A group of 2-week-old hamsters (n=6) were orally inoculated with 100 µl of MAV (10^5 $CCID_{50}$) each. After inoculation, all the animals were housed in a new cage for 2 hours before they were returned back to the original cage and housed together with the mother hamster. As part of the preparation for the animal experiments, preliminary studies were performed to establish the optimal viral dose, cage size and the number of infected animals needed per cage to transmit infection efficiently. All infected hamsters were observed daily for signs of infection such as limb weakness and/or paralysis, ruffled fur, and weight loss. Three additional hamsters were orally inoculated with PBS and served as negative controls.

3.3.2 Determining of 50% lethal dose (LD$_{50}$) in 2-week-old hamsters

Since preliminary results showed that 2-week-old hamsters could be consistently infected by the oral route, a 50% lethal dose (LD$_{50}$) study was performed on these animals. Six groups of hamsters (6 animals per group) were each orally-inoculated with 100 µl PBS containing 10^5, 10^4, 10^3, 10^2, 10, and 1 CCID$_{50}$ of MAV, respectively. The infective dose was delivered using a micropipette and without anesthesia. A group of mock-infected hamsters each for all experiments were kept separately and given PBS only. All animals were monitored twice daily up to 14 days, for signs of infection, such as weight loss, humped posture, ruffled fur and hindlimb paralysis. A total of 17 moribund animals defined as paralysis of ≥2 limbs or clinical score 4 (see Appendix F) (Lin et al., 2013b), were euthanized with isoflurane (1-4%) to minimize suffering (humane endpoints).

To determine the viral titers and histopathological analysis, another group of 2-week-old hamsters (n=8) were orally inoculated with 100 µl PBS containing 10^4 CCID$_{50}$ MAV. Animals were monitored, sacrificed at 4-5 dpi or moribund and various tissue including oral cavity, brain, spinal cord, thymus, heart, lung, liver, spleen, kidney, stomach, intestines, hind limb muscle, paws and skin were harvested for routine histology processing collected from 4 infected animals as before. The remaining 4 infected animals, serum and solid organs (brain, spinal cord, stomach, kidney, spleen, heart, adipose tissues, intestines, and hind limb muscle) were harvested for viral titration. In addition, oral washes and feces were also collected daily from all 8 infected animals for virus isolation and titration. Two additional mock-infected animals were served as negative controls.

3.3.4   Histopathology analysis

Infected and mock-infected hamster tissues from the LD_{50} study were harvested for histopathological analysis. Tissues from hamsters that were found dead (n=7) overnight were also harvested to determine the cause of death. However, the tissues were not included in the analysis. After adequate 10% neutral-buffered formalin fixation for about 2 weeks, the entire skin was first separated from the carcass before a set 20 standard tissues (oral cavity, brain, spinal cord, thymus, heart, lung, liver, spleen, kidney, stomach, intestines, hind limb muscle and paws) from each hamster was routinely processed and paraffin embedded. Formalin-fixed tissues were decalcified in 5% formic acid overnight followed by further formalin fixation for additional 2 days before routine processing and paraffin-embedded. In addition, various part of the skin tissues such as head, neck, chest, trunk, pelvic region, tail, fore and hind limbs, respectively, were dissected into 3 mm wide strips before sent for tissue processing.

3.3.5   Light Microscopy analysis

In all 3 animal experiments, tissue blocks (n=180, preliminary experiment), (n=840, LD_{50} study), (n=600, viral spread study), (n=120, transmission experiment 1) and (n=128, transmission experiment 2) were prepared, processed and paraffin-embedded. Tissue sections, 4 µm thick were cut from tissue blocks, dewaxed and stained with hematoxylin and eosin for light microscopy analysis.

3.3.6 Tissue controls for IHC and ISH analysis

EV-A71 infected and uninfected 1-day-old mouse, paraffin embedded tissue blocks, as previously prepared by Ong (2008) were obtained from Department of Pathology, Faculty of Medicine, University of Malay, were used as positive and negative controls, respectively.

3.3.7 IHC to detect EV-A71 antigens

IHC was performed using a modified immunoperoxidase technique as described previously (Ong et al., 2008b). Briefly, a monoclonal mouse anti-EV-A71 antibody (Light Diagnostics, UK) was applied onto tissue sections for 2 hours at RT followed by secondary antibody conjugated with horseradish peroxidase for 30 min at RT (Dako Real Envision, Denmark). The substrate chromogen 3,3' diaminobenzidine tetrahydrochloride was then applied (Dako, Denmark), followed by hematoxylin counterstaining and mounting. To confirm primary antibody specificity, primary antibody was replaced by mouse isotype control IgG1 or Tris buffered saline and IHC procedure repeated. EV-A71 infected mouse tissues (Ong et al., 2008b) were used as positive controls. Whereas, mock-infected hamster tissues were used as negative controls.

3.3.8 ISH to detect EV-A71 RNA

EV-A71 DNA probes were produced to detect the viral RNA in infected animal and human tissues throughout this project. Plasmids containing correct orientation of insert were provided by Dr. Ong Kien Chai, Department of Pathology, Faculty of Medicine, University of Malaya, to use as a template to produce DIG-labeled DNA probes. A 603 bp PCR amplicon was first produced from the VP1 of the EV-A71 genome using a pair of specific

primers (forward primer GTCTCAGTTCCATTCAT GTC and reverse primer CCTAGCAGGGTAATACTCGCTA). Digoxigenin (DIG)-labelled DNA probes were generated by incorporating DIG-11-dUTP (Roche, Germany) in a second PCR using the first amplicon as a template as previously described (Wong et al., 2008b). DNA probe labelling and PCR conditions are shown in Table 3.2. For the ISH procedure, after pre-treatment with 0.2 N HCL and proteinase K (100 µg/ml) for 20 min at 37˚C. Hybridization solution containing DNA probes were applied on tissue section and heated at 95˚C for 10 min to denature the DNA probes. Tissue sections were then incubated for 16 hours at 42˚C in a moist chamber. Hybridization signals was detected using anti-DIG-Alkaline-Phosphatase antibody (Roche, Germany) followed by nitroblue tetrazolium/5-bromo-4-chloro-3-indolyl phosphate (Roche, Germany) substrate to obtain a colour reaction. For negative controls, hybridization solution without probes were served as reagent control, and EV-A71 infected mouse tissues, mock-infected hamster tissues, and uninfected human skin cultured tissues were served as positive and negative controls, respectively.

3.3.9   Comparison of amino acid sequences of SCARB2 receptors

Amino acid sequences of SCARB2 receptors in human (Homo sapiens; accession no. KR709707), golden hamster (Mesocricetus auratus; accession no. NM_001281557), and mouse (Mus musculus; accession no. NM_007644) were downloaded from Genbank and aligned using MEGA 6.06 software in order to compare the homology of amino acid sequences of this EV-A71 receptor between these animal species.

Table 3.2 DNA probe labelling and PCR conditions.

Reagents mixture	
Buffer (10X)	5 µl
Primers (10 pmol/µl)	1 µl each
DNTP (A,G,C) (10mM)	1 µl
DTTP (1mM)	6.5 µl
Dig-11dUTP	3.5 µl
Taq DNA polymerase	0.5 µl
MgCl$_2$	4 µl
DNA	2 µl
H$_2$O to final volume	50 µl
PCR condition	
95ºC	3 min
95ºC	30 s
53ºC	30 s — 30 cycles
72ºC	1 min
72ºC	10 min
4ºC	Hold

3.3.10 Virus isolation from tissues, oral washes and feces

For virus isolation and titration, brain, upper spinal cord (thoracic cord segments), lower spinal cord (lower half thoracic and lumbosacral cord segments), stomach, intestines, heart, spleen, brown adipose, sera and hind-limb muscle tissues were collected from infected animals. Extra care was taken to minimize cross-contamination of tissues at harvesting. Tissues were weighed and immediately frozen at -80˚C for later use. Frozen tissues were then homogenized in PBS to obtain 10% (wt/vol) homogenation. Virus titration was performed with the micro-titration assay described above (see section 3.1.4).

To obtain oral washes, oral cavity of infected and mock-infected hamsters was rinsed 6 times each with 100 µl PBS. The pooled oral washes were then stored at -80˚C for processing later or immediately treated with chloroform (1:10). Treated oral washes were then centrifuged at 3500 rpm, for 20 min at 4˚C and the supernatants were harvested and stored at -80˚C until use (World Health Organization, 2004 Aug 31). Four or 5 fecal pellets expelled spontaneously from the anus during handling were collected from each hamster using sterile forceps. The collected fecal pellets were stored at -80˚C to be processed later, or immediately processed as described for oral washes, and stored until use.

3.4 Study of virus spread and distribution within CNS and non-CNS tissues

In this second animal experiment to study viral spread over time, 4 sets of experiments, 2-week-old hamsters (n=8 each group) were orally inoculated with 100 µl of PBS containing 10^5 CCID$_{50}$ of MAV. Groups of mock-infected hamsters given PBS only for each time point was served as negative controls and kept separately. All animals were monitored twice daily throughout the experiment for signs of infection, such as weight loss, humped posture, ruffled fur and hind limb paralysis. Each group of infected animals were sacrificed

at 1 dpi, 2 dpi, 3 dpi and 4 dpi, respectively for histopathological analysis (n=5 each). Fresh organs from 2, 3 and 4 dpi sacrificed animals (n=3 each time point) including brain, spinal cord, hind limb muscle and sera were harvested, processed and titrated as before (see sections: 3.3.9 and 3.1.4). Organs from animals sacrificed at 1 dpi were not performed for virus titration since histopathological analysis showed no viral antigens in all infected tissues. Oral wash and feces samples were also collected from all infected animals (n=8, each group) for viral isolation and titration. The procedure for oral wash and feces samples collection, processing and titration were performed as described before (see sections: 3.3.9 and 3.1.4). For histopathological analysis, the entire carcasses were fixed in 10% neutral buffered formalin for 2 weeks, routinely processed and prepared for light microscopy, IHC and ISH as described previously (see sections: 3.3.4, 3.3.5, 3.3.7 and 3.3.8).

3.5 Hamster viral transmission study

In this third animal study experiments were designed to investigate the suitability of the hamster as a model for person-to-person viral transmission.

3.5.1 Transmission experiment 1

Five groups of 2-week-old hamsters (n=6 per group) from 5 different mother hamsters were studied to investigate intra-hamster family transmission. From each group, 3 animals were orally infected with 10^4 CCID$_{50}$ of MAVS, and called "index case" hamsters (hereafter called index hamsters). After infection, index hereafter called contact hamsters), to reduce the likelihood of infection by the initial inoculum. After 2 hours, index hamsters (n=3) were returned to their respective mothers and contact littermates (n=3) and housed in the same cages (size 20 x 30 cm) for the duration of the experiment. Animals were observed a few

times a day for signs of infection including back hunching, ruffled fur, weight loss and hind limb paralysis. To determine the amount of live virus excretion, oral washes and feces were collected from index and contact animals daily from 4 groups of animals. Samples were immediately frozen in -80ºC for virus isolation and titration as described previously (see sections: 3.3.9, 3.1.4). Initial negative oral wash and feces results underwent a 2nd passage to confirm the absence of live viruses.

Animals showing severe hind limb paralysis or were moribund, were sacrificed by isoflurane inhalation, and sera collected via cardiac puncture for viral titration. Entire animal carcasses from 4 animal groups (n=24) were immediately fixed in 10% neutral buffered formalin for 2 weeks, and tissues harvested for routine processing and light microscopy analysis as described previously (see sections: 3.3.4, 3.3.5). From the 5th group of animals, (n=6) instead of fixing tissues, fresh organs/tissues including the brain, spinal cord, stomach and hind limb muscle were harvested and immediately frozen at -80ºC for virus isolation and titration as described (see sections: 3.3.9, 3.1.4).

3.5.2 Reverse-transcriptase PCR (RT-PCR) to detect MAVS viral RNA in oral wash and fecal samples

In order to confirm that viral cultures were truly positive or negative, RT-PCR was done. Total RNA was isolated from all oral wash and feces samples using High Pure Viral RNA Kit (Roche, Germany). The extracted RNA was synthesized using cDNA synthesis kit (Tetro cDNA Synthesis Kit, Bioline, UK) according to the manufacture's protocol. Single-stranded cDNA was then amplified using a pair of primers (forward primer GTCTCAGTTCCATTCATGTC and reverse primer CCTAGCAGGGTAATAC TCGCTA) binding to VP1 region of EV-A71 genome. The RT-PCR mixture and condition was shown in Table 3.3. Post-PCR products were loaded into 1% agarose gel, stained with ethidium

bromide, the expected 600 bp bands were visualised on a UV transilluminator (Alpha Imager HP, USA).

Table 3.3 RT-PCR mixture and conditions.

Master mix	
RT buffer (5X)	4 µl
Reverse transcriptase (200u/µl)	1 µl
RNase inhibitor (10u/µl)	1 µl
dNTP mix (10mM)	1 µl
Random hexamer primer mix	1 µl
Total RNA (5 µg)	~
DEPC-treated water to final volume	20 µl
RT-PCR condition	
25ºC	10 min
42ºC	30 min
85ºC	5 min
4ºC	Hold

3.5.3   Transmission experiment 2

In a separate experiment designed to study duration of viral exposure and transmission, 3 groups of 2-week-old index hamsters (n=4 per group; total 12 animals) were infected with a dose of 10^4 $CCID_{50}$ per animal, and returned to their respective mother hamsters. When index hamsters in each group developed signs of infection at 4 dpi, they were separated

from their mother and placed into a clean cage (size 10 x 20 cm) together with another group of uninfected 2-week-old contact hamsters (n=4) from a separate family. In this way, 3 groups of contact animals were separately exposed to 3 groups of index hamsters for 4, 8 and 12 hours, respectively. Index hamsters were sacrificed soon after at 4-5 dpi when they showed severe hind limb paralysis or were moribund. Contact hamsters upon return to their own mothers, were observed and sacrificed as before when severe disease occurred. Animal carcasses of both index and contact animals in the 12 hours-exposure experiment (n=4 each), were formalin-fixed for routine processing and light microscopy analysis (see sections: 3.3.4 and 3.3.5)

Oral washes and fecal samples were collected from all index hamsters just before placement with uninfected contact animals. In addition, oral washes and feces were also collected from all index and contact hamsters after exposure for virus titration as before (see sections: 3.3.9 and 3.1.4).

3.5.4   Light microscopy, IHC and ISH

Light microscopy analysis, IHC and ISH procedures were performed as described before (see sections: 3.3.5, 3.3.7 and 3.3.8).

3.5.5   Neutralizing antibody assay

Sera from all mother hamsters from experiment 1 (n=5) and experiment 2 (n=6), and contact hamsters (n=4) from the 4 hours-exposure group were collected at sacrifice after first exposure to infected offsprings to investigate seroconversion. Briefly, sera were serially diluted up to 1:512 and mixed equally with 100 $CCID_{50}$ of EV-A71 (Tan et al., 2016). Sera from uninfected or not exposed to infected animals were used as negative

control. The samples were then incubated at 4°C overnight before inoculation onto the Vero cell monolayers in 96-well plates and cultured for 7 days at 36°C. Monoclonal mouse anti-EV-A71 antibody was used as a positive control as previously described (Tan et al., 2016).

3.6 Human skin organotypic and primary squamous cell culture systems

3.6.1 Skin and lip/oral mucosa organotypic culture

In order to investigate cellular targets in human epidermis and oral mucosa, we infected human prepuce and lip skin, and lip mucosa organotypic tissues. The study was approved by the Medical Ethics Committee, University of Malaya Medical Centre in accordance with ICH Harmonised Tripartite Guidelines for Good Clinical Practice (Registration No. 920.1). All donors have given written informed consent prior to sample collection. Circumcised prepuce skin and lip skin/oral mucosa tissues were obtained from cleft-lip repair surgeries in children aged 3 months to 9 years. These biopsy samples were cultured as described previously with minor modifications (Maher et al., 2005; Taylor & Moffat, 2005b). After the surgery, the specimens were immediately transferred to the lab in a sterile tube containing cold phosphate buffered saline (PBS, pH 7.4). Next, the specimens were washed with PBS containing 0.1% penicillin and streptomycin (Sigma-Aldrich, USA) and fungizone (Sigma-Aldrich, USA). The specimens were further disinfected in 70% ethanol and washed twice in PBS before careful dissection to obtain approximately 1 mm x 3 mm tissue fragments. Eight fragments per well were placed on a 6-well transwell with a 0.4 µm pore size membrane (BD FalconTM, USA). Organotypic samples were cultured in 10% DMEM, at 37°C.

3.6.2 Cell proliferation assay

A cell proliferation assay using Celltiter 96® aqueous one solution (Promega, USA) was performed to assess general skin organotypic culture viability using prepuce tissues from 4 individual patients. The MTS Cell Proliferation Assay is a standard and sensitive colorimetric quantification of viable cells based on the reduction of MTS tetrazolium compound by NAD(P)H-dependent dehydrogenase enzymes in metabolically-active cells. Tissues cultured under the usual conditions as described above were harvested on days 0, 2, 4, 6 and 8, before transfer it to a standard 96-well plate for incubation with Celltiter aqueous solution for 4 hours at 37°C in the dark, according to manufacturer's protocol. After incubation, the absorption spectrum of the solution was measured at a wavelength of 490 nm with microplate reader (BioTek, USA). Since for each time point, 4 tissue fragments from each patient were harvested, a total of 80 fragments were assessed for viability.

3.6.3 Infection of human organotypic cultures

Seven sets of human prepuce skin organotypic cultures, derived from 7 patients, were grown in 6-well plates, and separately harvested for study at 2, 4 and 6 dpi. Each set consisting of 3 wells (10 tissue fragments/well) were infected with 2×10^6 $CCID_{50}$ of A104 virus per well. The plates were then shaker-incubated at 37°C for 2 hours to allow for virus attachment and entry. The specimens were then thoroughly washed 3 times with PBS containing antibiotics, before transfer onto transwell insert membranes placed in another set of 6-well plates each containing 3.2 ml/well of new medium. The medium was maintained unchanged for the whole experiment. To determine viral titers at 0 dpi, 100 µl of the medium and 2 tissue fragments were collected from each set of organotypic cultures very

soon after the new medium was added. At 2, 4 and 6 dpi, respectively, 6 tissue fragments and supernatant per well were collected for viral titration. Tissue fragments were washed with PBS 3 times, air-dried for about 10 minutes at room temperature (RT) before weighing and freezing at -80˚C for later viral titration. Tissues were then homogenized in PBS to obtain 10% (wt/vol) suspensions and virus titers were detected using microtitration assay in Vero cells (see section: 3.1.4).

The remaining 2 skin fragments per well were harvested for histopathological analysis. For negative uninfected skin control tissues, duplicate cultured specimens from all 7 patients were prepared in the same way and harvested for histopathological analysis at day 0, 2, 4 and 6 (n=8 each).

Lip skin/oral mucosa tissues were similarly infected as described for skin tissues using specimens from 5 patients (8 tissue fragments per patient, 8 fragments/well) which were respectively infected and shaker-incubated as before with the same viral dose. The medium was changed twice a week for the duration of the experiment. Two tissue fragments were harvested from each well at 1, 3, 5 and 7 dpi, respectively, for light microscopy, IHC and ISH. Negative uninfected controls, were prepared as before. Virus titration from this specimen was not performed due to limited size and availability of samples.

3.6.4   Primary epidermal keratinocyte monolayer culture

Human prepuce skin biopsies were cut into fragments about 3 x 3 mm and placed in a 30 mm dish containing 3-4 ml of PBS with antibiotics before treated with 2U/ml of Dispase (Sigma-Aldrich, USA) overnight at 4˚C. The epidermal layer was then carefully peeled off from the skin using sterile forceps and immediately washed with PBS/antibiotics before

further digestion with 0.05% trypsin for 30 min at 37˚C to obtain single keratinocyte cell suspensions. After washing with PBS, cell suspension was centrifugation at 1500 rpm for 5 min at RT, before resuspended in keratinocyte growth medium (Lonza, USA). Cell pellets were then resuspended in the fresh medium, loaded into the T25 flasks and cultured at 37˚C about 2-3 weeks until it's fully confluent.

3.6.5 Infection of primary epidermal keratinocytes

After the 1st passage, approximately $2x10^6$/well of keratinocytes were seeded into 12-well plates and cultured at 37˚C for 2 days. When 70-80% confluence was achieved, cells were then incubated with A104 virus at an MOI of 0.05 (10^5 $CCID_{50}$) at 37˚C for 2 hours for virus attachment and entry. The cells were then thoroughly washed with PBS containing antibiotics 3 times after pre-absorption and cultured up to 3 days. The supernatant was harvested from 4 well replicates every 24 hours for virus titration at 1, 2 and 3 dpi, respectively as described (see section: 3.1.4).

3.6.6 Light microscopy analysis

Two organotypic culture tissue fragments per well were harvested at 2, 4, 6 dpi from infected wells and day 0, 2, 4, 6 from uninfected wells were immediately fixed in 10% neutral-buffered formalin for routine processing and light microscopy analysis as described (see section: 3.3.4, 3.3.5).

3.6.7 IHC to detect EV-A71 viral antigens

A modified IHC technique was used to localize EV-A71 antigens in organotypic culture tissues. Four µm tissue sections were deparaffinised, followed by incubation with primary

monoclonal mouse anti-EV-A71 antibody (Light Diagnostics, UK) overnight at 4°C after antigen retrieval and normal serum blocking. Secondary antibody goat anti-mouse IgG conjugated with enzyme alkaline phosphatase (Santa Cruz Biotechnology, USA) was applied to the sections for 30 min at RT before colour development with Liquid Permanent Red chromogen (Dako, USA). The substrate Liquid Permanent Red chromogen (red end product) was used in organotypic cultures because in the skin organotypic cultures, the presence of normal occurring melanocytes which contain brown pigments may be misinterpreted as a positive result if 3,3' diaminobenzidine tetrahydrochloride (brown end product) were used. Hence, Liquid Permanent Red chromogen was used instead. Tissue sections were then counterstained with hematoxylin and mounted with DPX mounting media (Sigma-Aldrich, USA). For negative IHC controls, mouse isotype control IgG1 or Tris buffered saline (TBS) or anti-Japanese encephalitis virus antibodies was used instead of the primary antibody. Known EV-A71 infected mouse and hamster tissues were used as positive controls. A total of 42 infected tissue fragments from prepuce and 40 tissue fragments each for lip skin and oral mucosa were examined. IHC specificity testing was also done on corresponding uninfected cultured tissues as negative controls.

IHC using a mouse monoclonal anti-human cytokeratin AE1/3 (Dako, USA) was also performed to confirm that keratinocyte monolayers grown from human prepuce. Cells were incubated with primary antibody overnight at 4ºC after serial washing with 1 x TBS, followed by secondary antibody-horseradish peroxidase (Dako Real Envision, Denmark) for 30 min at RT. The substrate chromogen 3,3' diaminobenzidine tetrahydrochloride (Dako, Denmark) was then applied, followed by Mayer's hematoxylin counterstaining and mounting. The IHC chromogenic substrate 3,3' diaminobenzidine tetrahydrochloride (brown end product) was used for EV-A71 viral antigens in primary keratinocyte culture.

Because in primary keratinocyte culture, the superficial epidermal layer from which the cells were grown does not have melanocytes, therefore using 3,3' diaminobenzidine tetrahydrochloride will not pose a problem. For negative IHC controls, the primary antibody was replaced by mouse isotype control IgG1 or TBS.

IHC to detect viral antigens in infected primary keratinocytes was done at 3 dpi after serial washing with PBS and fixation in absolute methanol. The IHC procedure was similar to that for organotypic culture tissues except for incubation with secondary antibody-horseradish peroxidase for 30 min at RT (Dako Real Envision, Denmark) and a different substrate chromogen 3,3' diaminobenzidine tetrahydrochloride was applied (Dako, Denmark) before hematoxylin counterstaining and mounting. EV-A71 infected Vero cells were used as positive controls and uninfected primary keratinocytes were used as negative controls.

3.6.8   Double immunofluorescence (IF)

To demonstrate co-localization of EV-A71 antigens in cells with SCARB2, an important viral receptor, double IF was performed on selected organotypic prepuce (n=8) and lip (n=2) skin, and primary keratinocyte cultures (n=4) confirmed earlier by IHC to have viral antigens. Anti-EV-A71 antibody (Light Diagnostics, UK) was applied onto the tissue sections and incubated overnight at 4˚C followed by secondary antibody goat anti-mouse IgG conjugated with enzyme alkaline phosphatase (Santa Cruz Biotechnology, USA) for 30 min at RT in the dark before colour development with Liquid Permanent Red chromogen (Dako, USA). Next, a polyclonal rabbit anti-LIMPII/lgp85 antibody (GeneTex, USA) was applied and incubated overnight at 4˚C followed by goat anti-rabbit IgG conjugated with Alexa Fluor 488 (Life Technologies, USA) for 30 min at RT in the dark. The same anti-

EV-A71 antibody and a polyclonal rabbit anti-LIMPII/lgp85 (SCARB2) antibody (GeneTex, USA) which has been used extensively to detect SCARB2 were applied together onto the primary keratinocytes and incubated overnight at 4˚C followed by goat anti-mouse IgG conjugated with Alexa Fluor 488 (Life Technologies, USA) and goat anti-rabbit IgG conjugated with Alexa Fluor 594 for 30 min at RT in the dark. Tissues/cells were then counterstained with DAPI (4',6-diamidino-2-phenylindole, dihydrocholoride) (Molecular Probes, USA) for 1 minute followed by TBS washes. Slides were viewed with an inverted research microscope ECLIPSE Ti (Nikon, Japan).

Localization of viral antigens specifically within prepuce epidermis (n=8) and primary keratinocytes (n=4) was demonstrated by the same IF procedure using monoclonal mouse anti-human cytokeratin AE1/3 (Dako, USA) instead of anti-LIMPII/lgp85 antibody, and goat anti-mouse IgG conjugated with Alexa Fluor 488 was used. To detect viral antigen co-localization in skin Langerhans cells (n=16), the same IF procedure was followed except that an anti-S100 antibody (Abcam, UK), a well-known and reliable cell marker for Langerhans cells was applied instead of anti-LIMPII/lgp85 antibody, and goat anti-rabbit IgG conjugated with Alexa Fluor 488 was used. EV-A71-infected hamster tissues and Vero cells were used as positive controls, and uninfected keratinocytes as negative controls. Human rhabdomyosarcoma cells were used as positive controls for SCARB2 detection.

3.6.9 ISH to detect viral RNA

A ISH procedure as described in section (3.3.8) was used to detect EV-A71 RNA in infected human skin and/or oral mucosa tissues.

3.6.10 Immunoelectron microscopy

EV-A71 infected human prepuce skin tissues (n=10) were harvested at 2 dpi and fixed in 4% paraformaldehyde at 4˚C overnight. The tissues were then post-fixed in 0.75% glutaraldehyde at 4˚C for 1 hour, and washed with PBS as described previously (Ueno, 2009). After tissue fixation, tissues were dehydrated in graded ethanol (50% and 70%) for 30 min before infiltration with LR white resin (Sigma-Aldrich, USA) according the manufacturer's instructions 1:1 mixture of ethanol:LR white for 1 hour, 2:1 mixture of ethanol:LR white for 1 hour and then 100% LR white for 2 hours. Next, the specimens were infiltrated in fresh 100% LR white overnight, after that, transferred into gelatin capsules filled with fresh LR white and polymerized at 52ºC for 24 hours. Resin blocks were trimmed and ultra-thin sections of 70-100 nm thickness was obtained using an ultramicrotome (Leica, Austria).

The ultra-thin sections were washed in micro-filtered distilled water, serum blocking and applied anti-EV-A71 antibody (Light Diagnostics, UK) at 4˚C overnight followed by secondary antibody conjugated with gold particles (size, 20 nm) (BBinternational, UK) for 2 hours at RT. Ultra-thin sections were post-stained with 1% osmium tetroxide for 20 min at RT, before counterstained with uranyl acetate for 10 min and lead citrate for 5 min followed by several washing with micro-filtered water. Stained immunogold sections were viewed under transmission electron microscopy (Zeiss, Germany). For positive controls, monoclonal mouse anti-human cytokeratin AE1/3 (Dako, USA) was used as primary antibody and uninfected human skin tissues and Vero cells were also served as negative controls.

3.7   Statistics

To determine the significance of differences between mean viral titers, the one-way Anova followed by repeated t-test were performed using the IBM SPSS Statistics software version 23 throughout the project. The results were expressed as mean ± standard deviation. Statistical significance between the percentage of oral wash and fecal viral positivity was determined by the one-way Anova. P values < 0.05 were considered significant.

CHAPTER 4

RESULTS

4. 1   Hamster model

4.1.1   LD$_{50}$ study

Six groups of animals (n=6 per group) were orally infected with serially-diluted viral suspensions ranging from 10^5 to 1 CCID$_{50}$. Overall, hamsters were susceptible to infection, and survival was dose-dependent (Figure 4.1). All animals given doses $\geq 10^2$ CCID$_{50}$ died. The LD$_{50}$ dose calculated using the method of Reed and Muench (Reed & Muench, 1938) was 25 CCID$_{50}$. Animals consistently showed signs of infection such as hunchback posture, ruffled fur, weight loss and limb paralysis before succumbing to infection between 3 to 8 dpi. In the group given the low 10 CCID$_{50}$ dose, about 16.7% (n=1) died by 8 dpi, displaying signs of infection and pathological findings similar to those infected with higher doses (Figure 4.1). The surviving animals in this group did not show any signs of infection, and weight gain was consistent throughout the experiment. All the animals given the lowest 1 CCID$_{50}$ dose appeared healthy except for 1 animal which developed hind limb paralysis at 10 dpi before recovering at 14 dpi.
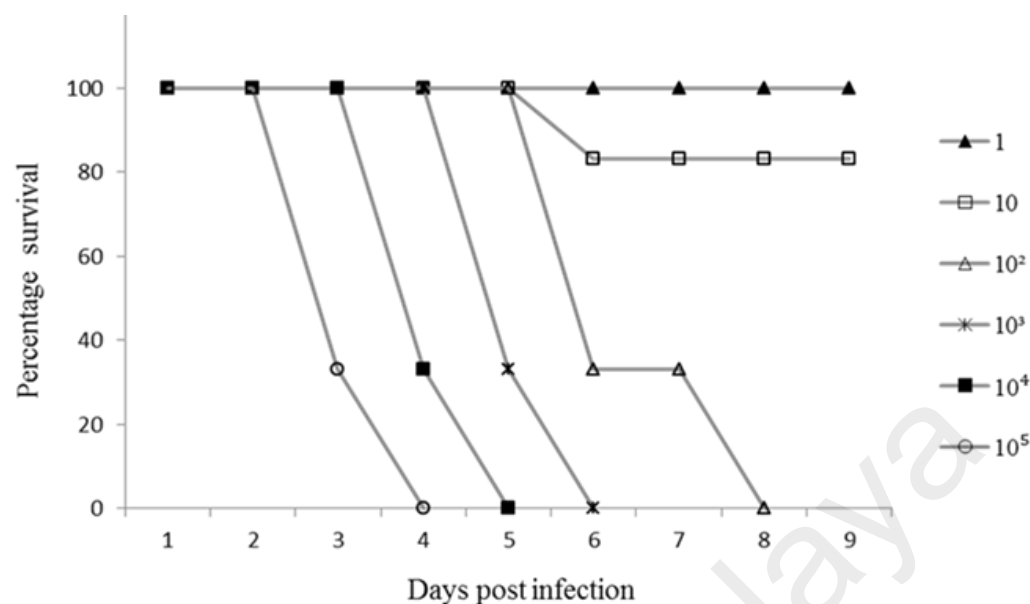
Figure 4.1. LD_{50} study: Survival graph of 2-week-old hamsters orally infected with six different viral doses (1-10^5 $CCID_{50}$). Each group given the same viral dose comprised 6 animals. All animals infected with 1 $CCID_{50}$ dose survived.

4.1.2 Pathological findings in 2-week-old hamster model

Macroscopic skin ulcers/lesions around the nose, lip and paw were visible in some of the infected hamsters given doses $\geq 10^2$ $CCID_{50}$ (Figure 4.2). In all the 21 animals with tissues available for light microscopy, small discrete foci of viral antigens/RNA as shown by strong IHC and ISH positive signals, respectively, were localized to squamous cells in the epithelium covering the lips, tongue and other parts of the oral cavity (Figure 4.3B, C). Similarly, viral antigens/RNA were also found in the epidermis, including hair follicle germinal epithelium, covering the paws (Figure 4.3D, H), limbs, head, neck, upper chest and pelvic areas (Figure 4.3F, G). These lesions generally showed minimal or mild inflammation, and some more superficial epidermal squamous lesions appeared vesicular. Viral antigens/RNA were also detected in esophageal squamous epithelium in 52% (n=9) of animals (Figure 4.4A) but were very focal and less dense than in squamous epithelia elsew-

59
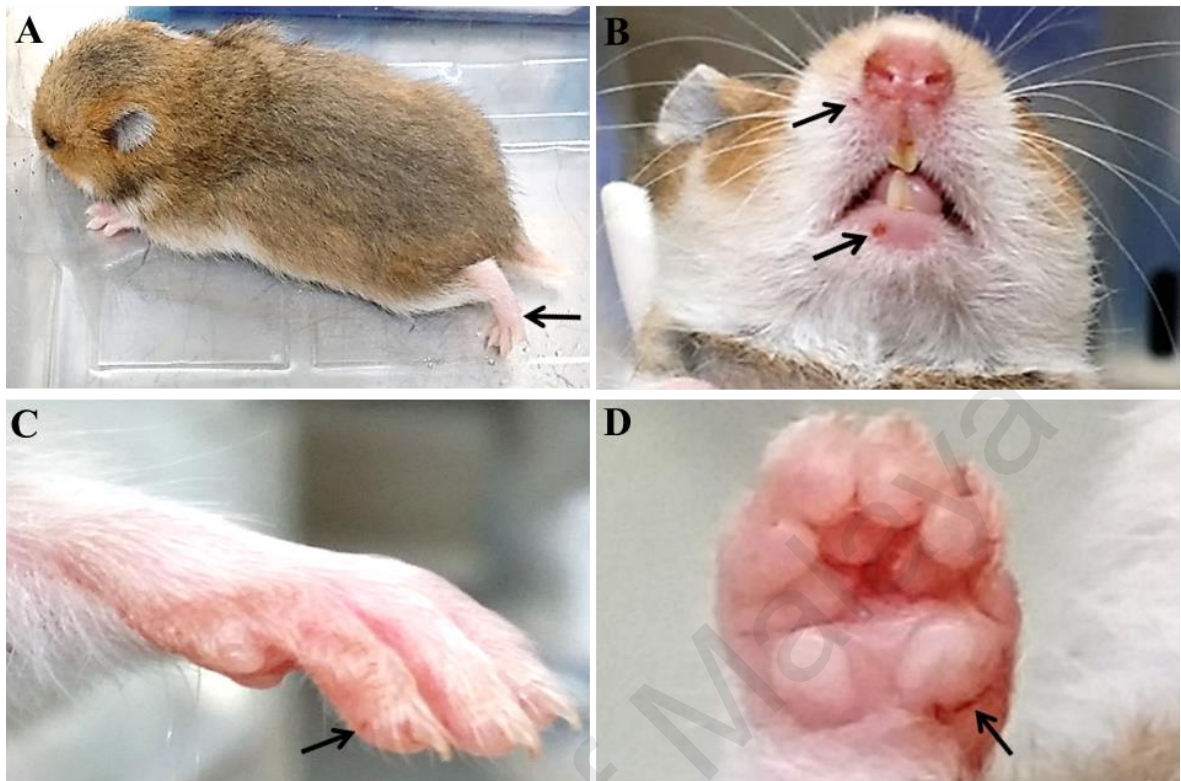
Figure 4.2. Signs of infection and macroscopic lesions in infected hamsters. Severely-infected hamster showing hind limb paralysis (A, arrow) at day 4 post-infection. Lesions on the lip (B, arrows), and paws (C, D, arrows) were observed in some animals.

here. Table 4.1 shows the distribution and relative density of viral antigens in squamous cells from various sites, CNS tissues and skeletal muscle fibres.

In the CNS, although inflammation was minimal or mild, viral antigens/RNA were demonstrated in neuronal bodies and processes in brainstems (62% of animals, n=3), spinal cord anterior horns (90%, n=19) (Table 4.1), and in sensory ganglia (90%, n=19), mainly in dorsal root ganglia, occasionally in trigeminal ganglia (Figure 4.5B-F). Neurons in other parts of the CNS e.g. cerebral and cerebellar cortex, and other cells/tissues such as oligodendrocyte, astrocyte, ependyma, blood vessel, choroid plexus, meninges, peripheral nerve and autonomic ganglion were all IHC and ISH negative.

Focal acinar cells in the parotid salivary gland (71% of animals, n=5) (Figure 4.4C, D) and lacrimal gland (64%, n=14), scattered liver hepatocytes (71%, n=15), (Figure 4.4E, H) and rare stomach epithelial cells (Figure 4.4B) were positive for viral antigens/RNA. Subcapsular sinus macrophages and lymphoid cells in other parts of lymph nodes from the head, neck and other areas were positive for viral antigens only (77% of animals, n=16) (Figure 4.4F), while some lymphoid cells in the spleen were positive for both viral antigens and RNA (62%, n=13) (Figure 4.4G). Viral antigens/RNA were densest in inflamed skeletal muscle fibres (Figure 4.5I, J) found in all the animals (Table 4.1). Conversely, only very rare foci of viral antigens/RNA were found in the smooth muscles of the intestine and stomach (Figure 4.5G), and myocardium (Figure 4.5H), although this was observed in all the animals. There was no myocarditis or pulmonary edema. Lymphoid cells in the thymus, intestinal Peyer's patches and mucosa, pancreas, kidney and lung were all negative for viral antigens/RNA.
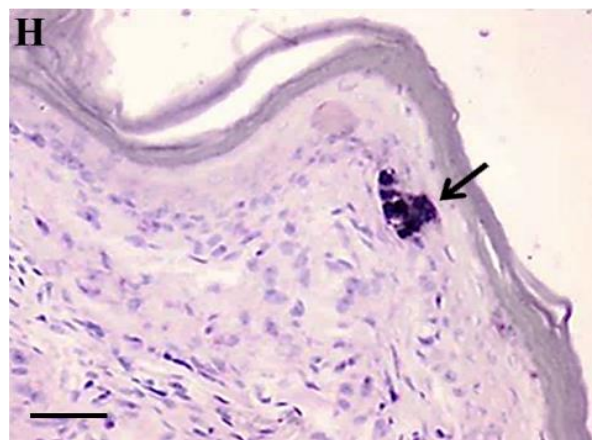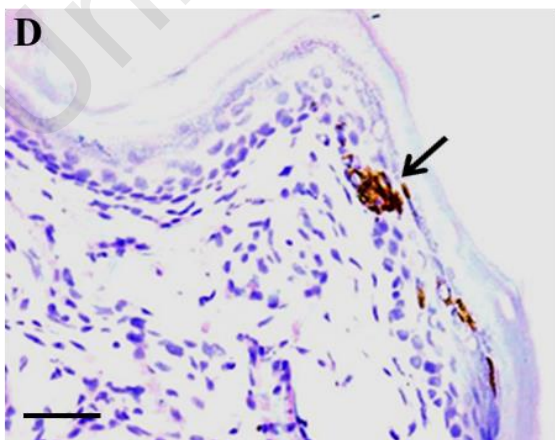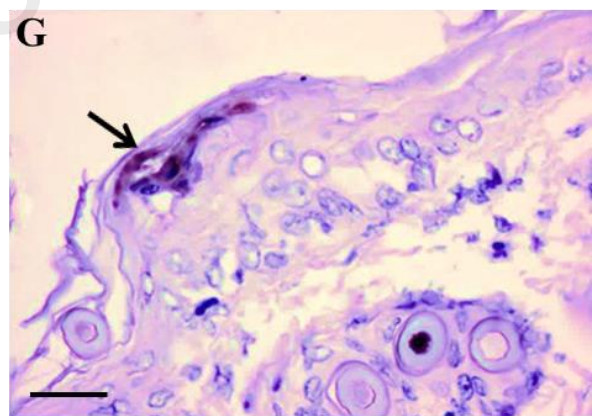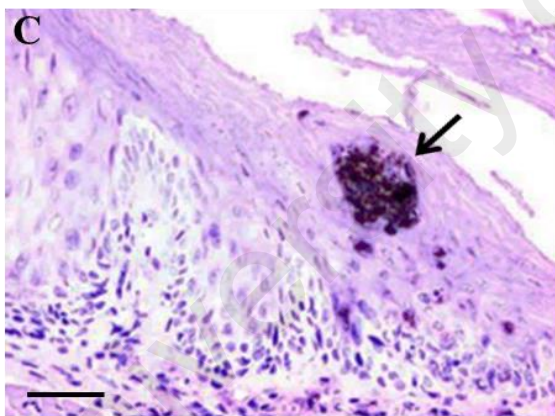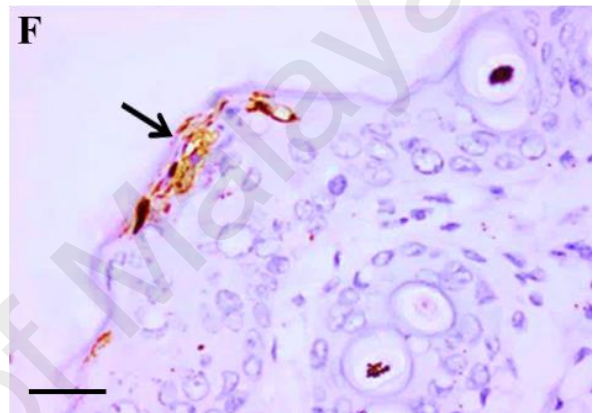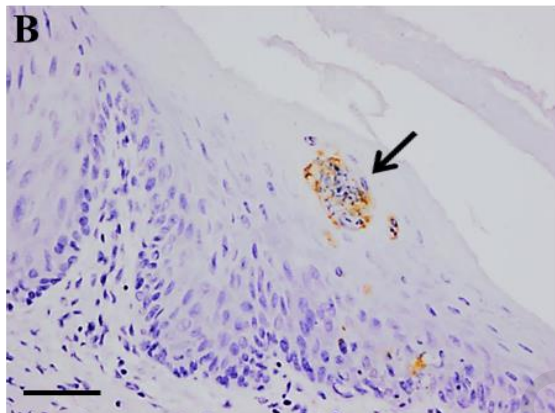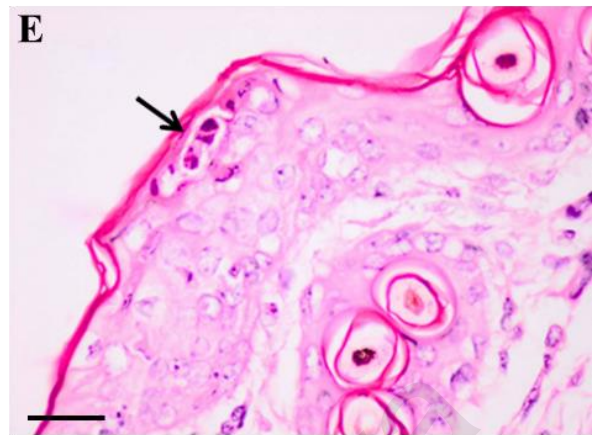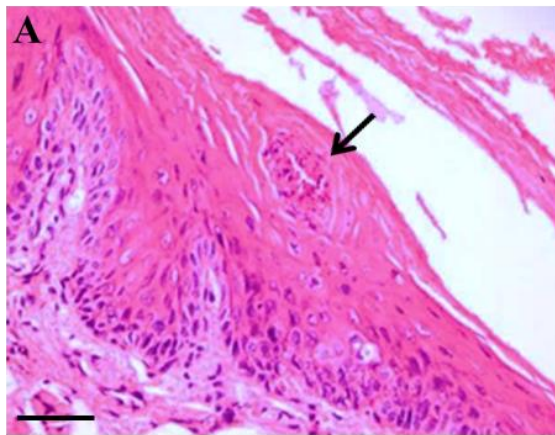
Figure 4.3. Pathological findings in EV-A71 infected hamsters at day 4 post-infection. Focal squamous inflammatory lesions in the oral mucosa (A, arrow) and skin epidermis showing mild inflammation and necrosis (E, arrow). These same lesions also demonstrated viral antigens (B, F, arrows) and RNA (C, G, arrows). Similarly, in the paw epidermis, viral antigens and RNA were localized to infected squamous cells (D, H, arrows). Stains: Hematoxylin and eosin (A, E), immunohistochemistry with 3, 3' diaminobenzidine-tetrahydrochloride chromogen/hematoxylin (B, D, F), and in situ hybridization with nitroblue tetrazolium/5-bromo-4-chloro-3-indolyl phosphate/hematoxylin (C, G, H). Original magnification: 20x objective (A-D, H), 40x objective (E-G). Scale bars: 30µm (A-D, H), 15µm (E-G).
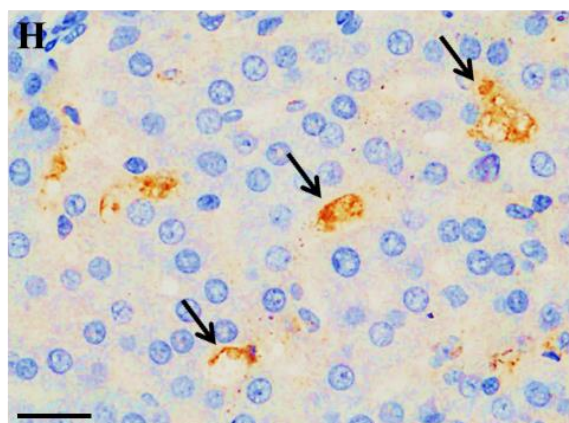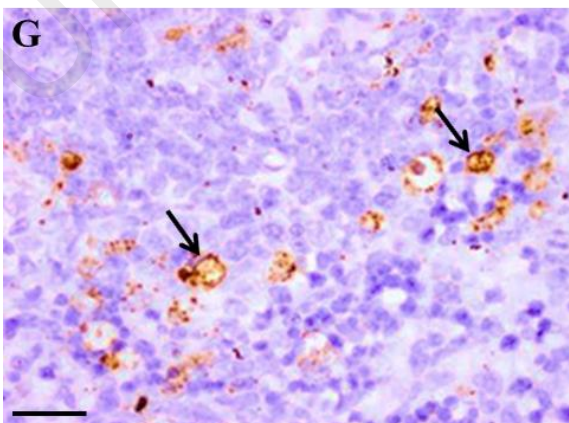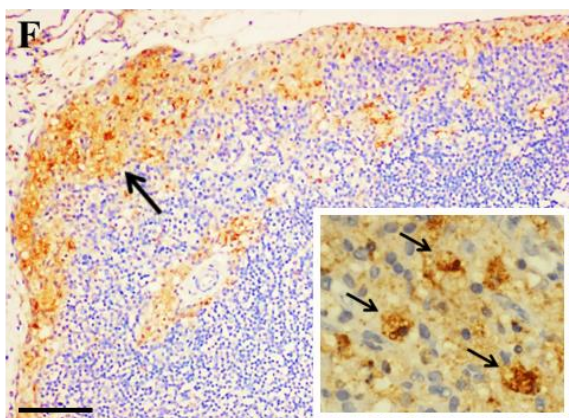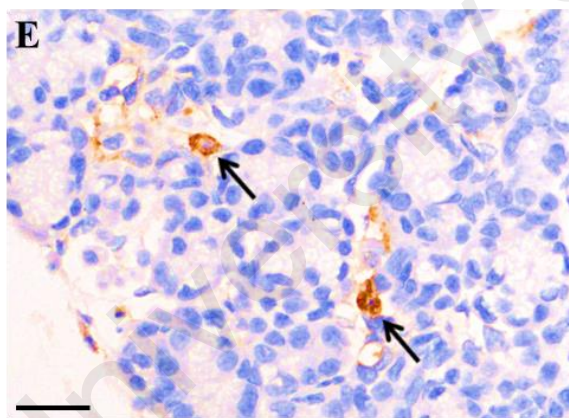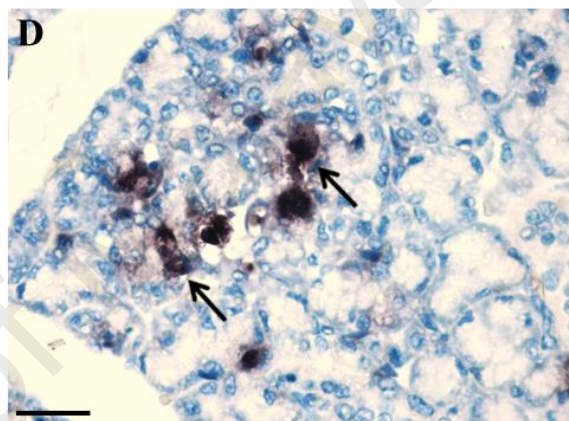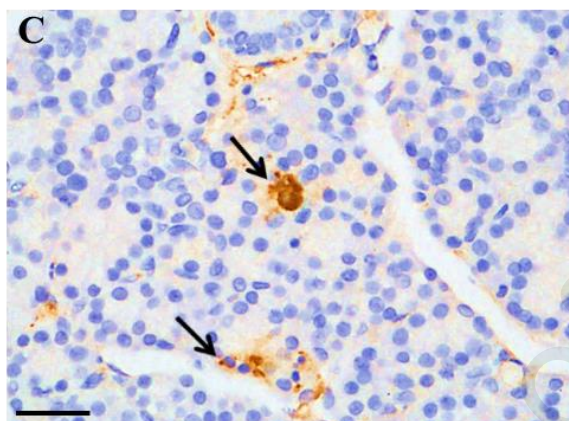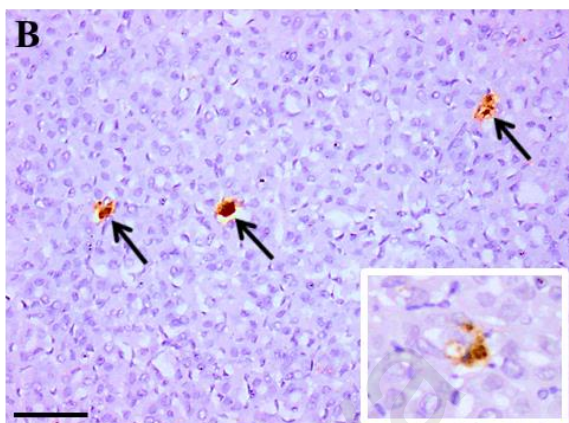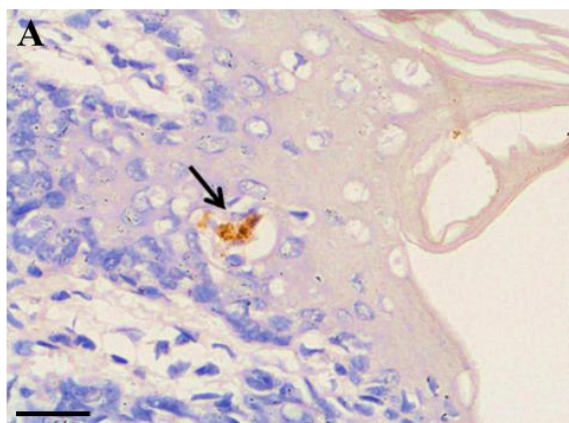
Figure 4.4. Pathological findings in non-CNS tissues from EV-A71 infected hamsters at day 4 post-infection. Viral antigens and/or RNA were detected in the esophageal epithelium (A, arrow), gastric epithelium (B, arrows), salivary gland acinar cells (C, D, arrows), lacrimal gland (E, arrows), lymph node (F and inset, arrows), spleen (G, arrows) and liver hepatocytes (H, arrows). Stains: Immunohistochemistry with 3, 3' diaminobenzidine-tetrahydrochloride chromogen/hematoxylin (A-C, E-H), and in situ hybridization with nitroblue tetrazolium/5-bromo-4-chloro-3-indolyl phosphate/hematoxylin (D). Original magnification: 10x objective (F), 20x objective (B), 40x objective (A, C-E, G, H, B-inset, F-inset). Scale bars: 50µm (F), 30µm (B), 15µm (A, C-E, G, H).
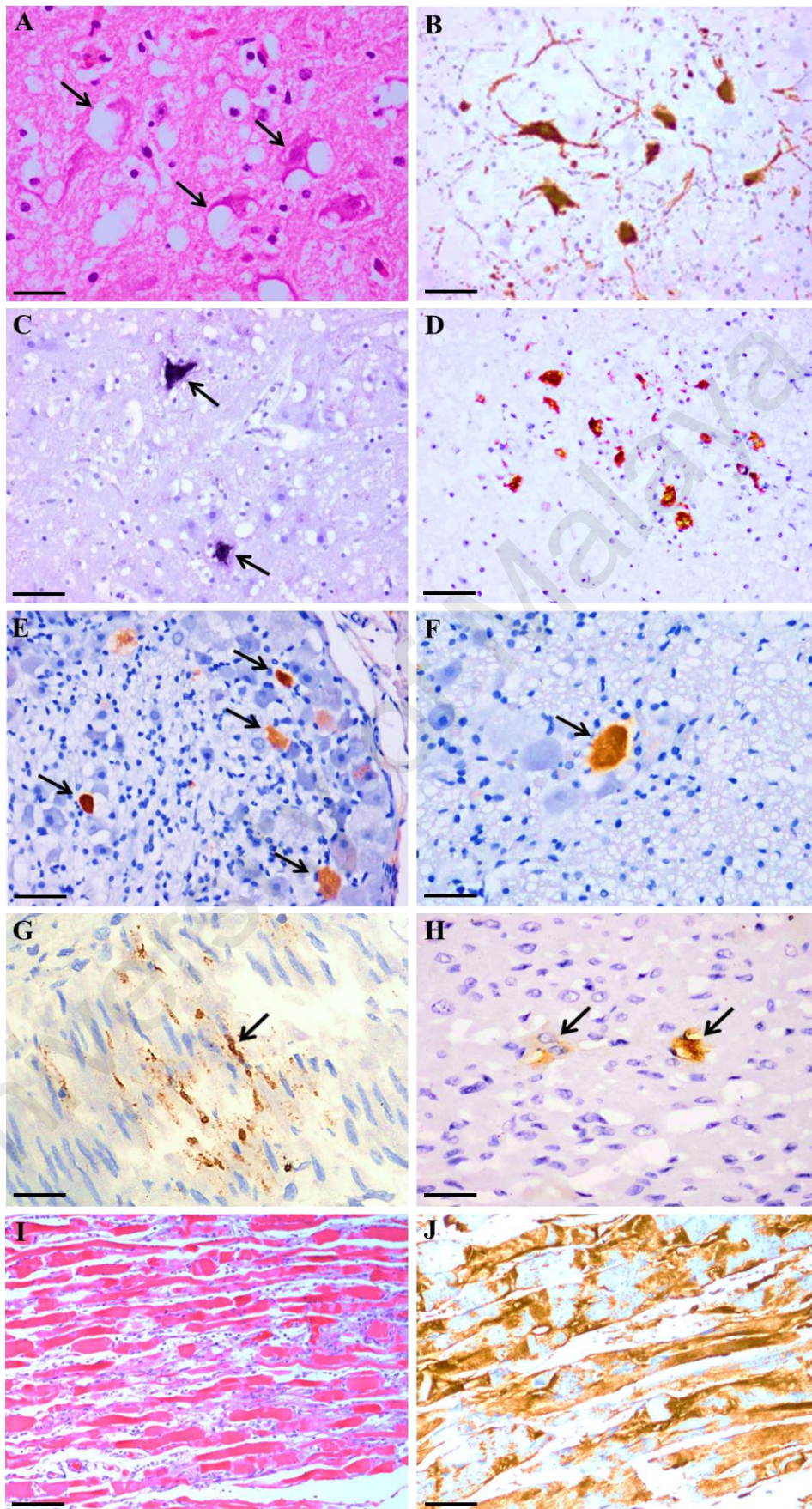
Figure 4.5. Pathological findings in CNS and muscle tissues from EV-A71 infected hamsters at day 4 post-infection. Vacuolation and degeneration in brainstem neurons (A, arrows) that also demonstrated viral antigens (B) and RNA (C, arrows). Viral antigens were also detected in spinal cord anterior horn cells (D), dorsal root ganglia (E, arrows) and trigeminal ganglion (F, arrows). Viral antigens were also localized in smooth muscle of intestines (G, arrow), myocardium (H, arrows), neutrophils infiltration and inflamed skeletal muscle fibres (I) and viral antigens (J). Stains: Hematoxylin and eosin (A, I), immunohistochemistry with 3, 3' diaminobenzidinetetrahydrochloride chromogen/ hematoxylin (B, D-F), and in situ hybridization with nitroblue tetrazolium/5-bromo-4-chloro-3-indolyl phosphate/hematoxylin (C). Original magnification: 20x objective (B-E, I), 40x objective (A, F). Scale bars: 30µm (B-E, I), 15µm (A, F).

Table 4.1 Localization of viral antigens in various tissues in animals (n=21) orally-infected with various *$CCID_{50}$ doses.

Dose/ Animal#	Oral** mucosa	Tongue mucosa	Esophageal mucosa	Skin epidermis	Paw epidermis	Brain stem	Spinal cord	Skeletal muscle***
10^5 $CCID_{50}$								
Animal 1	+	+	-	+	+	++	++	+++
Animal 2	+	+	-	+	+	-	++	+++
Animal 3	+	+	-	+	+	-	-	+++
Animal 4	+	+	+	+	+	-	-	+++
Animal 5	+	+	-	+	+	-	++	+++
Animal 6	+	+	+	+	+	++	++	+++
Animal 7	+	+	+	+	+	++	++	+++
Animal 8	+	+	-	+	-	++	++	+++
10^4 $CCID_{50}$								
Animal 1	+	+	-	+	+	-	++	+++
Animal 2	+	+	+	+	+	++	++	+++
Animal 3	+	+	+	+	+	++	++	+++
Animal 4	+	+	+	+	+	++	++	+++
Animal 5	+	+	+	+	+	-	++	+++
Animal 6	+	+	-	+	+	++	++	+++
10^3 $CCID_{50}$								
Animal 1	+	+	+	+	+	++	++	+++
Animal 2	+	+	NA	+	+	-	++	+++
Animal 3	+	+	-	+	+	++	++	+++
Animal 4	+	+	+	+	+	-	++	+++

Dose/ Animal#	Oral** mucosa	Tongue mucosa	Esophageal mucosa	Skin epidermis	Paw epidermis	Brain stem	Spinal cord	Skeletal muscle***
10^2 CCID$_{50}$								
Animal 1	+	+	NA	+	+	++	++	+++
Animal 2	+	+	-	+	+	++	++	+++
10 CCID$_{50}$								
Animal 1	+	+	NA	+	+	++	++	+++

*CCID$_{50}$ = 50% cell culture infectious dose.

**Oral mucosa includes lip, buccal mucosa and mucosa from other parts of oral cavity except the tongue.

***Since, skeletal muscle fibres invariably showed the highest density of viral antigens, the highest semi-quantitative score of +++ was assigned to skeletal muscle.

+++ = >50% area positive

++ = 10-50%

+ = <10%

NA = not available

10^5 CCID$_{50}$ dose = animals sacrificed at 3-4 dpi

10^4 CCID$_{50}$ dose = animals sacrificed at 4-5 dpi

10^3 CCID$_{50}$ dose = animals sacrificed at 5-6 dpi

10^2 CCID$_{50}$ dose = animals sacrificed at 6-8 dpi

10 CCID$_{50}$ dose = animal sacrificed at 6 dpi

4.1.3 Virus titration

Figure 4.6 shows virus titration in the sera, solid organs, oral washes and feces in the 4 animals from animals infected with the 10^4 CCID$_{50}$ dose. The highest titers were obtained in the serum, hind limb muscles and the CNS. From 4 dpi onwards, virus could be isolated from oral washes and feces, with virus titers of 10^3 CCID$_{50}$/ml and 10^2 CCID$_{50}$/ml, respectively.
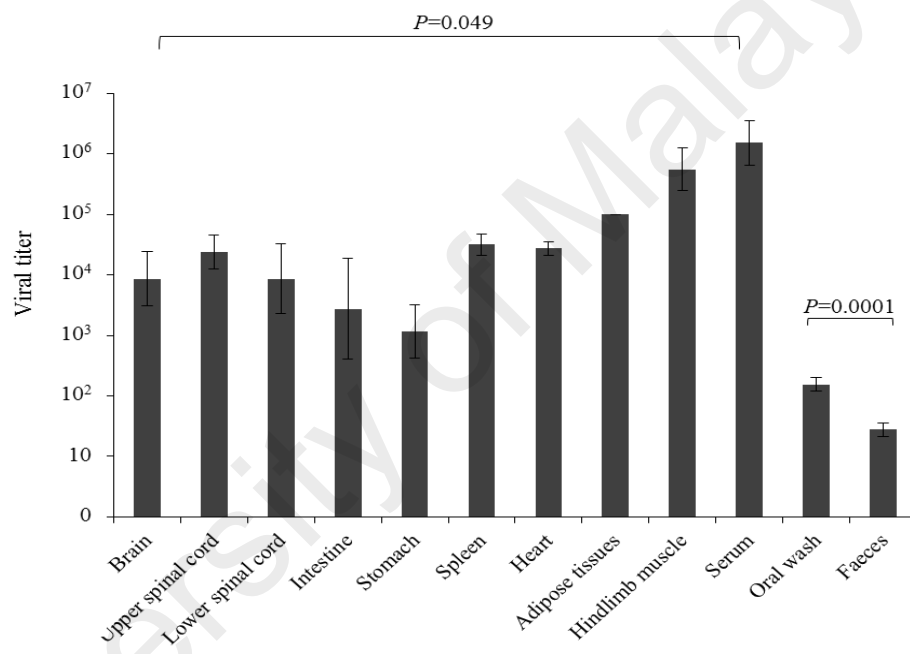
Figure 4.6. Viral titers in harvested tissues from EV-A71 infected hamsters infected with the 10^4 CCID$_{50}$ dose. Virus titer is expressed as the mean $\log_{10}$ CCID$_{50}$ ± standard error of mean per 10% (wt/vol) tissue homogenates derived from 4 hamsters at day 4 post-infection. The highest titters were obtained from serum and hind limb muscle and the overall viral titers between tissues (brain, upper spinal cord, lower spinal cord, intestine, stomach, spleen, heart, adipose tissues, hindlimb muscle and serum) were also statistically significant (P=0.049) by the one-way Anova. Oral wash viral titer was significantly higher than feces (P= 0.0001).

4.1.4 Amino acid sequences of SCARB2 receptors

Amino acid sequences of SCARB2 receptors in human (*Homo sapiens*; accession no. KR709707), golden hamster (*Mesocricetus auratus*; accession no. NM_001281557), and mouse (*Mus musculus*; accession no. NM_007644) downloaded from Genbank and aligned using MEGA 6.06 software were shown in Figure 4.7. The amino acid sequences conserved regions between all three sequences is about 82% and between hamster and mouse is about 90%.

```
Human          1 M G R C C F Y T A G T L S L L L L V T S V T L L V A R V F Q K A V D Q S I E K K I V L R N G T E A F D S W E K P P L P V Y T Q F Y F F N V T N P E E I L R G E T  80
Golden hamster . . . . . . . . . . . . . . A . . . . . . . . . T . . N M . . . . . . . V . . . . . . . . . . . . . . . . . . . . . . . . . . . . . Q . . I
Mouse          . . . . . . . . . . . . . . . . . . . T . . N M . . Q . . . K V . N . . . . . . . . . I . . . . . . . . . . . . . . . . . . Q . . I

Human         81 P R V E E V G P Y T Y R E L R N K A N I Q F G D N G T T I S A V S N K A Y V F E R D Q S V G D P K I D L I R T L N I P V L T V I E W S Q V H F L R E I I E A M L  160
Golden hamster . I L Q . . . . . . . . . . . . . . . . . E . . . . . . . . N . . . . . S N V . . . I . . L . . . V . L A . M P L . K . . . . . .
Mouse          . L L . . . . . . . . . . . . . . . . . . E . . . . . T . . . . . N . . . . . N V . . . I . . L . . . V D L A . L T L . . . L . . . .

Human        161 K A Y Q Q K L F V T H T V D E L L W G Y K D E I L S L I H V F R P D I S P Y F G L F Y E K N G T N D G D Y V F L T G E D S Y L N F T K I V E W N G K T S L D W W  240
Golden hamster . T . . . . . . . . . . H . . . . . . . . . V . I . K . . . . N . . . . . . . . . . . . . . . . N . . . . . . . . . . . . . . . . .
Mouse          . . . . . . . . I . . H . . . . . . . . . V . I . K . V . N . . . . R . . . E . . . . . . . . . . N . . . S . . . . . . . . . . . . .

Human        241 I T D K C N M I N G T D G D S F H P L I T K D E V L Y V F P S D F C R S V Y I T F S D Y E S V Q G L P A F R Y K V P A E I L A N T S D N A G F C I P E G N C L G  320
Golden hamster T . . E . . . . . . . . . . . . . . . . . . . . . . . . . . H . . . . G F . T . E . . . . . . . . . . . . . E . . . . . . . . M D
Mouse          T . . T . . . . . . . . . . . S . . . . . . L . . . L . . . H . . . . S F . N . E . . . . . . . . . . . . . E . . . . . . . . M D

Human        321 S G V L N V S I C K N G A P I I M S F P H F Y Q A D E R F V S A I E G M H P N Q E D N E T F V D I N P L T G I I L K A A K R F Q I N I Y V K K L D D F V E T G D  400
Golden hamster . . . . . . V . . V . . . . . . . . . . . K . . . K . R . K . H . S . . . . . . . . R . . . . . . . . . T . . . I . G I . . . . N
Mouse          . . . . I . . . . . . . . . . . . . . K . . . K . . . . . K . E H . S . . . . . . . . R G . . . . . . . T . . R . . . . . . . . . .

Human        401 I R T M V F P V M Y L N E S V H I D K E T A S R L K S M I N T T L I I T N I P Y I I M A L G V F F G L V F T W L A C K G Q G S M D E G T A D E R A P L I R T  478
Golden hamster . . . . . . . . . . L . . . . . . . V T S . . . . V . . . . . . . . . . . . . . . L . . . . . . . . R . . . P . . . . . . . . . . .
Mouse          . . . . . . . . . . L . . . . N Q . . . V . . . . V V . . . . . . . . . . . . . . . . . . . . . . R . . . . . . . . . . . . . . . . .
```

Figure 4.7. Amino acid sequence alignment of SCARB2 receptors in human, golden hamster and mouse shown in FASTA format. Overall amino acid alignment between 3 different species showed 82% similarity. Differences in amino acid sequence alignment between the species were shown in single-letter codes.

4.2   Viral spread in the hamster model

4.2.1   Susceptibility and sacrifice of infected hamsters at different time points

Groups of orally-infected animals (n=8 per group) each given 10^5 $CCID_{50}$ viral dose were sacrificed at various time points (1-4 dpi). At 1 dpi, animals were healthy and no signs of infection such as hunched back, ruffled fur, weight loss and limb paralysis were observed. A 2nd group of animals at 2 dpi also appeared healthy. At 3 dpi, the 3rd group of animals had severe hind limb paralysis and all the signs of infection. At 4 dpi, the 4th group animals also developed severe infection and some of them were moribund at sacrifice. All animals were sacrificed at their respective time points and entire carcasses (n=5 each group) were submitted for histological analysis as before (See section 3.3.4).

4.2.2   Viral distribution in EV-A71 infected hamster tissues

Tissues from all 4 animal groups were examined by light microscopy, IHC and ISH. No viral antigens/RNA were detected in all tissues submitted for both IHC and ISH from animals sacrificed at 1 dpi. Table 4.2 summarizes the IHC findings from animals tissues sacrificed at 2, 3 and 4 dpi. Despite showing no overt signs of infection, focal viral antigens were detected in animals sacrificed at 2 dpi including in squamous cells lining oral cavity (100%, n=5), tongue (80%, n=4), paws (40%, n=2), and skin (100%, n=5), and gastric epithelium (60%, n=3) (Figure 4.8A-D). Focal viral antigens in other non-CNS tissues were also detected, including salivary gland acinar cells (75%, n=3), cardiac (40%, n=2), smooth (20%, n=1) and skeletal muscles (100%, n=5) (Figure 4.9D). In the CNS, inflammation was very minimal or mild, and focal viral antigens were demonstrated in neurons in the motor cortex and medulla/pons regions (40% of animals, n=2) (Figure 4.10, Hamsters 4 and 5), and in sensory ganglia (dorsal root ganglia) in the same animals (40%, n=2),

Table 4.2 IHC findings in kinetics study of EV-A71 infected hamsters at 2, 3 and 4 dpi (n=5 each).

Time point/ Animal#	Oral mucosa	Tongue mucosa	Skin epidermis	Paw epidermis	Salivary gland	Stomach mucosa	Brain stem	Spinal cord	Dorsal root ganglion	Lymph node	Cardiac muscle	Smooth muscle	Hind limb muscle
2 dpi													
Animal 1	+	+	+	+	+	+	-	-	-	-	-		+
Animal 2	+	+	+	-	NA	-	-	-	-	-	+	-	++
Animal 3	+	-	+	-	+	+	-	-	-	+	-	-	+
Animal 4	+	+	+	+	+	+	+	-	+	+	-	-	+
Animal 5	+	+	+	-	-	-	++	-	+	+	+	+	++
Overall %	100%	80%	100%	40%	75%	60%	40%	0%	40%	60%	40%	20%	100%
3 dpi													
Animal 6	++	+	+	+	++	+	-	+	++	+	+	+	+++
Animal 7	++	++	+	++	++	+	++	++	+	NA	+	+	+++
Animal 8	+	+	+	++	+	+	++	++	++	+	+	+	+++
Animal 9	++	++	+	+	+	+	+	++	++	+	+	+	+++
Animal 10	++	++	+	+	++	+	++	+	+	NA	+	+	+++
Overall %	100%	100%	100%	100%	100%	100%	80%	100%	100%	100%	100%	100%	100%

Time point/ Animal#	Oral mucosa	Tongue mucosa	Skin epidermis	Paw epidermis	Salivary gland	Stomach mucosa	Brain stem	Spinal cord	Dorsal root ganglion	Lymph node	Cardiac muscle	Smooth muscle	Hind limb muscle
4 dpi													
Animal 11	++	+	+	+	+	+	+	++	++	+	+	+	+++
Animal 12	++	++	+	+	+	+	+	-	++	NA	+	+	+++
Animal 13	++	++	+	+	+	+	+	+	++	+	+	+	+++
Animal 14	+	++	+	NA	+	+	+	+	+	+	+	+	+++
Animal 15	++	+	+	-	+	+	-	++	++	+	+	+	+++
Overall %	100%	100%	100%	75%	100%	100%	80%	80%	100%	100%	100%	100%	100%

NA= not available

+++ = >50% area positive

++ = 10-50%

+ = <10%

(Figures 4.8A, C and Figure 4.10, Hamsters 4 and 5). No viral antigens were detected in anterior horn cells of spinal cords in all the animals (Figure 4.9B and Figure 4.10, Hamsters 1-5). Lymphoid cells in various parts of lymph nodes were also focally IHC positive (60% of animals, n=3) (Table 4.2).

At 3 dpi, vacuolated cytoplasm in some superficial epithelial squamous lesions in the mouth and skin appeared vesicular but minimal or only mild inflammation was observed (Figure 4.8E-H). More intense viral antigens were detected in tissues, with varying amounts of antigens/RNA in all major target organs. IHC findings in squamous cells lining oral cavity, tongue, paws, skin and gastric epithelium (Figure 4.8E-H) were similar to earlier findings (See section 4.12). Other non-CNS tissues such as salivary gland acinar cells, cardiac, smooth and skeletal muscles were also found to be IHC positive (Table 4.2). Positive skeletal muscle fibres were found to be strikingly extensive and dense (Figure 4.9H). In the CNS, viral antigens were detected mainly in the medulla, pons, and motor cortex, either unilaterally or bilaterally (Figures 4.9E and 4.10 Hamsters 7-10). In the spinal cord, viral antigens were found mainly in the cervical and thoracic anterior horn areas (Figure 4.9F and Figure 4.10, Hamsters 6-10). Viral antigens in sensory ganglia mainly in dorsal root ganglia (Figure 4.9G and Figure 4.10, Hamsters 6-10), and occasionally in trigeminal ganglion (Figure 4.10, Hamsters 6-8) were also detected. Neurons in other parts of the CNS, blood vessels, choroid plexus, meninges, peripheral nerves and autonomic ganglia were all negative. Viral antigens were also detected in lymphoid cells in various parts of lymph nodes (100%) (Table 4.2 and Figure 4.10, Hamsters 6, 8, 9).

Viral antigens detected in tissues harvested at 4 dpi were similar to findings at 3 dpi with detectable viral antigens in all major target organs. Viral antigens in neurons were

detected mainly in the medulla/pons, motor cortex (Figure 4.10, Hamsters 11-14), and cervical/thoracic cord anterior horn cells (Figure 4.9J and Figure 4.10, Hamsters 11-15) similar to 3 dpi animals. Viral antigens were detected in dorsal root ganglia (Figure 4.9G and Figure 4.10, Hamsters 11-15), and trigeminal ganglia (Figure 4.10, Hamsters 11 and 12). Consistent infection of anterior horn cells and sensory ganglia in 3 and 4 dpi animals were observed. Lymphoid cells in the thymus, intestinal Peyer's patches, intestinal mucosa, pancreas, kidney and lung were all negative for viral antigens/RNA in all infected animals at all time points.
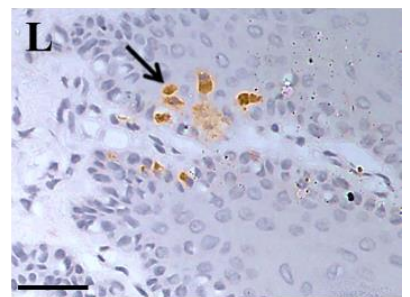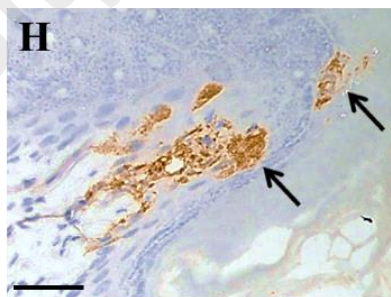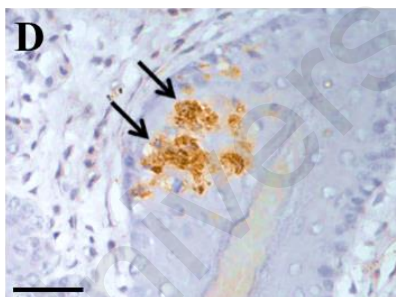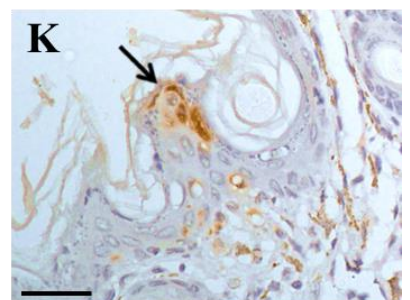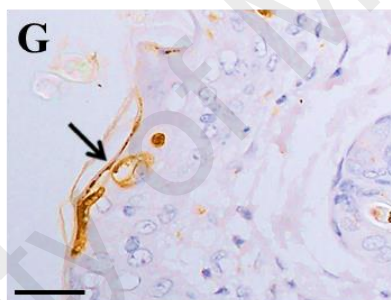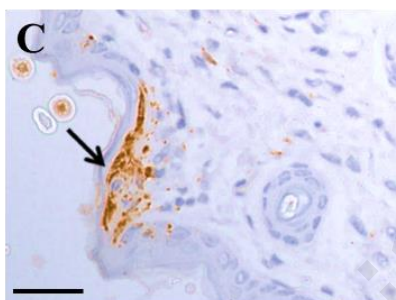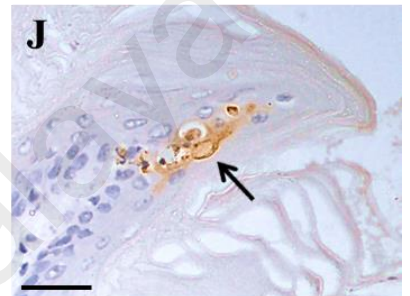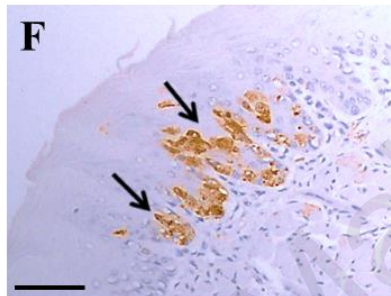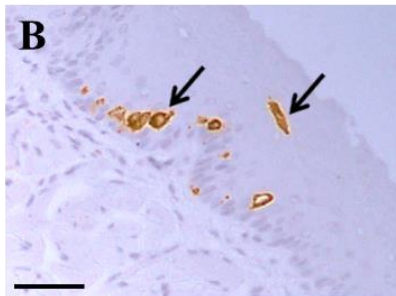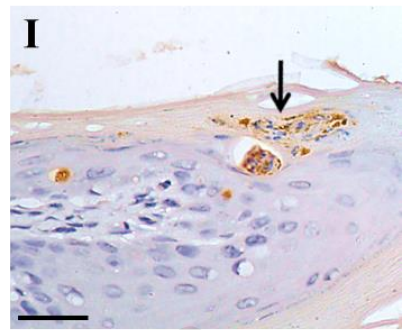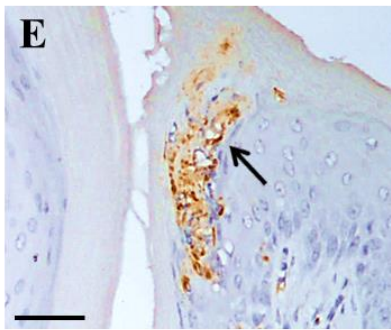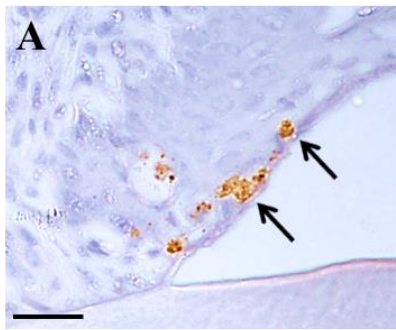
Figure 4.8. Pathological findings in EV-A71 infected hamsters at days 2, 3 and 4 post-infection. Viral antigens were localized in squamous inflammatory lesions in the oral mucosa (A, E, I, arrows) and tongue (B, F, J, arrows). Similarly, lesions in the skin epidermis (C, G, K, arrows) paw epidermis (D, H, L, arrows) also demonstrated viral antigens. Stains: Immunohistochemistry with 3, 3' diaminobenzidinetetrahydrochloride chromogen/hematoxylin. Original magnification: 20x objective (B, F), 40x objective (A, C-E, G-L). Scale bars: 30µm (B, F), 15µm (A, C-E, G-L).
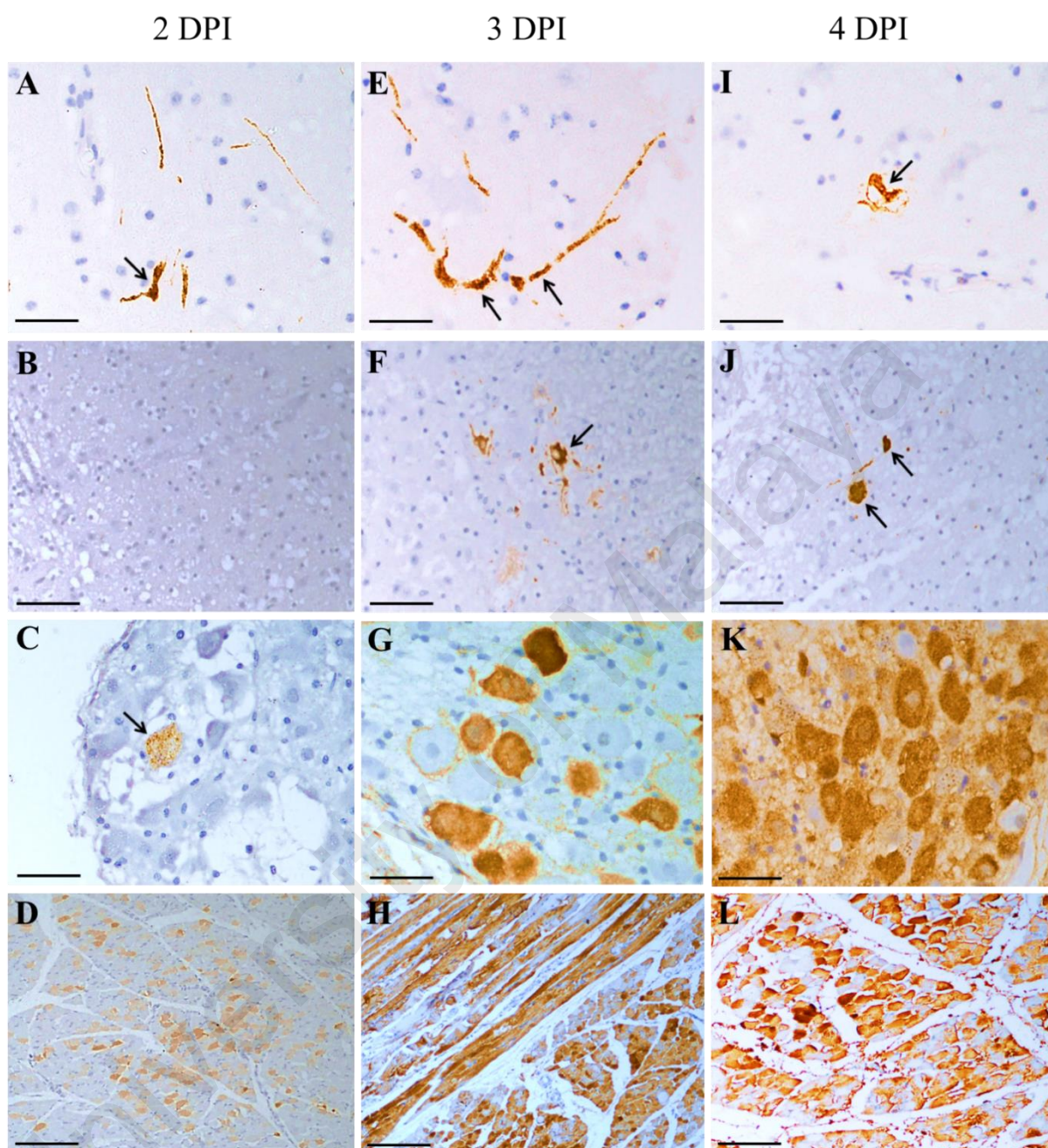
Figure 4.9. Pathological findings in CNS and non-CNS tissues of EV-A71 infected hamsters at days 2, 3 and 4 post-infection. Degenerated brainstem neurons demonstrated viral antigens (A, E, I, arrows). Viral antigens were also localized in spinal cord anterior horn cells (F, J, arrows), dorsal root ganglia (C, arrow, G, K) and hind limb skeletal muscles (D, H, L). Viral antigens were not detected in all levels of spinal cord in day 2 post-infected animals (B). Stains: Immunohistochemistry with 3, 3' diaminobenzidine-tetrahydrochloride chromogen/hematoxylin. Original magnification: 10x objective (D, H, L), 20x objective (B, F, J), 40x objective (A, C, E, I, G, K). Scale bars: 50µm (D, H, L), 30µm (B, F, J), 15µm (A, C, E, I, G, K).

Cerebral cortex													
Diencephalon/cortex													
Midbrain/cortex													
Rostral pons/ cerebellum													
Caudal pons/ medulla/cerebellum													
Cervical													
Thoracic													
Lumbar spinal cord													

| Hamster | 1-3 | 4 | 5 | 6 | 7 | 8 | 9 | 10 | 11 | 12 | 13 | 14 | 15 |

| Days
post-infection | 2 dpi | | | 3 dpi | | | | | 4 dpi | | | |
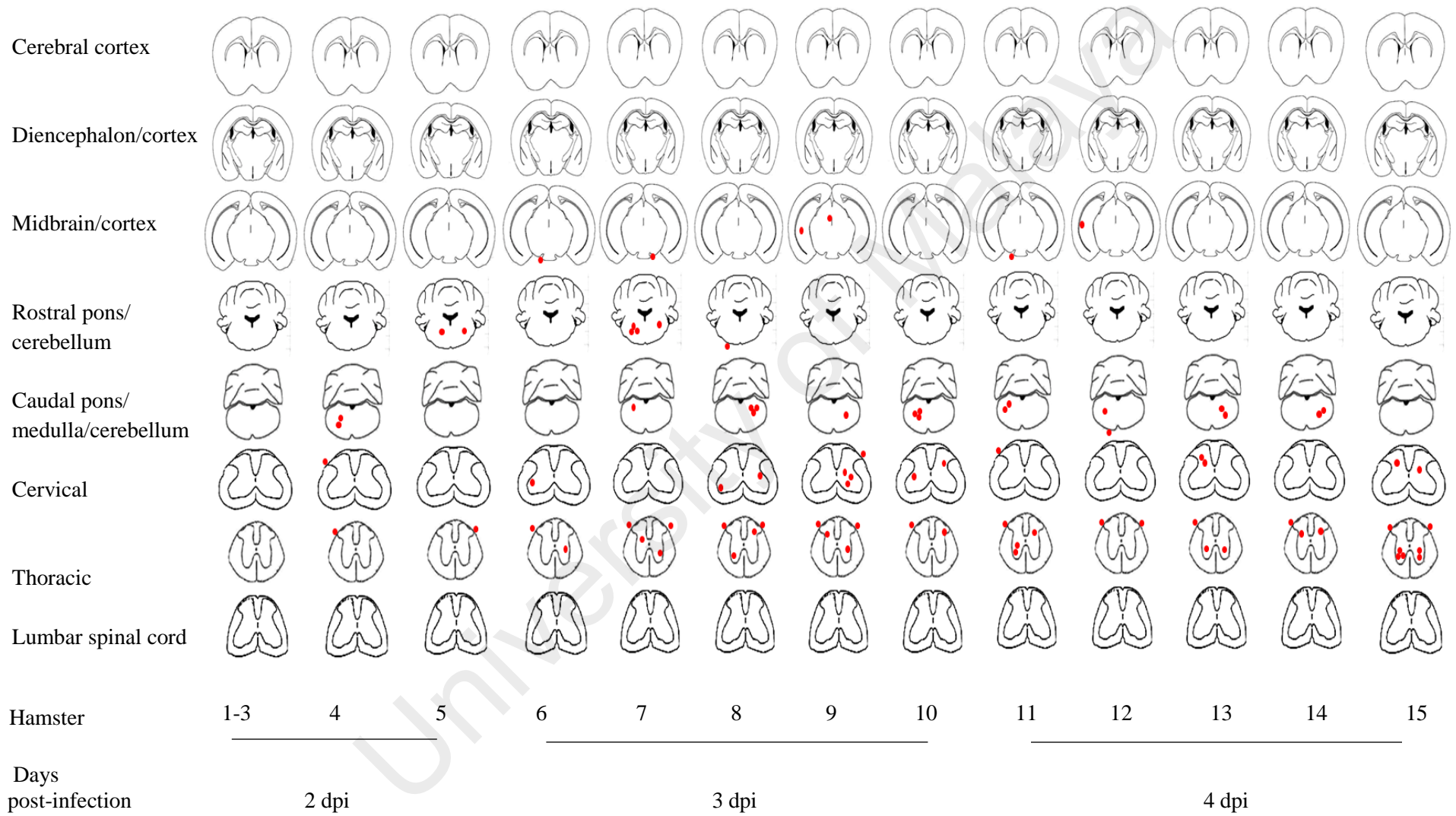
Figure 4.10. Topographic distribution of viral antigens in the CNS of animals (n=5 each group) sacrificed at 2, 3 and 4 days post-infection (dpi), respectively. Cross sections (from top to bottom) of the cerebral cortex, diencephalon/cortex, midbrain/cortex, rostral pons/cerebellum, caudal pons/medulla/cerebellum, medulla/cerebellum, cervical, thoracic, and lumbar spinal cords. Each red dot represents 2 positive neurons.

4.2.3 Virus titration

Viral cultures from animals sacrificed at 1 dpi including, brain, spinal cord, skeletal muscle, serum, oral wash and feces were all negative. As expected, the lowest viral titers from CNS, skeletal muscle and serum were obtained at 2 dpi (Figure 4.11) (P=0.0001). The highest viral titers from all tissues were determined at 3 dpi (Figure 4.11) (P=0.001). Viral titers from oral wash and feces at 2 dpi was not determined since majority of the samples were culture negative. Viral titers from oral washes and feces at 3 dpi was determined at 1×10^3 $CCID_{50}$/ml and 5×10^2 $CCID_{50}$/ml, and 4 dpi at 3×10^2 $CCID_{50}$/ml and 4×10^2 $CCID_{50}$/ml, respectively. Viral titers from oral washes at 3 dpi showed significantly higher than 4 dpi (P=0.002), however, the titers from feces at 3 and 4 dpi did not show significant (P=0.15) (Figure 4.12).
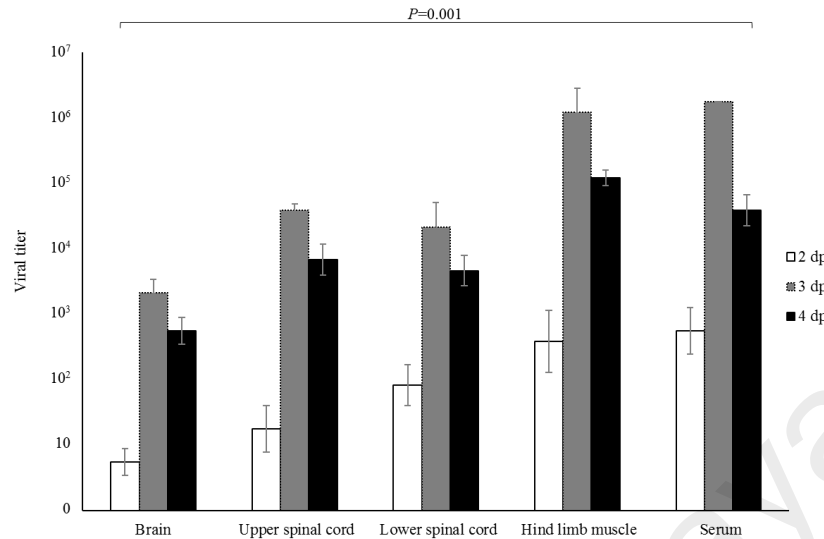
Figure 4.11. Viral titers in harvested tissues from EV-A71 infected hamsters. Virus titer is expressed as the mean $CCID_{50}$/ml $\pm$ standard error of mean per 10% (wt/vol) tissue homogenates derived from 3 hamsters at 2, 3 and 4 days post-infection. The highest titters were obtained from serum and hind limb muscle at all time points. Titers from all time points were statistically significant (P=0.001).
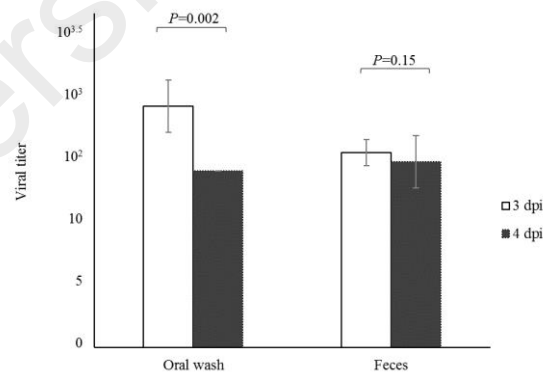
Figure 4.12. Viral titers of oral washes and feces from EV-A71 infected hamsters at 3 days post-infection (dpi) and 4 dpi (n=8 each). Viral titer is expressed as the mean $CCID_{50}$/ml $\pm$ standard error of mean per 10% (wt/vol) suspension. Oral titers at 3 dpi (P=0.002) was significantly higher than 4 dpi.

4.3 Hamster model for person-to-person transmission

4.3.1 Transmission experiment 1

Index animals orally-infected with 10^4 CCID$_{50}$ viral dose in experiment 1 showed typical signs of disease such as hunched back, ruffled fur, weight loss, and hind-limb paralysis at 4 dpi, and were sacrificed at 4-5 dpi (Table 4.3). All contact animals (littermates) showed signs of infection similar to index animals at 6-7 days post-exposure (2-3 days later than index animals), and were sacrificed at 7-8 days post-exposure.

Virus was isolated from oral washes in 9 index animals at 3-4 dpi (Table 4.3), 2 animals (B1, B2) at 1 dpi, and 1 animal at 5 dpi (D2). Virus isolation in feces was positive in the majority of 6 index animals (A3, B2, C1, C2, C3, D3) at 4 dpi, with a range of 3-5 dpi for all animals. Oral wash positivity was most commonly obtained before fecal positivity in 7 animals (ranging from 1-3 days before), followed by oral and fecal positivity on the same day in 4 animals (B3, C1, C2, D2), and fecal before oral positivity in 1 animal (A2).

Virus in oral washes were detected in 8 contact animals at 3-4 days post-exposure, followed by 4 animals (Table 4.3: A4, A5, A6, D4) in which positivity was obtained from 5-8 days post-exposure. Virus in feces was detected in the majority of 5 contact animals (A6, C4, C6, D4, D5) at 5 days post-exposure (range of 4-8 days for all animals). Similar to index animals, oral positivity in contact animals was most commonly obtained before fecal positivity in the majority of 7 animals (range 1-3 days before), followed by oral and fecal positivity on the same day in 4 animals (A6, B4, C4, D5), and fecal before oral positivity in 1 animal (D4). If only positive cultures in oral wash and feces were counted, oral wash positivity constituted 62% of the total, which was significantly higher than fecal positivity (P=0.003).

Table 4.3. Virus isolation from oral washes and feces in 4 groups of index and littermate contact hamsters (Experiment 1).

Legend:
- ■ Virus detected in oral wash[b]
- □ Virus detected in feces
- (gray) No virus detected

Group	Role		Sample	0	1	2	3	4	5	6	7	8
Group 1	**Index**	A1	Oral wash					*	X			
			Feces					*	X			
		A2	Oral wash					*	X			
			Feces				□	*	X			
		A3	Oral wash				*	X				
			Feces				*	X				
	Contact	A4	Oral wash						■	■	*	X
			Feces								*	X
		A5	Oral wash						■	■	*	X
			Feces								*	X
		A6	Oral wash						■	■	*	X
			Feces						□		*	X
Group 2	**Index**	B1	Oral wash	■	■		*	X				
			Feces				*	X				
		B2	Oral wash	■	■		*	X				
			Feces				*	X				
		B3	Oral wash				*	X				
			Feces				*	X				
	Contact	B4	Oral wash					■		*	X	
			Feces					□	□	*	X	
		B5	Oral wash				■	■	■	*	X	
			Feces					□		*	X	
		B6	Oral wash				■	■		*	X	
			Feces					□		*	X	
Group 3	**Index**	C1	Oral wash					*	X			
			Feces					*	X			
		C2	Oral wash					*	X			
			Feces					*	X			
		C3	Oral wash				*	X				
			Feces				*	X				
	Contact	C4	Oral wash						■	■	*	X
			Feces						□	□	*	X
		C5	Oral wash						■	■	*	X
			Feces							□	*	X
		C6	Oral wash						■	■	*	X
			Feces						□	□	*	X
Group 4	**Index**	D1	Oral wash					*	X			
			Feces					*	X			
		D2	Oral wash					*	X			

		Sample	1	2	3	4	5	6	7	8
		Feces					*	X		
	D3	Oral wash				■	*	X		
		Feces					*	X		
Contact	D4	Oral wash							*	X
		Feces						■	*	X
	D5	Oral wash						■	*	X
		Feces						■	*	X
	D6	Oral wash						■	*	X
		Feces							*	X

[a] Index animals are "index case" animals which after initial infection at the start of the experiment, spread viruses to "contact case" or contact animals. Because 2-week-old hamsters have to be kept with their mother for feeding purposes, after infection of index animals, they were returned to their mother and littermate contacts 2 hours later. Hence, the days post-infection of index animals and days post-exposure of contact animals started counting from the same day.

[b] Virus detected up to 2nd passage.

* Indicates onset of signs of infection

X = Time point animal is sacrificed.

Mean oral wash viral titer of index animals (n=4) at 4 dpi of 4×10^2 $CCID_{50}$/ml and the titer of contact animals (n=4) at 8 days post-exposure of 3×10^2 $CCID_{50}$/ml (Figure 4.13A), did not show statistically significant difference (P=0.65). The corresponding mean fecal viral titers of index and contact animals at 1×10^3 $CCID_{50}$/ml and 5×10^3 $CCID_{50}$/ml, respectively, also did not show significant difference (P=0.51).

Thus in general, the onset of oral virus shedding in the majority of index and contact animals was comparable, starting from 3-4 dpi or 3-4 days post-exposure, respectively. In the majority of index and contact animals, viruses in feces were usually detected later than in oral washes, although fecal virus was positive slightly earlier in index animals.

Virus titers in brain, spinal cord, stomach and hind-limb muscle tissues from index and contact animals (n=3 each) from experiment 1 showed no significant differences except for sera (P=0.03) (Figure 4.14).
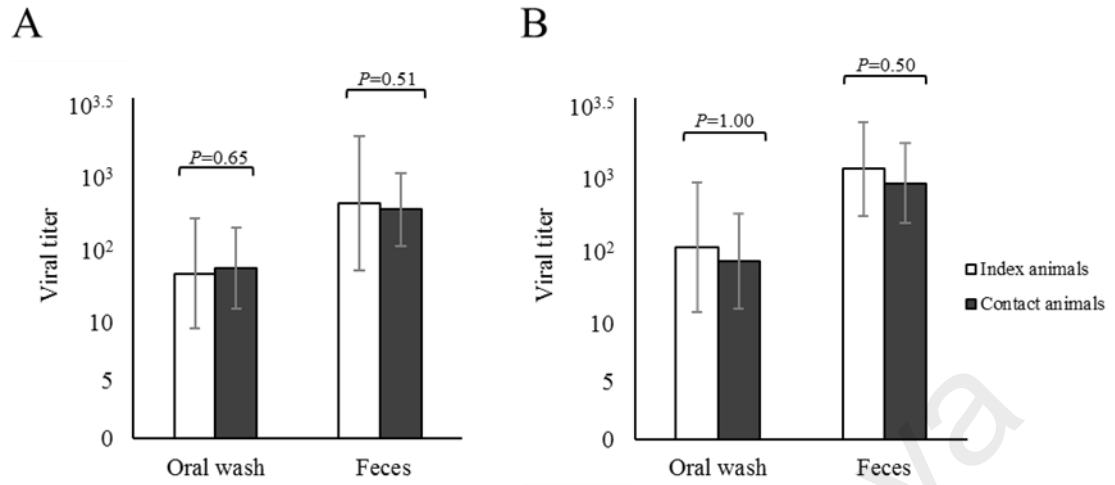
Figure 4.13. Oral wash and fecal viral titers in index and littermate contact animals (n=4 each) at 4 days post-infection and 8 days post-exposure, respectively, from transmission experiment 1 (A). Oral wash and fecal viral titers in index animals and non-littermate contact animals (n=4 each) in the 12-hour exposure group in transmission experiment 2 (B). Viral titer is expressed as the mean $CCID_{50}$/ml $\pm$ standard error of mean per 10% (wt/vol) suspension. There was no significant difference between titers as all P values were >0.05.
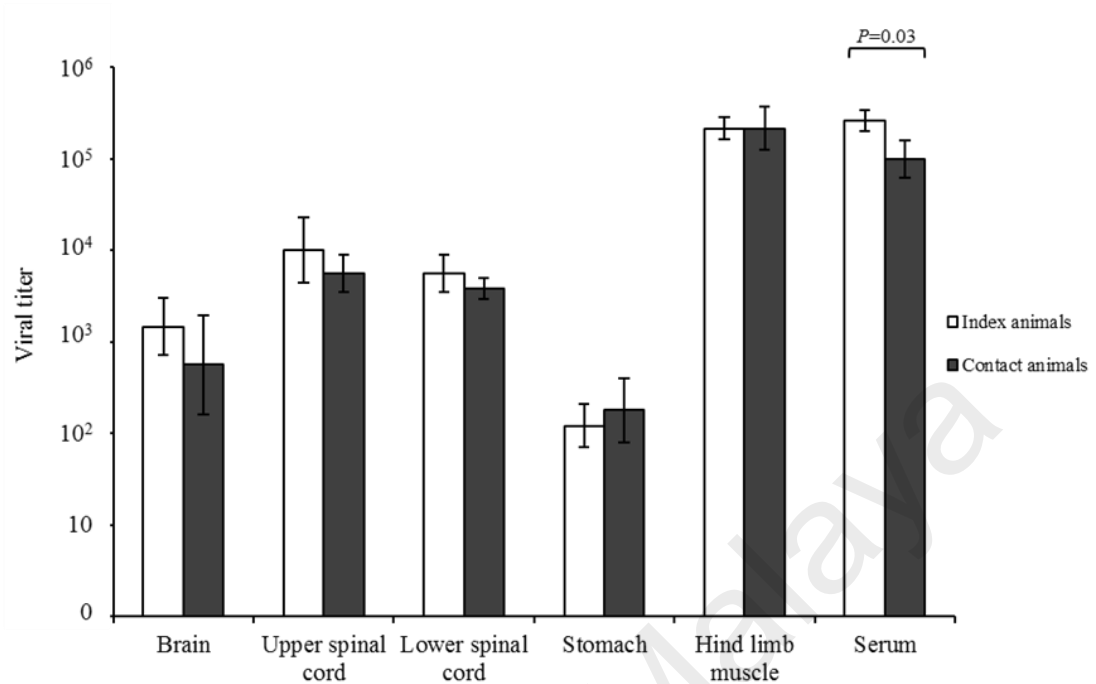
Figure 4.14. Viral titers from various tissues of index and littermate contact animals (n=3 each) in transmission experiment 1, at 4 days post-infection and 8 days post-exposure, respectively. Viral titer is expressed as the mean $CCID_{50}$/ml ± standard error of mean per 10% (wt/vol) tissue homogenates. Viral titer in sera is expressed as $CCID_{50}$/ml ± standard error of mean per 10% dilution. There were no significant differences between tissue viral titers as P values were >0.05, except for sera (P=0.03).

4.3.2 Viral RNA in oral washes and feces by PCR analysis

PCR analysis confirmed the absence of virus in negative oral wash and fecal cultures, and confirmed the presence of virus in positive samples in all samples from transmission experiment 1 (Figure 4.15). In addition, PCR confirmed all the results from virus culture in Table 4.3.
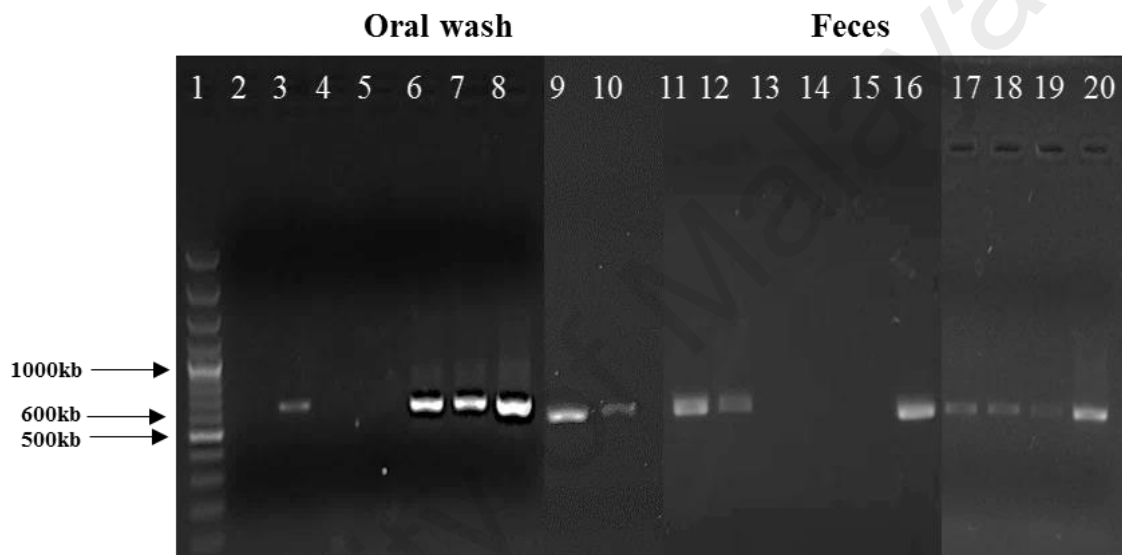
Figure 4.15. Agarose gel electrophoresis of PCR products from the VP1 region of EV-A71 genomes obtained from of oral washes and feces from both index and contact animals (transmission experiment 1). The expected PCR product size was 600 kb. Lane 1: 100 bp DNA ladder, Lane 2: control negative, Lane 3: control positive, Lanes 4-8: PCR products of the oral wash from index animals, Lanes 9-10: PCR products of oral wash from contact animals, Lanes 11-16: PCR products of the feces from index animals, Lanes 17-20: PCR products of the feces from contact animals. Lanes 4, 5: negative PCR products of oral wash from index animals, Lanes 13-16: negative PCR products of feces from index animals.

4.3.3   Transmission experiment 2

After 4 hours of exposure to 4 severely-infected index animals (Table 4.4, Animals E1-4), the 4 non-littermate, contact animals upon return to their respective mothers, remained healthy up to 14 days post-exposure, (Animals E5-E8). In the 8-hours exposure group, all 4 non-littermate contact animals (F5-F8) showed signs of infection such as hunched back, ruffled fur, weight loss and hind-limb paralysis at 6 days post-exposure, and were sacrificed at 6-8 days post-exposure. After 12 hours of exposure to index animals (G1-4), all 4 non-littermate contact animals (G5-G8) developed severe disease (clinical score 4; see Appendix G) earlier after 4 days post-exposure, and were sacrificed at 4-5 days post-exposure. The survival graphs for all contact animals from these 3 groups is shown in Figure 4.16.
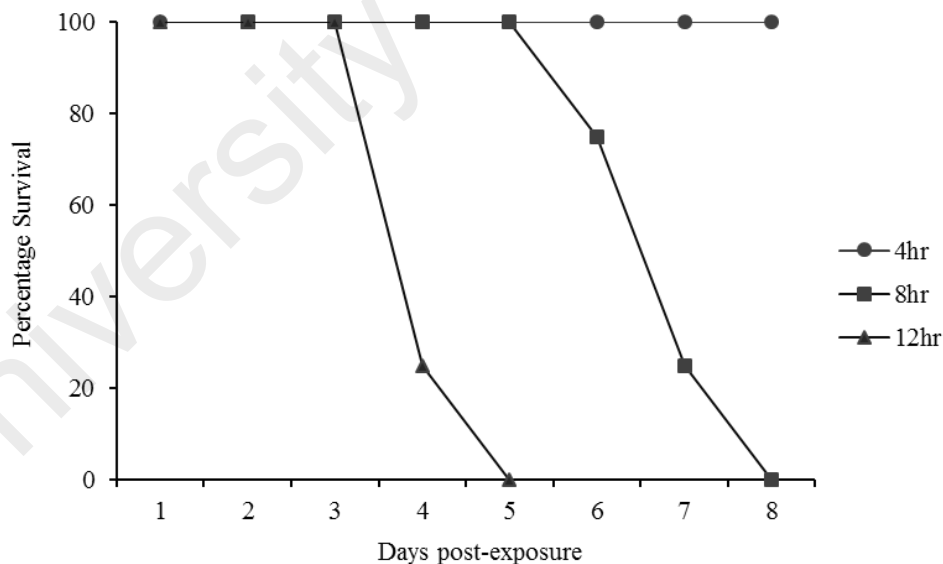
Figure 4.16. Survival graphs of 3 groups of littermate contact animals (n=4 each group) from experiment 2 with 4, 8 and 12 hour exposures to infected index animals.

In the 4 non-littermate contact animals with 4 hours exposure (E5-E8), oral or fecal virus isolation was negative between 1-14 days post-exposure, consistent with the observations that animals did not show any signs of disease. In the 8 hour-exposure group, virus isolation in oral washes was positive in all 4 non-littermate contact animals (F5-F8), and virus in feces, was positive in 2 animals (F5, F6) at 6-7 days post-exposure. In the 12 hour-exposure group, virus in oral washes and feces from all 4 non-littermate contact animals (G5-G8) were detected 4-5 days post-exposure (Table 4.4). Thus, as expected, virus was more likely to be detected in both oral wash and feces in non-littermate contact animals with the maximum 12 hours exposure.

All index animals developed severe disease as described in experiment 1 and were sacrificed at 4-5 dpi as before (Table 4.4). Virus was isolated from oral washes in the majority of 11 index animals (Table 4.4) at 4-5 dpi, except for 1 animal (F2) which was negative. Fecal virus was positive in 8 animals at 4-5 dpi and negative in 4 animals (E2, F3 G3 G4). Of the 7 animals in which both oral and fecal virus were positive, virus was detected on the same day.

Mean oral wash viral titers of index animals (n=4) at 4-5 dpi of 8×10^2 $CCID_{50}$/ml and titer of contact animals (n=4) at 4 days post-exposure of 3×10^2 $CCID_{50}$/ml (Figure 4.13B) showed no statistically significant difference (P=1.00). Similarly, the corresponding mean fecal viral titers of index and contact animals at 2×10^3 $CCID_{50}$/ml and 1×10^3 $CCID_{50}$/ml, respectively, also did not show significant difference (P=0.50).

Table 4.4. Virus isolation from oral washes and feces in 3 groups of index and non-littermate contact hamsters (Experiment 2)

				0/-	1/-	2/-	3/-	4/0	5/1	-/2	-/3	-/4	-/5	-/6	-/7	-/8	~	-/14[b]
Group 1	**Index**	E1	Oral wash					*	X									
			Feces					*	X									
		E2	Oral wash					*	X									
			Feces					*	X									
		E3	Oral wash					*	X									
			Feces					*	X									
		E4	Oral wash					*	X									
			Feces					*	X									
	Contact (4 hours)[c]	E5	Oral wash															X
			Feces															X
		E6	Oral wash															X
			Feces															X
		E7	Oral wash															X
			Feces															X
		E8	Oral wash															X
			Feces															X
Group 2	**Index**	F1	Oral wash				*	X										
			Feces				*	X										
		F2	Oral wash				*	X										
			Feces				*	X										
		F3	Oral wash				*	X										
			Feces				*	X										
		F4	Oral wash				*	X										
			Feces				*	X										

Days post-infection of index animals[a]/ days post-exposure of contact animals

■ Virus detected oral wash

■ Virus detected in feces

■ No virus detected

95

Contact (8 hours)	F5	Ora/ wash							X			
		Feces							X			
	F6	Oral wash							X	X		
		Feces								X		
	F7	Oral wash								X		
		Feces								X		
	F8	Oral wash								X	X	
		Feces									X	
Group 3	**Index**	G1	Oral wash		*	X						
			Feces		*	X						
		G2	Oral wash		*	X						
			Feces		*	X						
		G3	Oral wash		*	X						
			Feces		*	X						
		G4	Oral wash	*	X							
			Feces	*	X							
	Contact (12 hours)	G5	Oral wash				X					
			Feces				X					
		G6	Oral wash				X					
			Feces				X					
		G7	Oral wash				X					
			Feces				X					
		G8	Oral wash					X				
			Feces					X				

4.3.4   Pathological findings in index and contact animals

Macroscopic skin lesions around the oral cavity and on paws in some infected animals were observed similar to the original hamster model (see section 4.1.2). In the 14 severely-infected animals (transmission experiment 1: index and contact animals, n=3, respectively; experiment 2: index animals and contact animals, n=4 respectively), pathological findings were generally similar (Figures 4.17 and 4.18). Viral antigens/RNA were localized in the squamous mucosa in the oral cavity, tongue and esophagus, epidermis (paw and skin), gastric mucosa, and central nervous system neurons, muscle (skeletal, cardiac and smooth muscles), lymphoid tissues, liver, salivary and lacrimal glands. Viral antigens/RNA appears to be most widespread in the skeletal muscles, oral mucosa and tongue. Inflammation was absent or minimal in most infected tissues.

4.3.5   Neutralizing antibody

All mother hamsters from experiments 1 and 2 showed no signs of disease. Sera from sacrificed mother hamsters in transmission experiment 1 (n=5) collected at a mean of 22 days post-exposure (range 18-28 days), had neutralizing antibodies of 1:256. In transmission experiment 2, hamster mothers (n=3) of index animals, which were sacrificed at 19 days post-exposure, also developed neutralizing antibodies of 1:256. The mother hamster of the 4-hour exposure, contact animal group (Table 4.4) did not show seroconversion at 28 days post-exposure, but the mother hamsters in the 8 and 12-hour exposure groups both had neutralizing antibodies of 1:256 at 22 and 19 days post-exposure, respectively. Thus, all mother hamsters exposed to animals that showed signs of seroconversion. In the 4-hour exposure group, contact animals (n=4) did not show seroconversion.
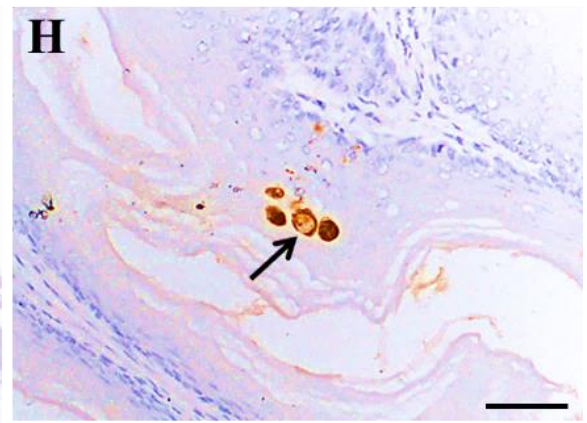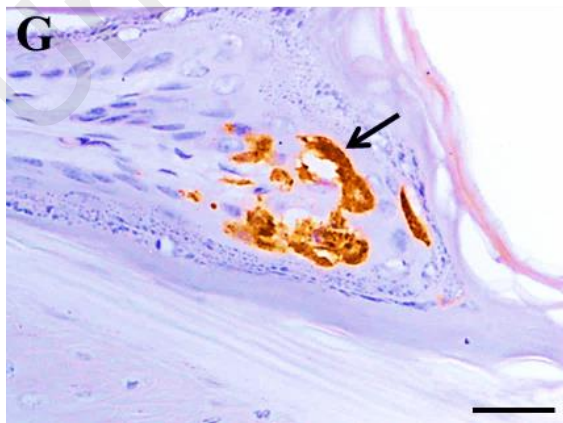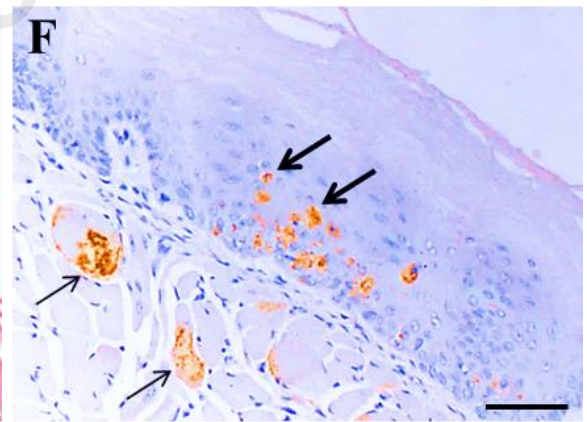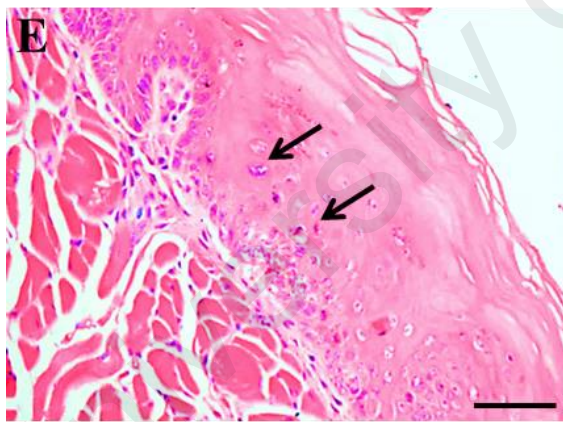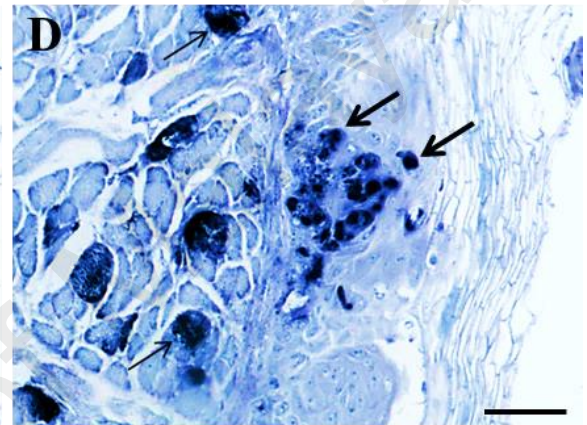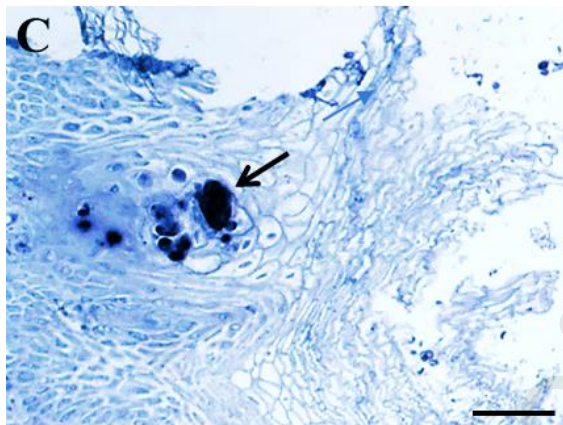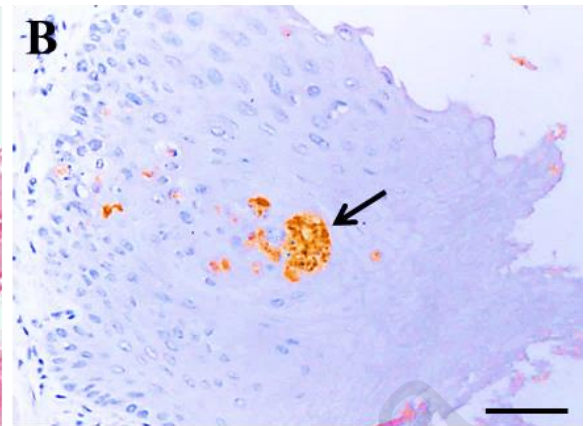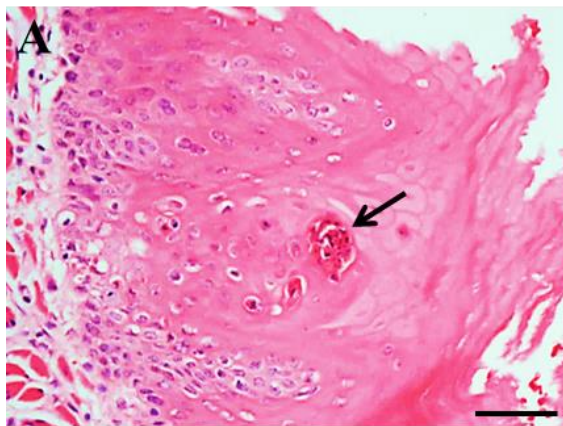
Figure 4.17. Pathological findings in squamous cells and skeletal muscle in littermate contact hamsters at 8 days post-exposure (transmission experiment 1). Squamous epithelial cell necrosis in the oral mucosa (A, arrow), localization of viral antigens (B, arrow) and viral RNA (C, arrow) in the same lesion in adjacent tissue sections. A mildly-inflamed lesion in tongue squamous epithelial cells (E, arrows) shows viral antigens in the same lesion (F, arrows) and skeletal muscle fibres (F, thin arrows) in adjacent tissue sections, and viral RNA in the same tongue squamous lesion (D, arrows) and skeletal muscle fibres (D, thin arrows). Viral antigens in squamous cells in paw epidermis (G, arrow) and oesophageal mucosa (H, arrow). Stains: Hematoxylin and eosin (A, E) immunohistochemistry with 3, 3' diaminobenzidinetetrahydrochloride chromogen/hematoxylin (B, F, G, H), and in situ hybridization with nitroblue tetrazolium/5-bromo-4-chloro-3-indolyl phosphate/hematoxylin (C, D). Original magnification: 20x objective (A, B, C, D, E, F, H), 40x objective (G). Scale bars: 30µm (A, B, C, D, E, F, H), 15µm (G).
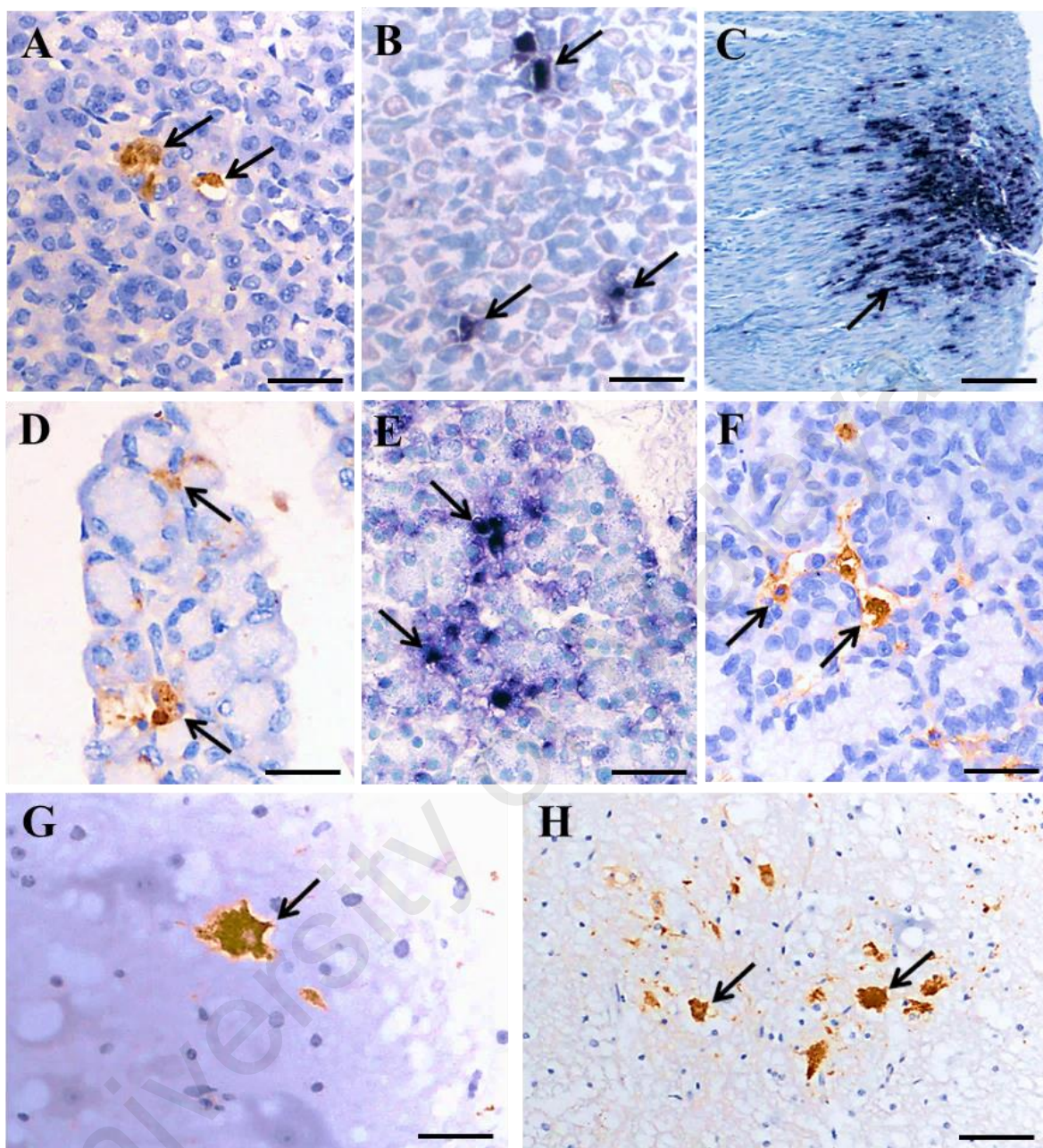
Figure 4.18. Pathological findings in the orodigestive tract and central nervous system in littermate contact hamsters at 8 days post-exposure (transmission experiment 1). Viral antigens (A, arrows) and viral RNA (B, arrows) in gastric mucosal epithelium, and viral RNA in gastric smooth muscle (C, arrows). Viral antigens (D, arrows) and viral RNA (E, arrows) were detected in salivary gland acinar cells. Viral antigens in lacrimal gland acinar cells (F, arrows), brainstem neurons (G, arrow) and spinal cord anterior horn cells (H, arrows). Stains: Immunohistochemistry with 3, 3' diaminobenzidinetetrahydrochloride chromogen/hematoxylin (A, D, F, G, H), and in situ hybridization with nitroblue tetrazolium/5-bromo-4-chloro-3-indolyl phosphate/hematoxylin (B, C, E). Original magnification: 10x objective (C), 20x objective (H), 40x objective (A, B, D, E, F, G). Scale bars: 50µm (C), 30µm (H), 15µm (A, B, D, E, F, G).

4.4   Human skin organotypic and primary squamous cell culture systems

4.4.1   Skin and lip/oral mucosa organotypic culture

Tissue viability of the skin organotypic cultures at days 0, 2, 4 and 6, respectively, as assessed by light microscopy, showed the morphology of the skin structure in day 0 and day 2 tissues to be largely intact (Figure 4.19). Day 4 tissues showed focal or spotty epidermal necrosis and nuclear pyknosis whereas, from day 6 onwards, most of the squamous cells started to detach from the superficial layers of the epidermis with only suprabasal or basal cells remaining attached to the basement membrane. The dermis and skin appendages appeared normal up to 6 days of culture. The morphology and viability of the lip skin and oral mucosa tissues were also found to be same as prepuce skin cultures.

The Celltiter 96 Cell Proliferation assay (Promega, USA) that was used to assess cell viability measured cell metabolic activity to determine the number of viable cells in cultured tissues (Connelly CA et al., 2000). Four replicates of organotypic tissue cultures at each time point showed tissue viability significantly dropped after day 4 of culture (Figure 4.20), in keeping with light microscopic observations.

4.4.2   Infection of human organotypic cultures

Following EV-A71 infection, squamous cells appeared degenerate and were characterized by vacuolation and nuclear shrinkage (Figure 4.21A). Focal viral antigens and RNA, respectively, were detected only in the cytoplasm of squamous cells in organotypic cultures from prepuce (Figure 4.21B, C, D) and lip skin (Figure 4.22A, B), and oral mucosa (Figure 4.22C, D). EV-A71 infected squamous cells in the prepuce and lip skin organotypic cultures were mostly found below stratum corneum, but in contrast, infected squamous cells could be found in the very superficial layer of the oral mucosa cultures. Table 4.5

summarizes the IHC and ISH findings in these tissues. EV-A71 infection of prepuce epidermis as demonstrated by IHC, averaged about 71% at 2 dpi, 64% at 4 dpi, and 36 % at 6 dpi, with an overall mean of 57% positive samples. In lip epidermis and/or oral mucosa, infection was about 15% at 1 dpi, 42% at 3dpi, and 35% at 5dpi, with an overall mean of 30% positive samples. Overall, the percentage of ISH positive fragments was lower than IHC (Table 4.5). Dermal connective tissues, blood vessels and other tissues were negative for viral antigens/RNA. Positive controls showed strong signals for viral antigens/RNA in respective tissues but were undetectable in the negative controls.

Epithelial marker AE1/3 and S100 protein were detected in human prepuce epidermis by specific IHC assay (Figure 4.23). Double IF using the epithelial marker AE1/3 and anti-EV-A71 antibody confirmed the localization of viral antigens in the cytoplasm of keratinocytes in the prepuce skin (Figure 4.24C). Similarly, the well-known EV-A71 receptor, SCARB2 co-localized with viral antigens in the keratinocytes (Figure 4.24F). Although S100 protein positive Langerhans cells (epidermal dendritic cells) were detectable by IF, we did not find convincing evidence of viral antigens in Langerhans cells using double IF (anti-S100 protein and viral antigens). Very rarely, a Langerhans cell may be seen adjacent to an infected cell (Figure 4.24I). Immuno-gold labelling of viral antigens in the cytoplasm of keratinocytes was observed in prepuce skin at 2 dpi (Figure 4.25A). Negative controls (using uninfected control tissues or a procedure that omitted the primary antibody) showed no immuno-gold labelling.
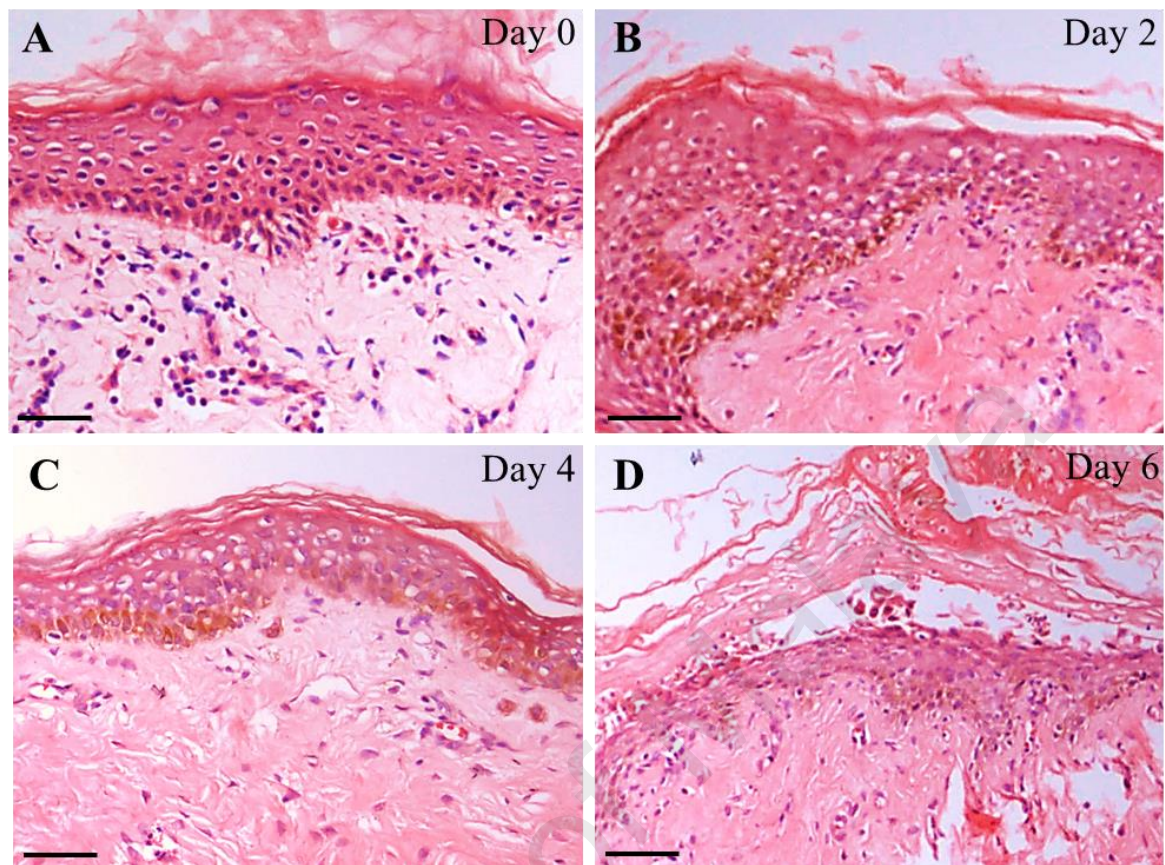
Figure 4.19. Histological analysis of the prepuce skin organotypic culture at 0, 2, 4, 6 days post-infection (A-D). Skin cultures at days 0 and 2 appeared normal and largely intact, whereas day 4 culture showed focal or spotty epidermal necrosis. Day 6 cultures showed nuclear pyknosis and the superficial epidermal layer has started to detach. Stains: Hematoxylin and eosin (A-D). Original magnification: 10x objective (D), 20x objective (A-C). Scale bars: 50 µm (D), 30µm (A-C).
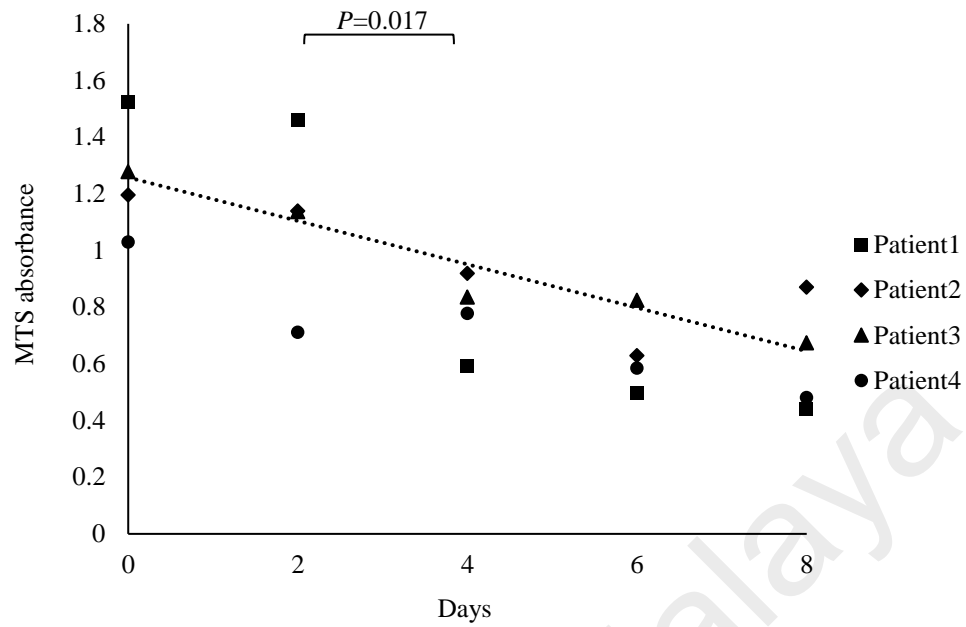
Figure 4.20. Viability of prepuce organotypic culture tissues was investigated using the Celltiter 96 Cell Proliferation assay, a colorimetric method for sensitive quantification of viable cells in proliferation and cytotoxicity that measured the absorbance of a novel proprietary tetrazolium compound called MTS at 490 nm. Pooled data of 4 replicates from 4 individual patients (n=80) per time point are presented. Tissue viability of day 2 cultures was significantly higher than day 4 (P=0.017).
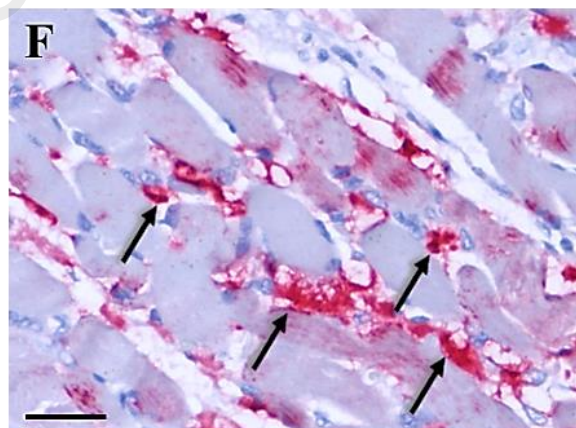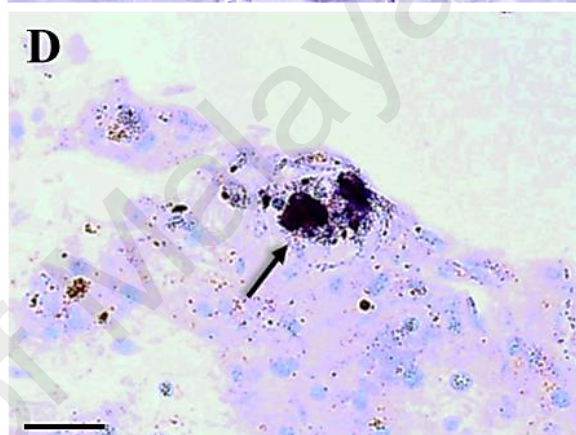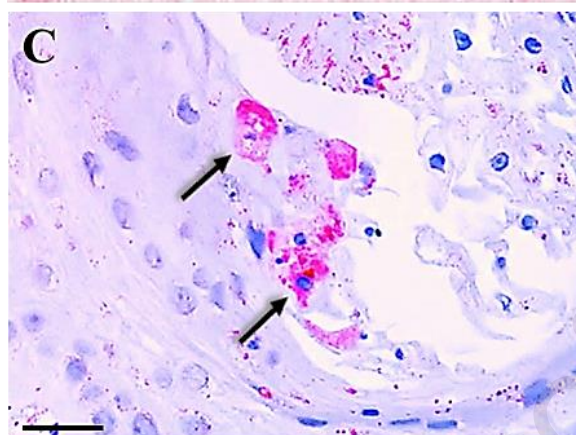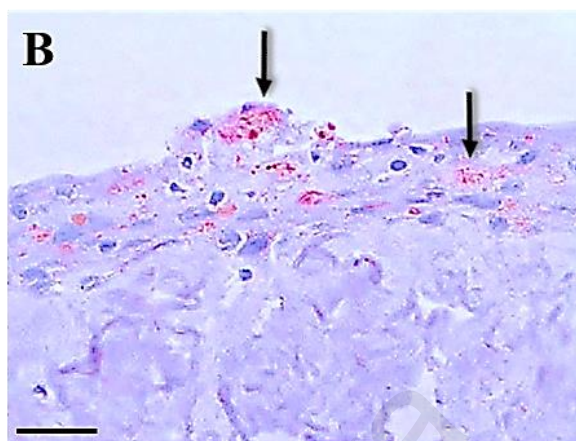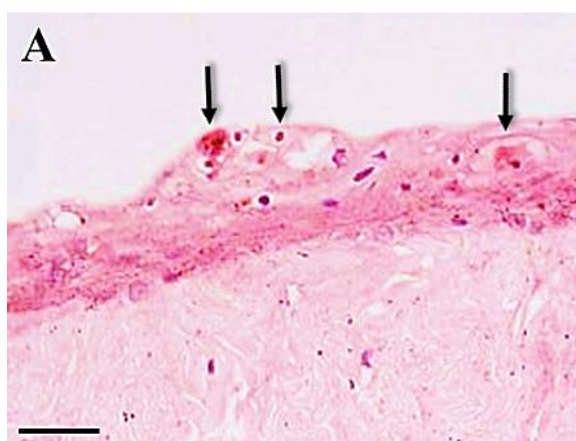
Figure 4.21. Pathological findings in EV-A71-infected organotypic culture epidermal squamous cells. At 2 days post-infection, prepuce epidermal squamous cells showed focal necrosis and vacuolated cytoplasm (A, arrows) and localization of viral antigens in the same lesion (B, arrows) and antigens (C, arrows) and viral RNA in other lesions (D, arrow). A negative control for the immunohistochemistry procedure that uses anti-Japanese encephalitis virus instead of anti-EV-A71 antibodies is shown in E (same lesion as in A and B). A positive tissue control using EV-A71-infected hamster skeletal muscle is shown in F (arrows). Stains: Hematoxylin and eosin (A), immunohistochemistry with permanent red chromogen/hematoxylin (B, C, E, F), and in situ hybridization with nitroblue tetrazolium/5-bromo-4-chloro-3-indolyl phosphate/hematoxylin (D). Original magnification: 20x objective (A, B, E), 40x objective (C, D, F). Scale bars: 30µm (A, B, E), 15µm (C, D, F).
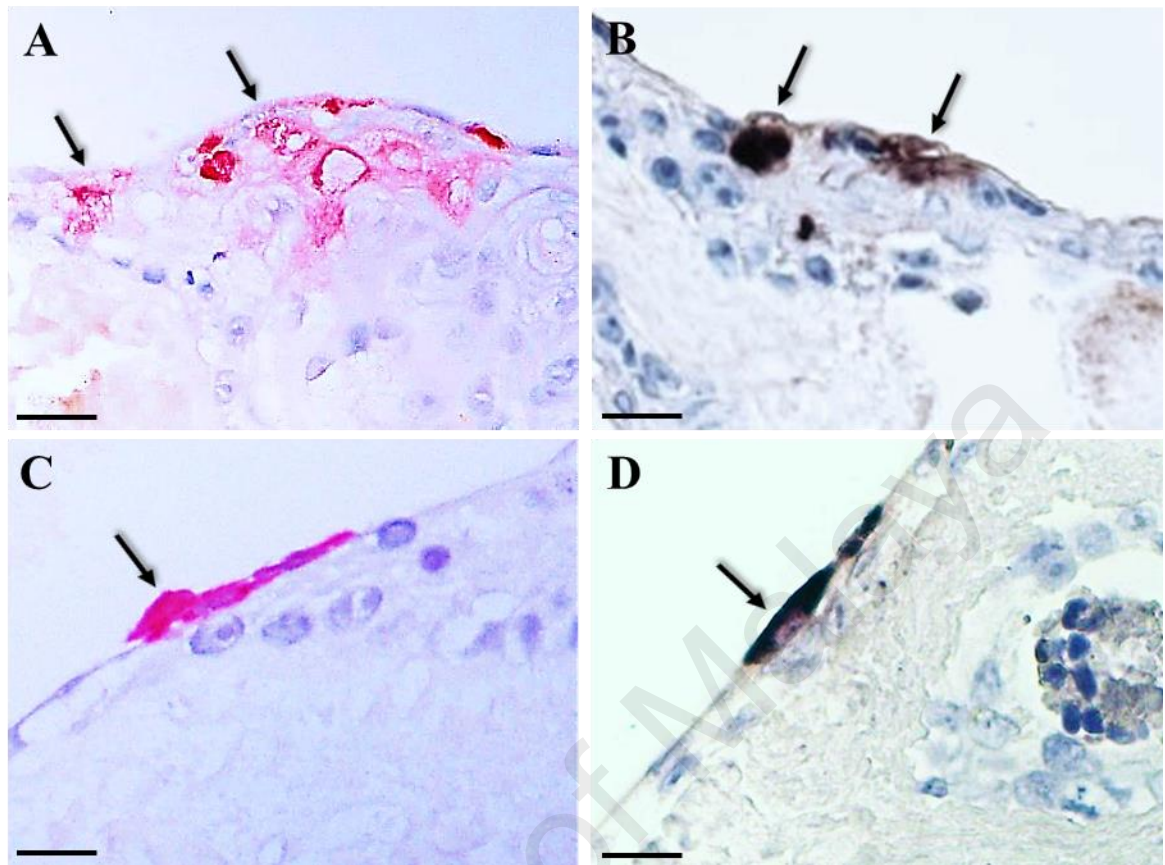
Figure 4.22. Pathological findings in EV-A71-infected lip epidermal and oral mucosa squamous cells. At 3 days post-infection, lip epidermal squamous lesions demonstrated viral antigens (A, arrows) and viral RNA (B, arrows). Similarly, viral antigens (C, arrow) and viral RNA (D, arrow) were detected in the same infected superficial oral squamous mucosa. Stains: Immunohistochemistry with permanent red chromogen/hematoxylin (A, C), and in situ hybridization with nitroblue tetrazolium/5-bromo-4-chloro-3-indolyl phosphate/hematoxylin (B, D). Original magnification: 40x objective (A, B), 60X objective (C, D). Scale bars: 15µm (A, B), 10µm (C, D).

Table 4.5. Immunohistochemsitry (IHC) and *in situ* hybridization (ISH) findings in human prepuce and lip organotypic cultures.

Organotypic culture	IHC results (no. of positive tissue fragments/ tissue total fragments)*			ISH results (no. of positive tissue fragments/total tissue fragments)*		
	2 dpi	4 dpi	6 dpi	2 dpi	4dpi	6dpi
Prepuce epidermis						
Case 1	1/2	1/2	0/2	0/2	1/2	0/2
Case 2	1/2	1/2	0/2	0/2	0/2	0/2
Case 3	2/2	2/2	0/2	2/2	0/2	0/2
Case 4	2/2	2/2	1/2	0/1	0/2	0/2
Case 5	1/2	1/2	2/2	1/2	0/2	0/2
Case 6	2/2	1/2	1/2	2/2	0/2	2/2
Case 7	1/2	1/2	1/2	2/2	1/2	1/2
Total positive fragments/total fragments	10/14 (71%)	9/14 (64%)	5/14 (36%)	7/13 (54%)	2/14 (14%)	3/14(21%)
	1dpi	3dpi	5dpi	1dpi	3dpi	5dpi
Lip epidermis and oral mucosa						
Case 1	1/2	3/4	1/1	0/2	1/3	0/1
Case 2	0/6	1/5	2/8	0/6	1/5	0/4
Case 3	0/4	2/4	2/4	0/4	0/4	0/4
Case 4	2/8	2/6	1/4	0/4	1/6	0/4
Total positive fragments/total fragments	3/20 (15%)	8/19 (42%)	6/17 (35%)	0/16 (0%)	3/18 (17%)	0/13 (0%)

dpi = days post-infection

* For IHC or ISH, 1 positive cell in each tissue fragment is sufficient for the fragment to be counted as a positive result.

110
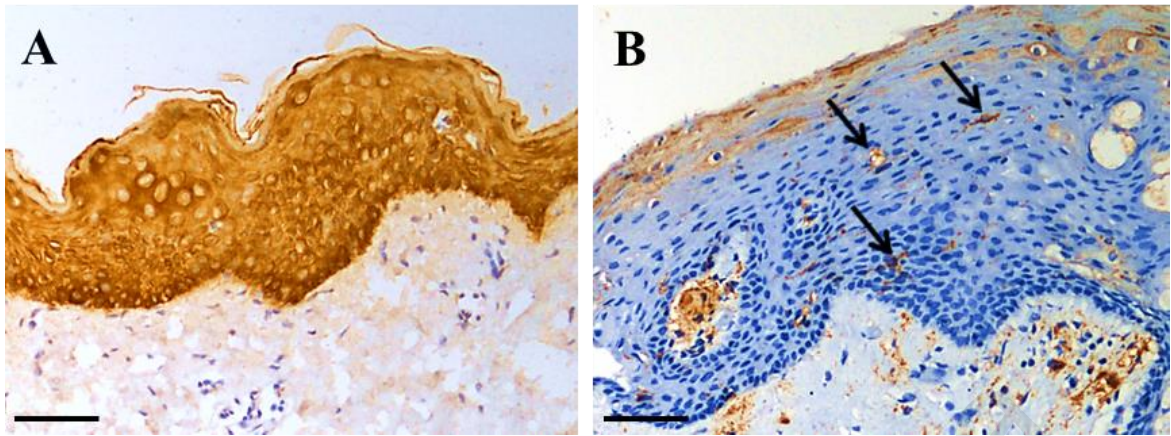
Figure 4.23. Epithelial cell marker AE1/3 staining of the whole epidermal thickness (A) and scattered S-100 positive Langerhans cells (B, arrows) in human prepuce skin. Stains: Immunohistochemistry with 3, 3' diaminobenzidinetetrahydrochloride chromogen/ hematoxylin. Original magnification: 20x objective (A, B). Scale bars: 30µm (A, B).
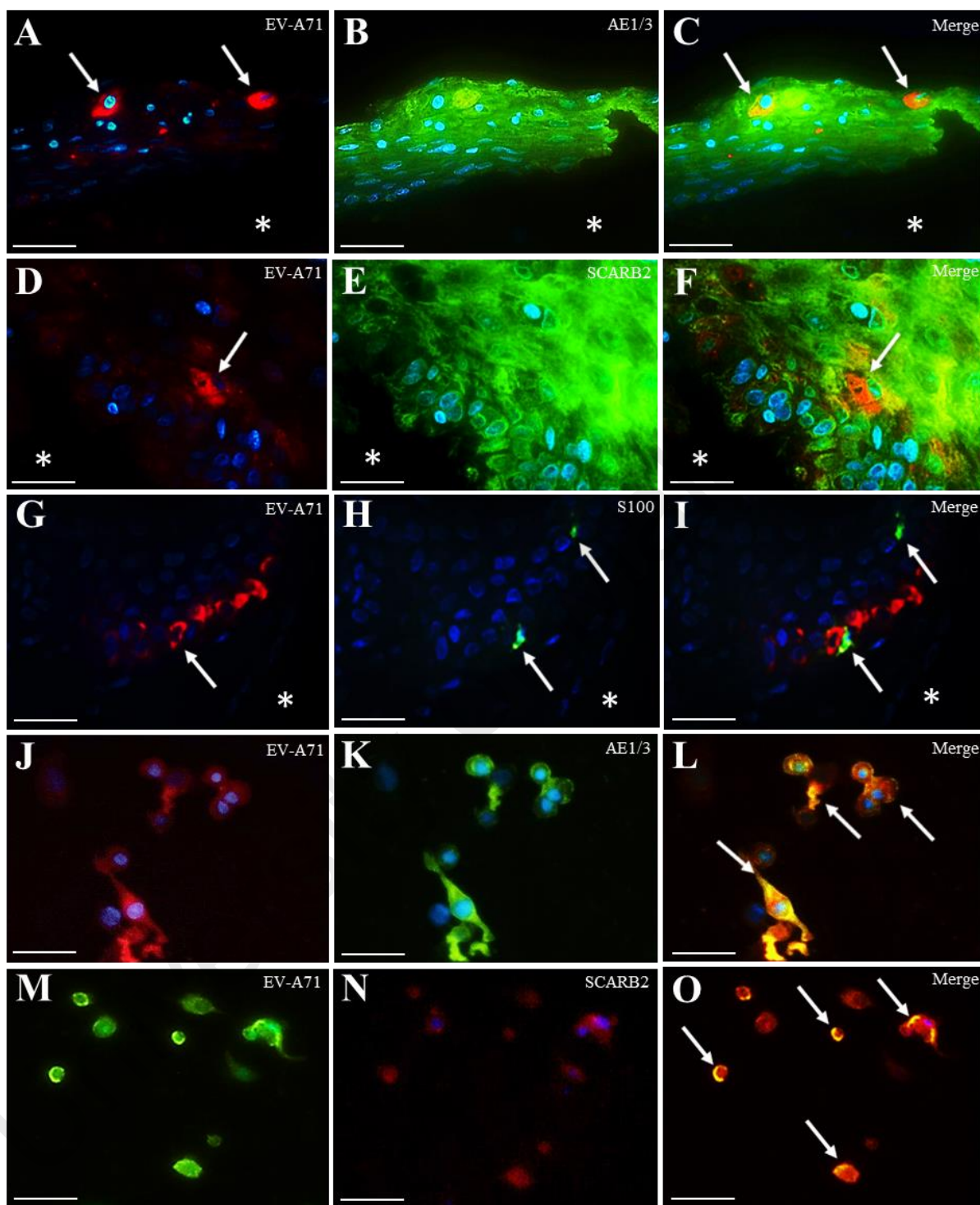
Figure 4.24. Double immunofluorescence staining of EV-A71-infected human prepuce and lip epidermis, and primary epidermal keratinocytes. Viral antigens were found in cytoplasm of prepuce epidermal keratinocytes (A, C, arrows) which were uniformly cytokeratin AE1/3 positive (B). Viral antigens in cytoplasm of prepuce epidermal keratinocytes (D, F, arrows) in uniformly SCARB2-protein positive keratinocytes (E). Both AE1/3 and SCARB2 (A-F) were negative in the dermal layers (∗). S100 protein-positive Langerhans cells (H, arrows) were found adjacent to keratinocytes with viral antigens (G, I, arrows). There was no apparent co-localization of viral antigens in Langerhans cells. The dermal layer (*) is negative for both S100 and viral antigens (H-I). Viral antigens were found in AE1/3-positive epidermal keratinocytes (J, K, L, arrows) and SCARB2-positive keratinocytes (M, N, O, arrows). Stains: Immunofluorescence staining with permanent red chromogen (A, D, G, J), anti-human cytokeratin AE1/3/IgG conjugated with Alexa Fluor 488 (B, K), SCARB2/IgG conjugated with Alexa Fluor 488 (E) and Alexa Fluor 594 (N), S100/IgG conjugated with Alexa Fluor 488 (H), and DAPI (4',6-diamidino-2-phenylindole, dihydrocholoride). Original magnification: 60x objective (A-O). Scale bars: 10µm (A-O).
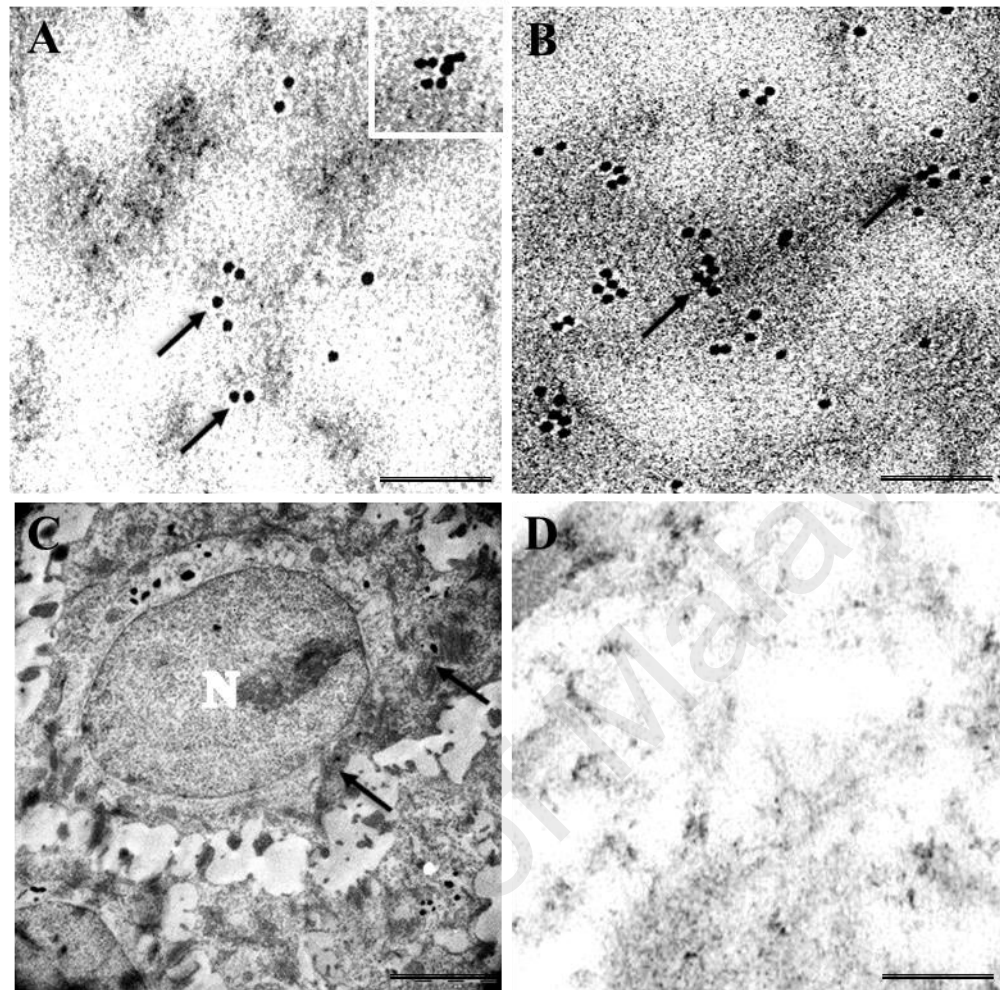
Figure 4.25. Ultra-thin sections of EV-A71 infected prepuce epidermal squamous cells. showing immuno-gold labelling of viruses (A and C, arrows).Immuno-gold labelling of the same tissues with AE1/3 antibody as positive control (B, arrows) and in the uninfected squamous cells as negative control (D). N= nucleus. Scale bars: 2µm (C), 200 nm (A, B, D).

4.4.3 Infection of human organotypic cultures

Viral titers from infected prepuce skin organotypic cultures are shown in Figure 4.26A. The combined viral titers from supernatant (extracellular titer) and tissue homogenates (intracellular titer) peaked at 2 dpi. The combined viral titer at 2 dpi of 7×10^4 $CCID_{50}$ (50% cell culture infective dose) was significantly higher (P=0.001) than at 6 dpi (1×10^4 $CCID_{50}$). Similarly, viral titers at 4 dpi (6×10^4 $CCID_{50}$) were also significantly higher (P=0.005) than at 6 dpi. Overall, corresponding viral titers derived from tissue homogenates collected from the same wells were approximately 10-fold higher than titers from supernatant at all time points.

4.4.4 Primary epidermal keratinocyte monolayer culture

Primary epidermal keratinocytes from human prepuce skin grown in KGM were observed from day 0 day 22 before trypsinizing when the keratinocyte monolayer was 70-80% confluent. Figure 4.27 showed the progress of primary cells growth from days 2 – 22 of cultures. Cells viability and the morphology of the primary cells assessed by inverted light microscopy showed gradual growth throughout the culture period.

A
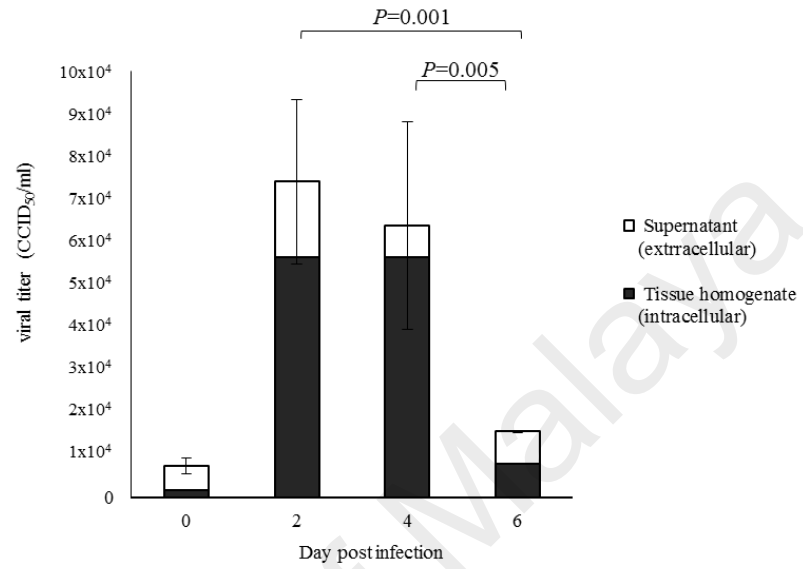
B
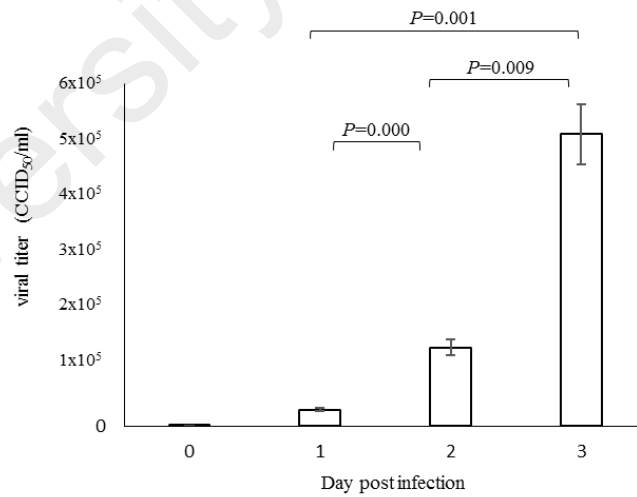
Figure 4.26. Virus replication in supernatant and tissue homogenates in EV-A71 infected human prepuce skin at 2, 4 and 6 days post-infection (dpi) (A), and primary epidermal keratinocytes at 1, 3, 5 dpi (B). Viral titers are expressed as $\log_{10}$ CCID$_{50}$ ± standard error of mean per 10%. Combined viral titers from organotypic tissue homogenate and supernatant (A) were statistically significant between 2 and 6 dpi (P=0.007) and between 4 and 6 dpi (P=0.005), respectively. Supernatant viral titers from primary epidermal keratinocytes (B) between all 3 time-points (1, 2 and 3 dpi) were significantly different (P=0.001).
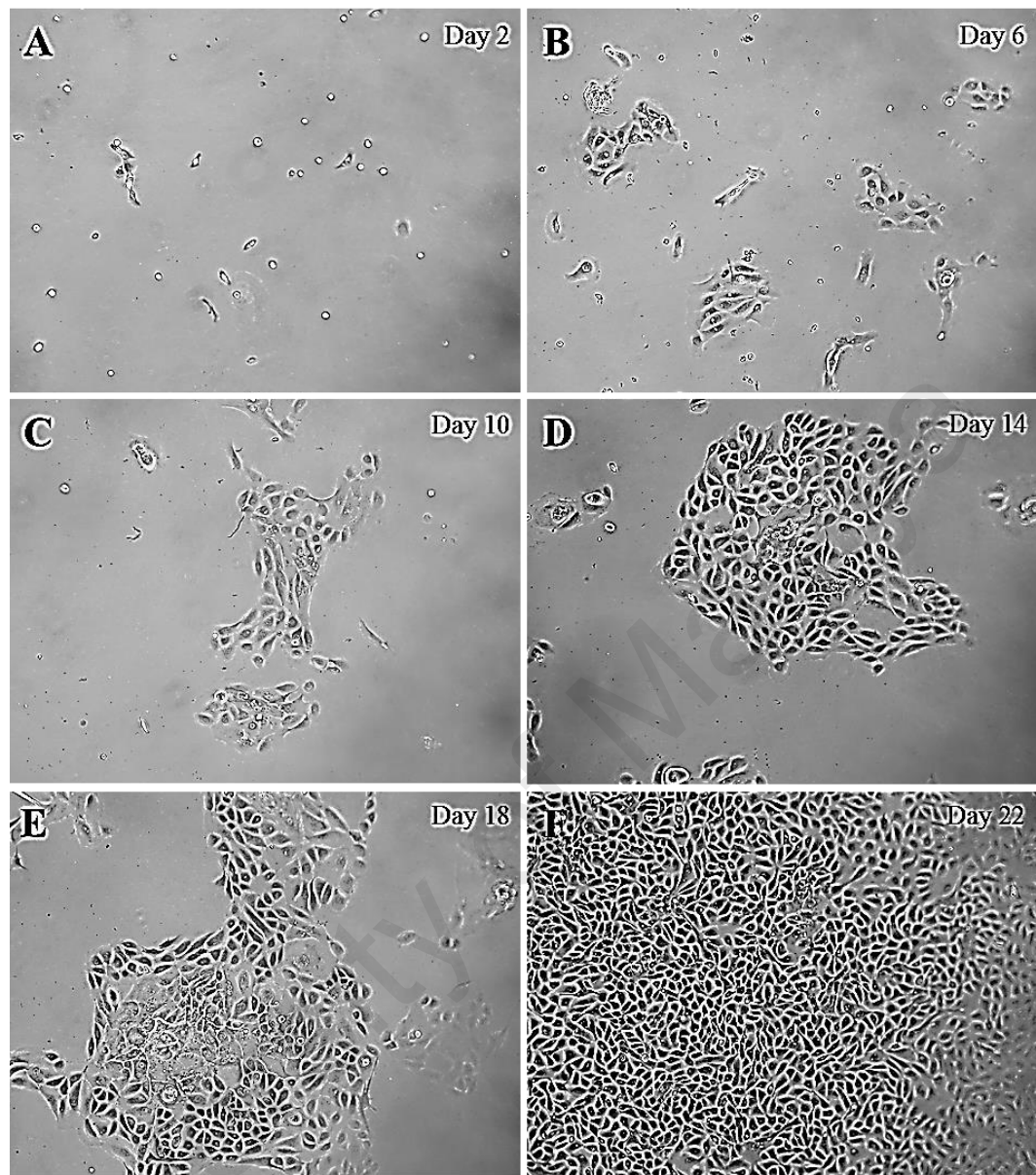
Figure 4.27. Primary epidermal keratinocyte cultures (days 2-22) with full confluence of viable cells at day 22. Original magnification: 20x objective (A-F).

4.4.5   Infection of primary epidermal keratinocytes

Susceptibility of human squamous EV-A71 infection was confirmed using a primary prepuce epidermis keratinocyte culture. Infection of keratinocyte monolayers at a MOI of 0.05 (10^5 CCID$_{50}$), from 2 dpi onwards showed cytopathic effects (CPE), consisting of swelling and rounding up of cells (Figure 4.28A). About 90% of cells showed CPE at 3 dpi, and viral antigens were demonstrated in these cells (Figure 4.28B, C). Uninfected primary keratinocyte controls showed no CPE. The cell monolayers were confirmed to be mostly keratinocytes, as nearly 100% of cells strongly stained positive for AE1/3 IHC (Figure 4.29A, B) and EV-A71 entry receptor SCARB2 protein (Figure 4.29C, D). Moreover, double IF (AE1/3 and viral antigen staining) confirmed keratinocyte infection (Figure 4.24J-L), and infected keratinocytes also strongly expressed SCARB2 receptors (Figure 4.24M-O).

Virus titration from the supernatant showed significant increase of titers for all time points (Figure 4.26B). The highest titer of 5×10^5 CCID$_{50}$ at 3 dpi was about 20-fold higher than 2×10^4 CCID$_{50}$ at 1 dpi (P = 0.001). The average supernatant viral titers from primary epidermal keratinocytes at 2 dpi (1×10^5 CCID$_{50}$) was about 7-fold higher than supernatant from infected organotypic culture at 2 dpi (1×10^4 CCID$_{50}$) (Figure 4.25). At 3 dpi (5×10^5 CCID$_{50}$), the titer was about 70-fold higher than organotypic tissue supernatant at 4 dpi (7×10^3 CCID$_{50}$). Thus, overall supernatant viral titers from primary epidermal keratinocytes were higher than from organotypic cultures. Viral titration from cell homogenates of primary keratinocyte cultures were not performed because all or almost all cells were lysed.
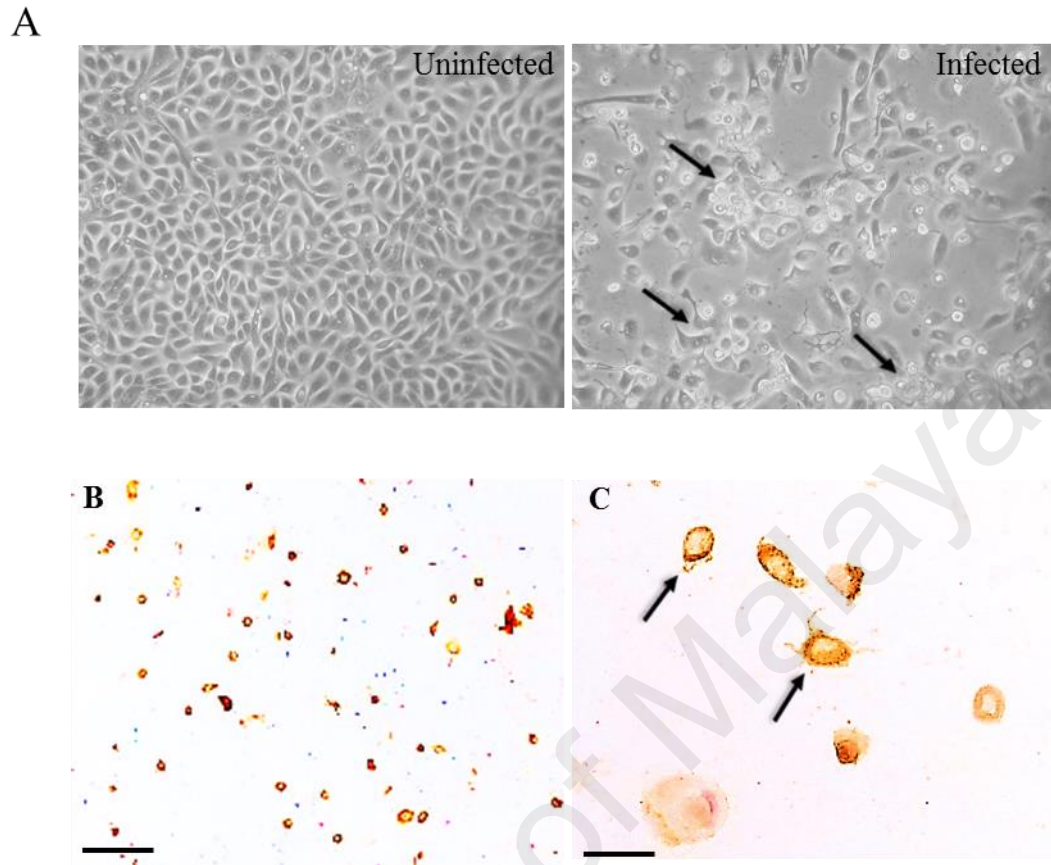
Figure 4.28. Primary epidermal keratinocytes showing cytopathic effect (arrows) at 3 days post-infection (A). EV-A71 infected primary epidermal keratinocytes (B) stained by immunohistochemistry with 3, 3' diaminobenzidinetetrahydrochloride chromogen/ hematoxylin. Original magnification: 20x objective (A, C), 40x objective (D). Scale bars: 30µm (A, C), 15µm (D).
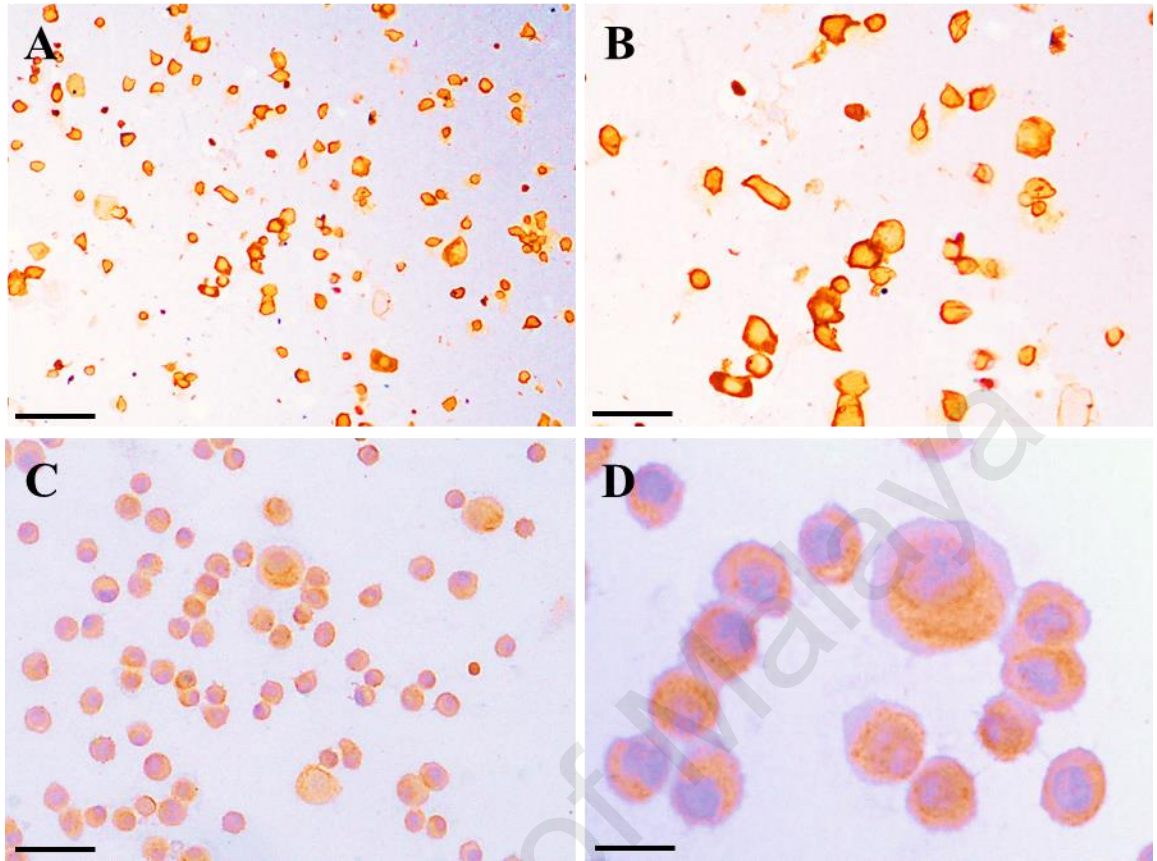
Figure 4.29. Epithelial cell marker AE1/3 (A, B) and viral entry receptor SCARB2 protein (C, D) were detected in primary epidermal keratinocytes. Stains: Immunohistochemistry with 3, 3' diaminobenzidinetetrahydrochloride chromogen/hematoxylin (A, B, C, D). Original magnification: 10x objective (A), 20x objective (B, C), 60x objective (D). Scale bars: 50µm (A), 30µm (B, C), 10µm (D).

CHAPTER 5

DISCUSSION

5.1 Orally-infected hamster model of EV-A71 infection

Many animal models have been developed for the study of EV-A71 infection as summarised in Table 5.1. Our hamster model is included for comparison. The first animal model was a cynomolgus monkey in 2002 (Nagata et al., 2004a; Nagata et al., 2002a) and subsequently mouse models in 2004 (Chen et al., 2004a; Wang et al., 2004a). In more recent years, other researchers have developed rhesus monkey, AG129 mouse, hSCARB2 transgenic, hSCARB2 knock-in, and PSGL-1 transgenic mouse models and pig model to investigate the pathogenesis of EV-A71 infection, neurotropism and to test vaccines (Fujii et al., 2013a; Khong et al., 2012a; Lin et al., 2013b; Liu et al., 2012; Liu et al., 2011a; Ong et al., 2008b; Xiu et al., 2013; Yang et al., 2014; Yu et al., 2014b; Zhou et al., 2016). Recently, neurogenic pulmonary oedema in a mouse model was reported as the main cause of EV-A71 infection-related mortality (Victorio et al., 2016), but pulmonary oedema was not found in this hamster model or indeed in other animal models. The routes of inoculation in many models, were mostly parental, and failed to reproduce all the important features of HFMD and encephalomyelitis, except for the 1-day-old transgenic mouse which could convincingly demonstrate CNS, oral mucosa and skin infections (Fujii et al., 2013a). Another transgenic mouse and SCARB2 knock-in mouse models also demonstrated CNS and skin infections by histopathological analysis but oral mucosa infection was not detected (Lin et al., 2013b; Zhou et al., 2016).

In an orally-infected 1-day-old mouse, although HFMD-like skin lesions such as patchy areas of hair loss, and viral antigens apparently demonstrated in the skin, the

122

localization of the viral antigens in which part of the skin was not clearly demonstrated. Viral shedding and isolation in oral and fecal samples were also not reported (Chen et al., 2004a; Lin et al., 2013b) (Table 5.1). In another orally-infected, 7-day-old mouse model, although skin infection was not observed, the animal developed hindlimb paralysis and CNS infection, and virus isolation in the feces was reported (Wang et al., 2004a). Other mouse models including the AG129 mouse model, did not show either skin infection or viral shedding (Khong et al., 2012a; Ong et al., 2008b; Xiu et al., 2013; Yu et al., 2014b). In the 4-week-old SCARB2 knock-in mouse, although the animals developed CNS, and skin infection in footpads, the author did not report viral isolation and shedding (Zhou et al., 2016). In the cynomolgus monkey model, although limb paralysis and CNS infection was demonstrated, skin involvement in this model was not reported (Nagata et al., 2004a). In another neonatal rhesus monkey model, vesicular lesions were found on the mouth and foot, however, viral antigens were not demonstrated in these regions (Liu et al., 2011a). In the gnotobiotic pig model, limb paralysis, skin vesicular lesions and virus shedding from rectal swabs were reported, however, the infection was inconsistent since all the animals survived and the pathological changes of the infected tissues were not convincingly demonstrated (Yang et al., 2014).

The evidence from the LD_{50} results (see section: 4.1.1) showed that the natural oral route employed by EV-A71 in human infections could be used to consistently infect this unique hamster model. With sufficiently high viral doses ($\geq 10^2$ $CCID_{50}$), the hamster invariably developed squamous lesions in the paw, skin and oral cavity, and encephalomyelitis that strikingly resembled complicated HFMD (Table 5.1). Although, similar infection using a clinical isolate of EV-A71 was not performed in this study, it is intriguing that the involvement of oral cavity and paws corresponded so well with the

mucocutaneous lesions in HFMD. Based on these findings, the pathological basis for the oral lesions, skin rashes and vesicles in HFMD, is viral squamous epitheliotropism, first suggested in a recent SCARB2 transgenic mouse, which showed viral antigens in oral squamous epithelium and distal limb epidermis. However, these findings were only observed in subcutaneously-infected, neonatal transgenic mice, but not in older mice (Table 5.1) (Fujii et al., 2013b). From its extensive involvement, the squamous epithelium in the oral cavity/tongue is likely to be an important primary viral replication site that contributes significantly to oral viral shedding.

The strong positive IHC and ISH signals in the infected hamster oral mucosa and skin tissues suggested active viral replication, and that viral infection and cytolysis played an important role in the inflammation and necrosis of squamous cells. Moreover, active viral replication in salivary gland acinar cells may also contribute to viral shedding via its secretions. The relatively high viral titres obtained from oral washes in hamster model, ≥4 dpi (Figure 4.5), suggested that these viruses represented viral progeny rather than the original inoculum. Viral replication in the human palatine tonsil has been suggested as an important source site for primary viral replication contributing to viral shedding in oral secretions and feces (He et al., 2013). Hamster do not have tonsils. Interestingly, lacrimal gland acinar cell infection in this model raises the possibility that human tears may also be a source of shed virus.

As shown in the hamster epidermis, infection of human epidermal squamous cells probably occurs, leading to acute inflammation and skin vesicle/rash formation. Hitherto, there is no data on human epidermal squamous cell infection (He et al., 2013) but virus has been cultured in fluid from skin vesicles (Chan et al., 2003a; Chatproedprai et al., 2010; Podin et al., 2006a). Although EV-A71 associated skin lesions in mouse and monkey

models have been reported before (Chen et al., 2004b; Lin et al., 2013a; Liu et al., 2011b), only in the SCARB2 transgenic mouse model was epidermal involvement convincingly demonstrated (Fujii et al., 2013a).

Table 5.1 EV-A71 infection in animal models.

Animal type	Age	Dose	Route of infection	Clinical findings	Pathological findings	References
Monkey, cynomolgus	6-17-year-old	$10^{5.5}$ TCID$_{50}$	Intravenous, Intraspinal	CNS infection, limb paralysis, death Skin: NA	Viral antigens: Brain Virus culture: CNS, Lymph node, sensory ganglia, tonsil	Nagata et al., 2004
Monkey, rhesus	Neonatal	$10^{4.5}$ CCID$_{50}$	Respiratory tract	CNS infection, vesicular lesions on the mouth and foot, no death	Viral antigens: NA, Virus culture: CNS, peripheral nerves	Liu et al., 2011
Mouse, ICR	7-day-old	5×10^6 PFU	Oral	CNS infection, hind limb paralysis, death	Viral antigens: thoracic spinal cord Virus culture: CNS, heart, spleen, lung, liver, kidney, muscle, blood, feces	Wang et al., 2004
Mouse, ICR	1-day-old	1×10^6 or 1×10^7 PFU	Oral	CNS infection, skin infection, hind limb paralysis, death	Viral antigens: CNS, intestine, heart, skin, skeletal muscle Virus culture: CNS, intestine, spleen, heart, liver, lung, muscle, skin	Chen et al., 2004

Animal type	Age	Dose	Route of infection	Clinical findings	Pathological findings	References
Mouse, ICR	2-week-old	3×10^4 CCID$_{50}$ 1×10^4 CCID$_{50}$ 6×10^4 CCID$_{50}$ 28×10^4 CCID$_{50}$	Intracerebral, Intramuscular, Intraperitoneal, Subcutaneous	CNS infection, hind limb paralysis, death Skin: NA	Viral antigens and RNA: CNS, skeletal muscle Virus culture: CNS, skeletal muscle, adipose tissues, heart, lung, spleen, serum	Ong et al., 2008
Mouse, ICR	2-week-old	NA	Oral	CNS infection, hind limb paralysis, no death Skin: NA	Viral antigens and RNA: NA Virus culture: NA	Ong et al., 2008
Mouse, ICR	2-week-old	2×10^6 TCID$_{50}$/ gram of weight	Intraperitoneal, Intramuscular, Intracerebral	CNS infection, hind limb paralysis, death Skin: NA	Viral antigens: skeletal muscle Virus culture: NA	Xiu et al., 2013
Mouse, BALB/c	10-day-old	10^5 TCID$_{50}$	Intraperitoneal	CNS infection, limb paralysis, death Skin: NA	Viral antigens: CNS, jejunum, lymph node, lung, skeletal muscle Virus culture: NA	Yu et al., 2014
Mouse, BALB/c	6-day-old	10^6 CCID$_{50}$	Intraperitoneal	CNS infection, limb paralysis, neurogenic	Viral antigens: Brain, spinal cord Virus culture: NA	Victorio et al., 2016

127

Animal type	Age	Dose	Route of infection	Clinical findings	Pathological findings	References
				pulmonary oedema, death		
Mouse, AG129	2-week-old or younger	10^3-10^7 PFU	Intraperitoneal, oral	CNS infection, hind limb paralysis, death Skin: NA	Viral antigens: Brain Virus culture: CNS, kidney, liver, spleen, lung, intestine, lymph node, skeletal muscle	Khong et al., 2012
Mouse, hSCARB2 transgenic	1-day-old 7-day-old	1×10^7 PFU 3×10^4 PFU	Subcutaneous	CNS infection, skin infection, hind limb paralysis, death	Viral antigens: CNS, intestine, lung, muscle, skin Virus culture: NA	Lin et al., 2013
Mouse, hSCARB2 transgenic	3-week-old or adults	1×10^6 TCID$_{50}$	Intravenous	CNS infection, hind limb paralysis, death Skin: NA	Viral antigens: CNS Virus culture: Brain, spinal cord	Fujii et al., 2013
Mouse, hSCARB2 transgenic	1-day-old	1×10^4 TCID$_{50}$	Subcutaneous	CNS infection, oral mucosa and skin infection, hind limb paralysis, death	Viral antigens: Oral mucosa, skin Virus culture: NA	Fujii et al., 2013

128

Animal type	Age	Dose	Route of infection	Clinical findings	Pathological findings	References
Mouse, hSCARB2 transgenic	1-3-week-old	106-108 PFU/mouse	Intraperitoneal	CNS infection, limb paralysis, death Skin: NA	Viral antigens: Brain, CNS Virus culture: NA	Liou et al., 2016
Mouse, hSCARB2 knock-in	4-week-old	1×10^8 and 5×10^8 PFU	Intravenous	CNS infection, skin infection, limb paralysis, no death	Viral antigens: Brain, footpad Virus culture: NA	Zhou et al., 2016
Mouse, human PSGL-1 transgenic	10-day-old	5×10^6 TCID$_{50}$	Intraperitoneal	CNS infection, hind limb paralysis, no death	Viral antigens: NA Virus culture: NA	Liu et al., 2012
Mouse, immunodeficient	1-week-old	10^5-10^8 PFU/mouse	Intraperitoneal, Subcutaneous, Oral	CNS infection, skin lesions, hind limb paralysis, death	Viral antigens: Brain, CNS Virus culture: Intestine, spleen, kidney, heart, lung, muscle, brain, spinal cord	Liao et al., 2014
Pig, gnotobiotic	Neonatal	5×10^8 FFU 4.5×10^8 FFU/oral and	Oral Combined Oral-nasal	Vesicles on the snouts and lung lesions, fever, limb paralysis, no death	Viral antigens: NA Virus culture: NA	Yang et al., 2014

129

Animal type	Age	Dose	Route of infection	Clinical findings	Pathological findings	References
		5×10^7 FFU/nasal				
Hamster, syrian golden (Current study)	2-week-old	10^5 CCID$_{50}$ 10^4 CCID$_{50}$ 10^3 CCID$_{50}$ 10^2 CCID$_{50}$ 10 CCID$_{50}$	Oral	CNS infection, oral cavity, paw and skin infection, lesions on the mouth and paws, hind limb paralysis, death	Viral antigens: Oral, tongue, esophageal and stomach mucosa, paw and skin epidermis, salivary gland, lacrimal gland, brain, spinal cord, sensory ganglia, lymph node, heart, spleen, liver, smooth muscle, skeletal muscle Virus culture: CNS, intestines, stomach, spleen, heart, adipose tissues, skeletal muscle, serum, oral wash, feces	-
Hamster, syrian golden (Current study)	2-week-old	1 CCID$_{50}$	Oral	No limb paralysis, No death	Viral antigens: NA Virus culture: oral wash, feces	-

AG129 mouse: alpha/beta interferon (IFN-α/β) and IFN-γ receptor genes knockout

TCID$_{50}$: median tissue culture infective dose

CCID$_{50}$: median cell culture infective dose

PFU: plaque-forming uni

FFU: focus forming unit

In skin rashes/vesicles of herpes simplex and varicella zoster infections, viral antigens and virions in epidermal squamous cells have been previously demonstrated (Sperling et al., 2012; Taylor & Moffat, 2005a). Based on the extent and severity of infection in the hamster model, although viremia may be more likely to lead to skin infection, it could also be speculated that the epidermis could be an important secondary viral replication site contributing significantly to viremia. Furthermore, if sufficient viable virus is shed from the skin, significantly person-to-person transmission via a cutaneous-oral route could possibly occur. While it may be assumed that skin infection itself resulted from viremia, further investigations are needed to exclude the possibility that direct percutaneous infection may occur after exposure to viruses in the environment.

In human studies and other animal models, significant viral replication sites in the gastrointestinal tract mucosa have never been convincingly demonstrated (Chan et al., 2003a; Chen et al., 2004b; Fujii et al., 2013b; Khong et al., 2012b; Lin et al., 2013a; Yu et al., 2014a). Generally, in the hamster model no evidence of viral replication in gastrointestinal epithelium (except very focally in gastric epithelium) or any infection of pancreatic acinar cells and bile ducts were found, suggesting that virus shedding into the gastrointestinal tract from these tissues/organs may be insignificant. In fact, the main source of fecal virus may be the oral cavity, and to a much lesser extent, the esophageal mucosa and gastric epithelium. In human infections, it was reported that throat/oral swabs were more likely to be positive for virus than rectal swabs (Chang et al., 1999; Podin et al., 2006a). Of course, it is still possible that significant amounts of virus could be actively secreted into the digestive tract without mucosal viral replication but so far there is no evidence to support this. Hepatocyte infection may contribute to secondary viremia but virus may not be shed into the intestine via bile secretions. Similar to tonsillar crypt

131

epithelium (He et al., 2013), it is also possible that the relatively thin oral/esophageal squamous epithelium upon infection could be portal for viral entry into the blood vessels in the subepithelial stroma.

The neuronotropism or neuronal infection demonstrated mainly in the spinal cord and brainstem in this hamster model confirmed findings in other animal models and human autopsy studies (Fujii et al., 2013b; Nagata et al., 2002b; Ong et al., 2008a; Tan et al., 2014a; Wong et al., 2008a). Neuronal infection in EV-A71 encephalomyelitis is a central feature that could account for fatal outcomes in complicated EV-A71 infection. Based on animal and autopsy findings, it was suggested that retrograde axonal transport up peripheral and cranial motor nerves is an important route for viral entry into the CNS, resulting in early infection of motor neurons in the cord and brainstem. Following intramuscular inoculation of virus into hind limb muscles of 2 week old mice, (Table 5.1), viral antigens was first localized to motor neurons (anterior horn cells) of the ipsilateral spinal cord. Moreover, viral antigens/RNA were demonstrated in peripheral spinal nerves (Ong et al., 2008b). In another similar experiment, intramuscular viral inoculation into facial/jaw muscles resulted in initial infection of the ipsilateral motor trigeminal nucleus in the brainstem (Tan et al., 2014b). In human autopsy studies, the distribution of inflammation and virus was stereotyped and clearly shows the early involvement of motor neurons of the spinal cord and motor cortex, features that are consistent with entry into the CNS via motor components of peripheral nerves (Wong et al., 2008b). However, most of the animal models in previous studies that suggested retrograde viral transmission up motor nerves were infected by parenteral routes (Fujii et al., 2013b; Ong et al., 2008a; Tan et al., 2014a), hence the findings in this orally-infected hamster model provided further corroborative

evidence for this hypothesis. As was shown, (see section: 4.1.2, Figure 4.5B, D), motor neurons in the spinal cord and brainstem showed early infection.

Viral antigens/RNA has been localized to sensory ganglia in this model (see section: 4.1.2, Figure 4.5E, F), and also in the transgenic mouse model (Fujii et al., 2013b). So far, only inflammation in human dorsal root ganglion without viral antigens/RNA had been reported previously (Wong et al., 2008a). Dorsal root ganglia involvement may be due to viral transmission from infected anterior horn cells crossing into sensory nerves via the reflex arc or may even be the result of viral transmission up peripheral sensory nerve endings. It is possible that following epidermal/oral mucosa infection virus could directly infect peripheral sensory nerve endings found in these areas. Sensory nerve and dorsal root ganglion involvement in EV-A71 has to be further investigated.

The very focal viral antigens/RNA found in hamster myocardium without significant myocarditis, have also been reported in mouse models (Chen et al., 2004b; Fujii et al., 2013b). Human viral myocarditis and/or viral antigens/RNA localization in the myocardium have not been unequivocally demonstrated (Chan et al., 2003a; Chen et al., 2007b; He et al., 2013; Ho et al., 1999; Wong et al., 2008a). The extensive skeletal muscle involvement in this hamster model is similar to most other mouse models, including a SCARB2 transgenic mouse (Lin et al., 2013a; Zhou et al., 2016). The highest viral titers observed in hind limb muscle at all time-points suggested skeletal muscle is highly susceptible to the virus, which also contributes significantly to the major viremia. So far, autopsy studies have not yielded any evidence of myositis nor shown localization of viral antigens/RNA in skeletal muscle (Chan et al., 2003b; He et al., 2013; Wong et al., 2008a; Yu et al., 2014a), but there have been very few studies. Interestingly, rhabdomyosarcoma cells readily support viral replication *in vitro* (Shi et al., 2012; Zhang et al., 2014).

Hamster model, which was orally-infected by MAV produced by passaging virus in mouse brains, was serendipitously found to be more susceptible to infection (Table 5.1) than the original mouse model (Chen et al., 2004a; Ong et al., 2008a; Wang et al., 2004a). In all other previous mouse models, including a transgenic mouse, oral/intragastric inoculation did not consistently cause infection (Chen et al., 2004b; Fujii et al., 2013b; Khong et al., 2012b; Ong et al., 2008a; Wang et al., 2004b). Similarly, oral infection in a pig model was inconsistent (Yang et al., 2014), and so far there has been no reports of orally-infected monkey models (Liu et al., 2011b; Nagata et al., 2004b; Nagata et al., 2002b) (Table 5.1). Based on IHC and ISH evidence of infection in the salivary and lacrimal glands, esophageal mucosa, gastric epithelium, and gastrointestinal smooth muscle, this hamster model demonstrated a wider tissue tropism than previously observed in animal models or human studies (Chan et al., 2003a; Chen et al., 2004b; Fujii et al., 2013b; He et al., 2013; Lin et al., 2013a; Liu et al., 2011b; Nagata et al., 2004b; Ong et al., 2008a; Wang et al., 2004b; Wong et al., 2008a) (Table 5.1). Squamous cell infection in oral mucosa and epidermis has only been demonstrated in one other animal model, a transgenic mouse model (Fujii et al., 2013b). In another transgenic mouse, and other mouse and monkey models, in which skin infection was investigated, squamous epitheliotropism was not convincingly demonstrated (Chen et al., 2004b; Lin et al., 2013a; Liu et al., 2011b) (Table 5.1).

Unlike poliovirus, EV-A71 genomic mutations that could determine neurovirulence have not been confirmed (Ong & Wong, 2015). However, mutations in EV-A71 structural and non-structural genes that probably trigger or attenuate neurovirulence in mice and monkey models have been demonstrated (Arita et al., 2008; Arita et al., 2007). Similarly, it is also possible that the mutations in EV-A71 MAVS (P5D1) structural genes could

134

determine neurovirulence in mice and hamsters. In human SCARB2 mapping study, amino acids 142 to 204 is important for EV-A71 binding and infection (Yamayoshi et al., 2012). However, it is reported that mouse SCARB2 does not serve as the receptor for EV-A71 infection although mouse SCARB2 shares 85.8 % homology to human SCARB2 (Lin et al., 2013b). Amino acid sequences of SCARB2 receptor in hamster shows 87 % similarity to human SCARB2 (Figure 4.7), but it is still unknown whether hamster SCARB2 may serve as an important receptor for EV-A71 binding and infection. Further analysis of *in vitro* infection should be done to confirm this hypothesis using non-susceptible hamster SCARB2 expressing cells.

5.2   Study of viral spread and distribution in the hamster model

In order to study sequential viral spread in the hamster model, groups of infected animals were sacrificed at 2, 3 and 4 dpi, respectively (see section: 3.4). A relatively higher viral dose of 10^5 $CCID_{50}$ was used in this study since animals given the lower dose of 10^3-10^2 $CCID_{50}$ developed disease only after 5-6 dpi (a longer incubation period) and a relatively higher number of animals may need to be used as well. It is also interesting to use a lower viral dose to study viral spread in this hamster model and to compare with the viral distribution found in animals infected by a higher dose. Histopathological findings of viral distribution in this orally-infected hamster model showed only minimal traces of viral antigens at 2 dpi in all major organ each distant organs rapidly. These results support the possibility that squamous epithelial cells in oral cavity and orodigestive tract could be primary viral replication sites where virus first infected and replicated here before virus progeny reaches to the blood stream, and spread to other major target organs. Superficial involvement of oral mucosa and/or tongue epithelia cells at 2 dpi also suggests that virus might be able to infect these areas directly upon oral infection (Figure 4.7). However,

135

infected animal tissues at 1 dpi showed negative IHC and virus isolation in all tissues, including serum, perhaps because it is too early for virus to establish infection in the organs/tissues examined. However, the degree of infection in oral cavity and orodigestive tract were consistently increased after 2 dpi, and the cellular necrosis and inflammation were also clearly observed at 3-4 dpi, suggesting that virus was actively replicating at these primary sites (Table 4.2, Figure 4.8). The most severe and intense degree of infection was seen in all animals at 3 dpi by IHC analysis and virus titration as well and its wider tissue tropisms was also similar to original orally-infected hamster model.

Focal, early infection in dorsal root ganglia at 2 dpi in 2 animals without apparent infection in anterior horn cells may suggest virus transmission and neuroinvasion via sensory nerves. However, dorsal root ganglia involvement may be viral transmission from infected anterior horn cells crossing into sensory nerves via the reflex arc as well. This was more apparent in the sensory ganglia at 3 and 4 dpi where simultaneous involvement of dorsal root and anterior horn cells were observed. It was previously suggested that peripheral autonomic and sensory nervous system do not seem to be involved in viral spread into the CNS. However, in human autopsies, mouse and monkey models, occasional and rare involvement of the dorsal root ganglion may still suggest anterograde viral spread via sensory nerves (Wong et al., 2008b). Further investigations are needed to confirm the role of neuropathology in CNS infection.

Higher degree of anterior horn cell and brainstem neuron infections detected at 3 and 4 dpi may also be associated with extensive skeletal muscle infection at late time points since it was postulated that virus cross from neuromuscular junctions where motor neurons terminate on skeletal muscles (Too et al., 2016). Skeletal muscle involvement and likely retrograde axonal transport of virus spread into the CNS through neuromuscular junctions

was also suggested in poliovirus infection in transgenic mice (Ohka et al., 2004). Involvement of anterior horn cells and motor trigeminal nucleus infection in this hamster model also support the retrograde motor nerve viral transmission hypothesis of viral entry to the brainstem and spinal cord.

Significantly higher titers of oral washes (1×10^3 $CCID_{50}$/ml) at 3 dpi than 4 dpi (3×10^2 $CCID_{50}$/ml) (P=0.002) suggest that the virus was most actively shedding at 3 dpi. It is also correlated well with the strong and extensive viral antigens and inflammation detected in oral cavities at 3 dpi (Figures 4.8 and 4.12). At 4 dpi, although the animals showed signs of infection and relatively strong viral antigens detected in all major target organs, overall degree of infections appear to be less than of animals at 3 dpi. Viral titers in various organs also support the gradual increase of viral load from 2 dpi with the highest viral titers at 3 dpi (Figures 4.9 and 4.11).
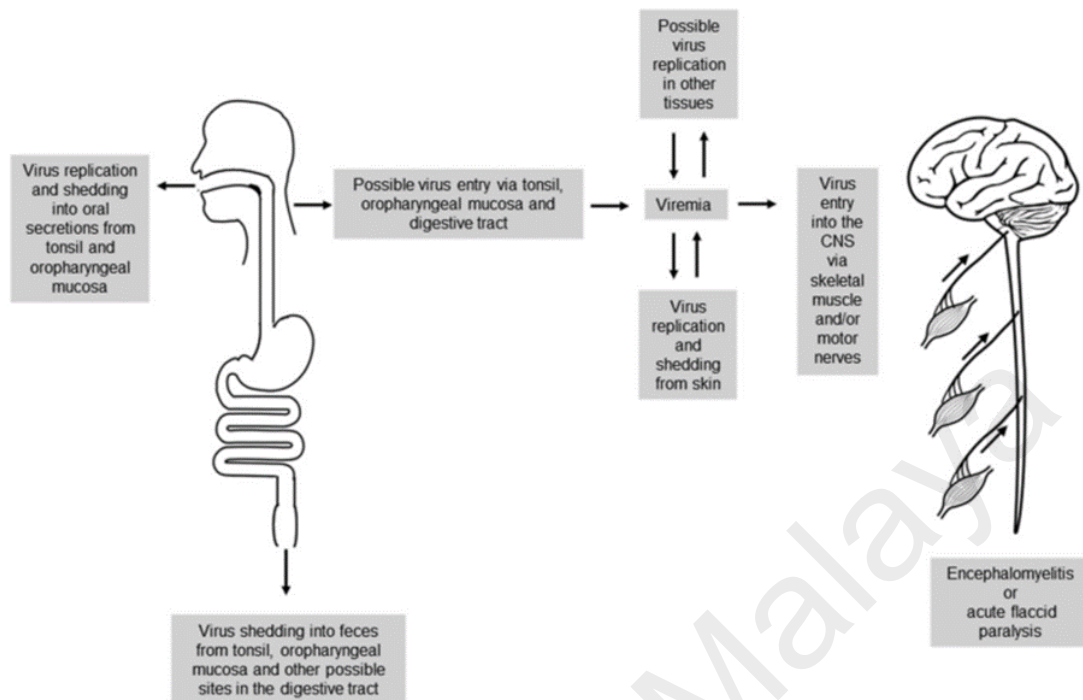
Figure 5.1. Hypothesis for the route of viral entry, primary viral replication sites, viral dissemination to the CNS and other non-CNS tissues, viral shedding and person-to-person-to-person transmission in human EV-A71 infection. Adapted from Ong & Wong, 2015.

Ong & Wong, 2015 has previously hypothesized the possible viral entry and primary replication sites, and viral shedding in EV-A71 encephalomyelitis, based on human and animal studies (Figure 5.1). Evidence of virus replication and shedding from oral cavity, oral wash and feces in this hamster model is consistent with primary replication sites in the oral cavity and upper orodigestive tracts. Viremia and neuroinvasion follows soon after (Figure 5.2). However, the results suggest that neuroinvasion by sensory nerves may be possible and needs to be further investigated.
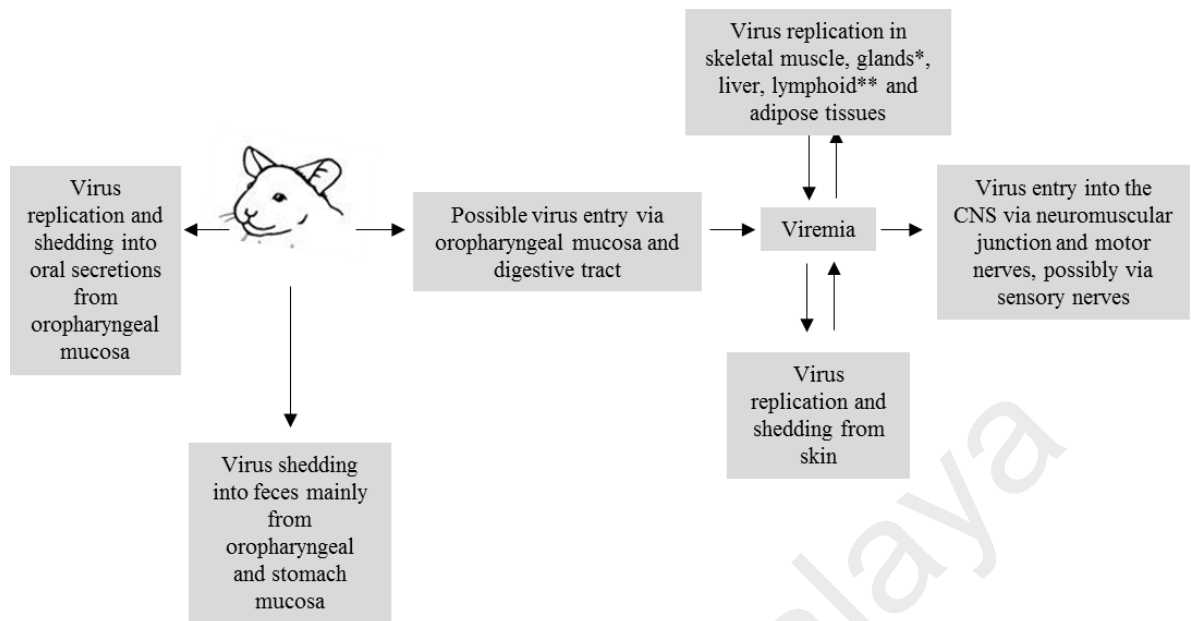
Figure 5.2. Hypothesis of the route of viral entry, primary viral replication sites, viral dissemination to the CNS and other non-CNS tissues, viral shedding in the hamster model. (*) salivary glands, lacrimal glands. (**) lymph node, spleen.

5.3   Hamster model of person-to-person transmission

The orally-infected hamster model was used to investigate person-to-person transmission in this study because it consistently developed disease reminiscent of HFMD and encephalomyelitis. In our opinion, our results show that this hamster model is likely to prove useful to study person-to-person transmission, including using the model to test drugs and other prevention strategies to interrupt viral transmission. So far, neither a consistent orally-infected animal model for EV-A71 nor a model for person-to-person transmission has been described before. Previous results had alluded to the possibility of using animals to model person-to-person EV-A71 transmission. In an EV-A71 orally-infected, 1-day-old mouse model, viral transmission to littermates has been observed. However, the animals

developed only very mild skin lesions, no pathological changes, and survived. Although no attempt was made to isolate virus in oral fluids or feces, the authors had suggested fecal-oral transmission (Chen et al., 2004a). In another study, involving orally-infected 7-day-old mouse models, virus were detected in stools of healthy littermate animals suggesting oral-fecal viral transmission but no further investigations were done (Wang et al., 2004a). In the oro-nasal and orally-infected gnotobiotic pig models, rectal swabs were positive for virus in infected animals, but not in control animals in which only very mild fever was observed (Yang et al., 2014). A promising SCARB2 (a well-recognised viral receptor) transgenic mouse model for EV-A71 infection could not be consistently orally-infected (Fujii et al., 2013a) and therefore may not be suitable to study person-to-person transmission.

In transmission experiment 1 (see section 4.3.1), both index and littermate contact animals (exposed to index animals) developed similar signs and pathology of disease. However, as expected, contact animals consistently developed disease later at 6-7 days post-exposure, probably because the index animals began to shed the virus from 3 dpi onwards. Moreover, littermate contact animals could be exposed to viruses found in oral fluids, feces and/or environment in doses that may be relatively lower than the initial doses given to index animals. Experiment 2 (see section 4.3.3) showed that exposure of 8 hours or more to index animals successfully enabled viral transmission to non-littermate contact animals, and the 12 hours-exposure group developed disease the earliest, while the 4 hours-exposure group remained healthy with no seroconversion. Interestingly, after 4 days post-exposure, the 12 hours-exposure group developed severe disease similar to the all index animals, suggesting that a relatively short exposure to active infective sources (4 index animals) was sufficient for viral transmission to cause severe infection. Although the cumulative infective doses received by severely infected littermate and non-littermate

contact animals are unknown, our results showed that oral and fecal virus titers from index

animals of 3×10^2 to 8×10^2 CCID$_{50}$/ml and 1×10^3 to 2×10^3 CCID$_{50}$/ml, respectively, were

sufficient for viral transmission. These results correlated with the previous findings (see

section 4.1.3) in the hamster model in which viral doses of 10^2 to 10^3 CCID$_{50}$ given orally

were sufficient to cause severe disease.

In the majority of index and contact animals in experiment 1, oral virus shedding

was comparable, starting from 3-4 dpi or days post-exposure, respectively. However, in

most animals, oral wash viruses were usually detected earlier than fecal viruses. In the

orodigestive tract, viral antigens/RNA were consistently detected most abundantly in the

oral mucosa and tongue, and more focally in salivary and lacrimal glands, oesophageal and

stomach epithelia. Importantly, viral antigens/RNA in other parts of the orodigestive tract,

including intestines, were not detected. These data suggest that in the hamster model, the

main source of oral viral shedding was the oral cavity, and possibly to a lesser extent, the

salivary gland as well. Therefore, these results suggest that fecal virus may be mainly

derived from viruses in swallowed oral secretions with some contribution from viral

replication in oesophageal and stomach epithelia. This may be a reason why fecal viruses

were detected relatively later. EV-A71, poliovirus and other enteroviruses (Knipe &

Howley, 2001; Solomon et al., 2010) are able to resist gastric acid, thus virus from the oral

cavity, esophagus and stomach may remain viable once excreted in the feces. Viral titres

from oral washes and feces showed no significant differences although fecal titres were

consistently higher (Figure 4.12). The percentage of positive oral viral isolation was higher

at 62% than fecal positivity at 38% (P=0.003), consistent with human studies in which

throat swabs were more likely to be positive for virus than rectal swabs or stools (Podin et

al., 2006b). In humans, the reason for this is uncertain but it has been postulated that this

141

may be because palatine tonsils and oral mucosa are major viral replication sites (He et al., 2014). Tonsils are not found in hamsters so this organ did not play a role in viral infection and/or shedding. Although possibility of person-to-person EV-A71 transmission via respiratory droplets has been suggested, there is no evidence or *in vivo* animal models available so far.

After exposure to infected offsprings, seroconversion without any signs of disease suggested that mother hamsters probably had the human equivalent of asymptomatic infection. It has been observed that all family members may be susceptible to be infection through close contact with EV-A71 infected patients but may or may not develop overt signs of infection (Chang et al., 2004; Chen et al., 2008). In addition, the study showed that seroconversion in adults was >50% and seropositive rates among family members may be as high as 93% (Chang et al., 2004; Chen et al., 2008). Intra-family transmission rate among family members, especially between siblings, was reported to be the highest (Chen et al., 2008). It was also suggested that in some circumstances, asymptomatic or mildly symptomatic adults/parents may be a source of infection in young children. Interestingly, adults may even develop encephalomyelitis after viral transmission from children who only have the milder HFMD, suggesting that other factors, including a higher infective viral dose and host immune system, may be responsible for neurovirulence (Chang et al., 2004; Hamaguchi et al., 2008; Kuo & Shih, 2013; McMinn et al., 2001). In a 7-day-old mouse model, non-neutralizing, anti-EV-A71 antibodies was detected in dams of infected animals and control littermates although animals remained healthy (Wang et al., 2004a).

5.4 Enterovirus A71 squamous epitheliotropism

Based on clinical observations and viral culture results, the human skin in various parts of the body especially in the hand, foot, lips, buttock, and oral mucosa are well known to be infected but the cellular target/s of virus in these tissues have remained unknown. In this study, squamous cells derived from human prepuce and lip epidermis, and oral mucosa, and viably maintained by organotypic culture, were found to be infected by EV-A71. Focal squamous cell degeneration and necrosis was associated with EV-A71 antigens/RNA as demonstrated by specific IHC and ISH assays within the cytoplasm of epidermal keratinocytes and oral mucosa squamous cells (Figure 4.21, 4.22). This was confirmed by immunogold labelling (Figure 4.25). This is the first time that EV-A71 squamous epitheliotropism has been reported in human tissues by *in vitro* analysis. Due to a lack of suitable naturally-infected human tissues for investigation, very little data has been published except in one available skin sample in which viral antigens were not detected (He et al., 2014). Nevertheless, the authors found palatine tonsil crypt squamous epithelia to be infected by EV-A71. Further investigations using human autopsy or biopsy tissues are needed to confirm EV-A71 squamous epitheliotropism.

In EV-A71-infected hamsters, multiple, focal inflammatory skin lesions were found on footpads/paws, lips and other parts of the skin following oral infection. Viral antigens/RNA were also localized within the cytoplasm of epidermal squamous cells found in these areas, as well as squamous cells of the oral and oesophageal mucosa. Similarly, a SCARB2 transgenic mouse model has also convincingly demonstrated viral antigens in squamous cells in the oral mucosa and in the skin on limbs (Fujii et al., 2013a). In human primary epidermal keratinocytes, viral antigens found in SCARB2-positive (Figure 4.24O) and AE1/3-positive keratinocytes (Figure 4.24L) confirming squamous epitheliotropism

and SCARB2 as a major receptor for EV-A71 infection (Lin & Shih, 2014; Yamayoshi et al., 2014; Yamayoshi et al., 2009). Other HFMD-causing, SCARB2-associated enteroviruses such as CVA-7, CVA-14 and CVA-16 (Yamayoshi et al., 2012) may likewise infect squamous cells but so far there is no evidence for this. HFMD-causing but non-SCARB2-associated CVA-6 viral antigens have been demonstrated in keratinocytes found around a skin lesion of epidermal necrosis and vesicle formation in a naturally-infected human case (Muehlenbachs et al., 2015). Hence, other viral receptors in squamous cells may facilitate CVA-6 entry. In other viral infections that cause skin vesicles and rashes such as herpes simplex and varicella zoster, viral antigens have been demonstrated within squamous cells (Cunningham et al., 2006; Jones et al., 2014; Muehlenbachs et al., 2015; Rahn et al., 2015; Taylor & Moffat, 2005b).

In EV-A71-infected prepuce skin organotypic cultures, the highest viral titers were observed at 2 dpi which significantly dropped after 4 dpi suggesting that virus was probably most actively replicating from 2 dpi to 4 dpi. The reasons for the reduction in viral titers at 4 dpi may in part be related to tissue viability, which also appeared to be reduced after 4 days of culture. EV-A71 replication in primary epidermal keratinocytes increased from 1 dpi to reach the highest titers at 3 dpi, confirming robust growth in keratinocytes. Although virus from skin vesicle fluid/swabs of HFMD patients could be isolated, and up to 60% of cases were positive by viral culture (Chan et al., 2003b; Chang et al., 2004; Podin et al., 2006b), there are no published data on viral titrations from these samples. Moreover, PCR has been increasingly used for viral detection and reported as either positive or negative. These data provides an indication that viral replication in epidermal keratinocytes is very active and this may also be the case *in vivo*. Hence, virus shedding from skin vesicles may even be sufficient to facilitate significant person-to-person transmission by the cutaneous-

to-oral route. Taken together with these results, it is speculated that cutaneous-to-oral transmission probably occurs more readily than oral-to-cutaneous route because the most superficial epidermal corneal layer is well known to resist infection. Theoretically, transmission via an oral-to-cutaneous route may still be possible if a sufficient viral dose is delivered onto the skin followed by direct infection of the more superficial layers of the epidermis (Knipe & Howley, 2001; Santermans et al., 2015). However, in the prepuce and lip skin organotypic cultures, infected squamous cells were mostly below the superficial corneal layer. However, skin breaches, in the form of cuts or abrasions, may predispose to infection. Conversely, devoid of a corneal layer, oral squamous mucosa would probably be more readily infected directly by virus. In fact, this study was able to demonstrate that the most superficial squamous mucosal cells could be infected (Figure 4.22A and C). Thus, apart from tonsillar crypt epithelium (He et al., 2014), oral mucosa could be another major primary replication site for EV-A71 (Ong & Wong, 2015), and indeed may be a portal for viral entry in the body as well. Having gained entry, viremia is likely to spread virus to the epidermis in the feet, buttocks and other areas, which are less likely to be exposed to direct viral contact. In this case, the skin lesions would represent secondary viral replication sites. Thus, these data support the hypothesis of squamous epitheliotropism plays a crucial role in the viral replication and dissemination in the body. Since skin lesions are more commonly observed in the perioral skin, hands and feet, it is possible that viral growth in epidermal keratinocytes in these areas will be higher than in the prepuce and other parts of the body. The factors that could explain EV-A71 predilection for skin in these parts of the body have to be further investigated.

Viral antigens/RNA in dermal fibroblasts, blood vessels, peripheral nerves or other cells/tissues were not detected, suggesting that these cells/tissues were not susceptible to

the infection. Epidermal dendritic cells such Langerhans cells (LCs) were not shown to have viral antigens in this organotypic skin cultures but this possibility should be investigated more thoroughly. In *in vitro* experiments, EV-A71 has been shown to infect dendritic cells, which are professional antigen-presenting cells that prime T lymphocytes (Lin et al., 2009; Shi et al., 2014). In this study, no viral antigens were detected in LCs for possible reasons including a reduction in the viability of LCs in skin organotypic cultures and a relatively short period of culture that precludes phagocytosis of viral antigens. Further experiments are needed to investigate the role of LCs in EV-A71 skin infection.

5.5   Future prospects

Virus infection using EV-A71 clinical isolated strains or other HFMD-causing virus such as CVA-16 should be further studied in the hamster model. Other clinical signs such as neurogenic pulmonary oedema in the lung should be studied as well. In the viral spread study, lower viral dose may also be used to determine the viral dissemination in this hamster model as a comparison with the higher viral doses used in this current study (10^5 $CCID_{50}$). In addition, viral genetic diversity and mutations after transmission over several cohorts of animals could possibly be studied in the hamster model. Similarly, other HFMD-causing, SCARB2 associated and non-SCARB2 associated enterovirus such as CVA-16 and CVA-6, respectively, could be employed in primary squamous cell cultures infection.

CHAPTER 6

CONCLUSION

In conclusion, this 2-week-old hamster model invariably developed consistent CNS infection and squamous epithelial lesions in the paws, skin and oral cavity that is strikingly reminiscent of HFMD with CNS involvement. In addition, a relatively high degree of homology of SCARB2 receptors in the hamster and the mouse (90%) may explain why the former was also susceptible to MAV (Figure 4.7) but there may be other reasons. The most consistent results were obtained in 2-week-old or younger hamsters, just like in other mouse models (Khong et al., 2012b; Lin et al., 2013a; Ong et al., 2008a). The reasons are not clear just as the reasons for a much higher incidence of complicated HFMD in children less than 5 years old are also not fully understood (Mcminn, 2003), but may due to immune system immaturity, relative availability of viral receptors or other unknown factors.

Based on the results, this orally-infected hamster is a good small animal model to further investigate viral pathogenesis, model person-to-person transmission of EV-A71 infection, and to test the effectiveness of anti-viral drugs and vaccines (Ch'ng et al., 2012a). Possible primary viral replication sites in the orodigestive tract and skeletal muscles could lead to viremia and neuroinvasion. It is not clear if the orodigestive tract is a portal for viral entry into the body to give rise to viraemia. Infection of skeletal muscles could enable retrograde viral transmission up motor nerves to enter the CNS. The results also indicate the possibility for the involvement of sensory nerves and dorsal root ganglion for neuroinvasion.

Active oral and fecal viral excretion confirmed oral-oral and oral-fecal routes as important for EV-A71 transmission between animals just as in the human population. The data from the results showed that hamster-to-hamster viral transmission was population and

147

duration-of-exposure dependent. The results suggest that viral excretion was mainly from the orodigestive tract especially, the oral cavity, and that fecal viral excretion probably originated from the upper orodigestive tract. Focal inflammation and cellular necrosis in hamster oral mucosa and skin epidermal squamous cells strongly support squamous epitheliotropism of EV-A71suggesting that HFMD-causing EV-A71 infection in humans may also demonstrate squamous epitheliotropism. This was confirmed by evidence from the human skin, lip and/or oral mucosa organotypic cultures and primary human squamous cell cultures. Human squamous cells/keratinocytes are important viral targets and represent may represent important primary and/or secondary viral replication sites that may contribute significantly to viremia and person-to-person transmission (oral-cutaneous and/or cutaneous-oral transmission). Judging from the very similar clinical manifestations, this study predicts that all enteroviruses that cause HFMD are essentially squamoepitheliotropic.

REFERENCES

Arita, M., Ami, Y., Wakita, T., & Shimizu, H. (2008). Cooperative effect of the attenuation determinants derived from poliovirus sabin 1 strain is essential for attenuation of enterovirus 71 in the NOD/SCID mouse infection model. *J Virol, 82*(4): 1787-1797.

Arita, M., Nagata, N., Iwata, N., Ami, Y., Suzaki, Y., Mizuta, K., Iwasaki, T., Sata, T., Wakita, T., & Shimizu, H. (2007). An attenuated strain of enterovirus 71 belonging to genotype a showed a broad spectrum of antigenicity with attenuated neurovirulence in cynomolgus monkeys. *J Virol, 81*(17): 9386-9395.

Brown, B. A., Oberste, M. S., Alexander, J. P., Kennett, M. L., & Pallansch, M. A. (1999). Molecular epidemiology and evolution of enterovirus 71 strains isolated from 1970 to 1998. *J Virol, 73*: 9969-9975.

Brown, B. A., & Pallansch, M. A. (1995). Complete nucleotide sequence of enterovirus 71 is distinct from poliovirus. *Virus Res, 39*: 195-205.

Ch'ng, W. C., Stanbridge, E. J., Wong, K. T., Ong, K. C., Yusoff, K., & Shafee, N. (2012a). Immunization with recombinant enterovirus 71 viral capsid protein 1 fragment stimulated antibody responses in hamsters. *Virol J, 9*: 1-5. doi: 10.1186/1743-422X-9-155.

Ch'ng, W. C., Stanbridge, E. J., Wong, K. T., Ong, K. C., Yusoff, K., & Shafee, N. (2012b). Immunization with recombinant enterovirus 71 viral capsid protein 1 fragment stimulated antibody responses in hamsters. *Virology, 9*(155).

Chan, K. P., Goh, K. T., Chong, C. Y., Teo, E. S., Lau, G., & Ling, A. E. (2003a). Epidemic hand, foot and mouth disease caused by human EV71, Singapore. *Emerg Infect Dis, Vol. 9*.

Chan, K. P., Goh, K. T., Chong, C. Y., Teo, E. S., Lau, G., & Ling, A. E. (2003b). Epidemic hand, foot and mouth disease caused by human EV71, Singapore. *Emerg Infect Dis, 9*(1): 78-85.

Chang, L. Y., Lin, T. Y., Huang, Y. C., Tsao, K. C., Shih, S. R., Kuo, M. L., Ning, H. C., & Chung, P. W. (1999). Comparison of enterovirus 71 and coxsackievirus A16 clinical illnesses during the Taiwan enterovirus epidemic, 1998. *Pediatr Infect Dis J., 18*(12): 1092-1096.

Chang, L. Y., Tsao, K. C., Hsia, S. H., Shih, S. R., Huang, C. C., Chan, W. K., Hsu, K. H., Fang, T. Y., Huang, Y. C., & Lin, T. Y. (2004). Transmission and clinical features of enterovirus 71 infections in household contacts in Taiwan. *JAMA, 291*(2): 222-227.

Chatproedprai S, Theanboonlers A, Korkong S, Thongmee C, Wananukul S, & Poovorawan, Y. (2010). Clinical and molecular characterization of hand-foot and mouth disease in Thailand, 2008-2009. *Jpn J Infect Dis* (63): 229-233.

Chatproedprai, S., Theanboonlers, A., Korkong, S., Thongmee, C., Wananukul, S., & Poovorawan, Y. (2010). Clinical and molecular characterization of hand-foot-and-mouth disease in Thailand, 2008-2009. *Jpn. J. Infect. Dis, 63*: 229-233.

Chen, K. T., Chang, H. L., Wang, S. T., Cheng, Y. T., & Yang, J. Y. (2007a). Epidemiologic features of hand-foot-mouth disease and herpangina caused by enterovirus 71 in Taiwan, 1998-2005. *Pediatrics, 120*(2): 244-252.

Chen, K. T., Chang, H. L., Wang, S. T., Cheng, Y. T., & Yang, J. Y. (2007b). Epidemiologic features of hand-foot-mouth disease and herpangina caused by enterovirus 71 in Taiwan, 1998 2005. *Pediatrics, 120*(2): e244-e252.

Chen, K. T., Lee, T. C., Chang, H. L., Yu, M. C., & Tang, L. H. (2008). Human enterovirus 71 disease clinical features, epidemiology, virology, and management. *Open Epidemiol J, 1*: 10-16.

Chen, P., Song, Z., Qi, Y., Feng, X., Xu, N., Sun, Y., Wu, X., Yao, X., Mao, Q., Li, X., Dong, W., Wan, X., Huang, N., Shen, X., Liang, Z., & Li, W. (2012). Molecular determinants of enterovirus 71 viral entry: cleft around GLN-172 on VP1 protein interacts with variable region on scavenge receptor B 2. *J Biol Chem, 287*(9): 6406-6420.

Chen, T. C., Lai, Y. K., Yu, C. K., & Juang, J. L. (2007c). Enterovirus 71 triggering of neuronal apoptosis through activation of Abl-Cdk5 signalling. *Cell Microbiol, 9*(11): 2676-2688.

ous system involvement. *J Gen Virol, 85*(Pt 1): 69-77. doi: 10.1099/vir.0.19423-0
Chen, Y. C., Yu, C. K., Wang, Y. F., Liu, C. C., Su, I. J., & Lei, H. Y. (2004b). A murine oral EV71 infection model with central nervous system involvement. *J Gen Virol, 85*: 69-77.

Chong, C. Y., Chan, K. P., Ng, W. Y. M., Lau, G., Teo, T. S., Lai, S. H., Ling, A. E., & Shah, V. (2003). Hand, foot and mouth disease in Singapore: a comparison of fatal and non-fatal cases. *Acta Paediatr, 92*(10): 1163-1169.

Connelly CA, Chen LC, & Colquhoun, S. D. (2000). Metabolic activity of cultured rat brainstem, hippocampal and spinal cord slices. *J Neurosci Methods, 99*: 1-7.

Cunningham, A. L., Diefenbach, R. J., Miranda, S. M., Bosnjak, L., Kim, M., Jones, C., & Douglas, M. W. (2006). The cycle of human herpes simplex virus infection: virus transport and immune control. *J Infect Dis, 194*: S11-18.

Deshpande, J. M., Nadkarni, S. S., & P., F. P. (2003). Enterovirus 71 isolated from a case of acute flaccid paralysis in India represents a new genotype. *Curr Sci, 84*: 1350-1353.

Fujii, K., Nagata, N., Sato, Y., Ong, K., Wong, K., Yamayoshi, S., Shimanuki, M., Shitara, H., Taya, C., & Koike, S. (2013a). Transgenic mouse model for the study of enterovirus 71 neuropathogenesis. *Proc Natl Acad Sci U S A, 110*(13): 14753-14758.

Fujii, K., Nagata, N., Sato, Y., Ong, K., Wong, K., Yamayoshi, S., Shimanuki, M., Shitara, H., Taya, C., & Koike, S. (2013b). Transgenic mouse model for the study of enterovirus 71 neuropathogenesis. *Proc Natl Acad Sci U S A., 110*(36): 14753-14758.

Hajjar, K. A., & Acharya, S. S. (2000). Annexin II and regulation of cell surface fibrinolysis. *Ann N Y Acad Sci*(902): 265-271.

Hamaguchi, T., Fujisawa, H., Sakai, K., Okino, S., Kurosaki, N., Nishimura, Y., Shimizu, H., & Yamada, M. (2008). Acute encephalitis caused by intrafamilial transmission of EV71 in adult. *Emerg Infect Dis*(14): 828-830.

Han, J., Ma, X. J., Wan, J. F., Liu, Y. H., Han, Y. L., Chen, C., Tian, C., Gao, C., Wang, M., & Dong, X. P. (2010). Long persistence of EV71 specific nucleotides in respiratory and feces samples of the patients with hand-foot-mouth disease after recovery. *BMC Infect Dis, 10*: 178.

He, Y., Ong, K. C., Gao, Z., Zhao, X., Anderson, V. M., Mcnutt, M. A., Wong, K. T., & Lu, M. (2013). Tonsillar crypt epithelium as an important extra central vervous system site for viral replication in EV71 encephalomyelitis. *Am J Pathol, 184*: 715-720.

He, Y., Ong, K. C., Gao, Z., Zhao, X., Anderson, V. M., McNutt, M. A., Wong, K. T., & Lu, M. (2014). Tonsillar crypt epithelium is an important extracentral nervous system site for viral replication in EV71 encephalomyelitis. *Am J Pathol, 184*(3): 715-720.

Ho, M., Chen, E. R., Hsu, K. H., Twu, S. J., Chen, K. T., Tsai, S. F., Wang, J. R., & Shih, S. R. (1999). An epidemic of enterovirus 71 infection in Taiwan. *N Engl J Med, 341*(13): 929-935.

Hsiung, G. D., & Wang, J. R. (2000). Enterovirus infection with special reference to enterovirus 71. *J Microbiol Immunol Infect, 33*: 1-8.

Hsueh, C., Jung, S. M., Shih, S. R., Kuo, T. T., Shieh, W. J., Zaki, S., Lin, T. Y., Chang, L. Y., Ning, H. C., & Yen, D. C. (2000). Acute encephalomyelitis during an outbreak of enterovirus Type 71 infection in Taiwan: report of an autopsy case with pathologic, immunofluorescence, and molecular studies. *Mod Pathol, 13*(11): 1200-1205.

Huang, P. N., & Shih, S. R. (2014). Update on enterovirus 71 infection. *Curr Opin Virol, 5*: 98-104.

Huang, S. W., Kiang, D., Smith, D. J., & Wang, J. R. (2011). Evolution of re-emergent virus and its impact on enterovirus 71 epidemics. *Exp Biol Med (Maywood), 236*(8): 899-908.

Hubiche, T., Schuffenecker, I., Boralevi, F., Leaute, L. C., Bornebusch, L., Chiaverini, C., Phan, A., Maruani, A., Miquel, J., Lafon, M. E., Lina, B., Del, G. P., & Clinical Research Group of the French Society of Pediatric Dermatology Groupe de Recherche Clinique de la Societe Francaise de Dermatologie, P. (2014). Dermatological spectrum of hand, foot and mouth disease from classical to generalized exanthema. *Pediatr Infect Dis J, 33*(4): 92-98.

Hyypia, T., Hovi, T., Knowles, N. J., & Stanway, G. (1997). Classification of enteroviruses based on molecular and biological properties. *J Gen Virol, 78*: 1-11.

Jones, M., Dry, I. R., Frampton, D., Singh, M., Kanda, R. K., Yee, M. B., Kellam, P., Hollinshead, M., Kinchington, P. R., O'Toole, E. A., & Breuer, J. (2014). RNA-seq analysis of host and viral gene expression highlights interaction between varicella zoster virus and keratinocyte differentiation. *PLoS Pathog, 10*(1): e1003896.

Karber, G. (1931). Beitrag zur kollektiven Behandling pharmakologischer Reihenversuche. *Arch Exp Pathol Pharmakol, 162*: 480-483.

Khong, W. X., Yan, B., Yeo, H., Tan, E. L., Lee, J. J., Ng, J. K., Chow, V. T., & Alonso, S. (2012a). A non-mouse-adapted enterovirus 71 (EV71) strain exhibits neurotropism, causing neurological manifestations in a novel mouse model of EV71 infection. *J Virol, 86*(4): 2121-2131.

Khong, W. X., Yan, B., Yeo, H., Tan, E. L., Lee, J. J., Ng, J. K., Chow, V. T., & Alonso, S. (2012b). A non-mouse-adapted enterovirus 71 (EV71) strain exhibits neurotropism, causing neurological manifestations in a novel mouse model of EV71 infection. *J Virol, 86*(4): 2121-2131.

Knipe DM, & Howley, P. M. (2001). Enteroviruses: polioviruses, coxsackieviruses, echoviruses, and newer enteroviruses. *USA: Lippincott Williams & Wilkins,*.

Knipe, D. M., & Howley, P. M. (2001). Enteroviruses: polioviruses, coxsackieviruses, echoviruses, and newer enteroviruses. In D. E. Griffin, R. A. Lamb, M. A. Martin, B. Roizman & S. E. Stratus (Eds.), *Fields Virology* (4th ed., Vol. 1, pp. 723-775): Lippincott Williams & Wilkins, USA.

Kuo, R. L., & Shih, S. R. (2013). Strategies to develop antivirals against enterovirus 71. *Virol J, 10*(28).

Lai, J. K., Sam, I. C., & Chan, Y. F. (2016). The autophagic machinery in enterovirus infection. *Viruses, 8*(2).

Li, R., Zou, Q., Chen, L., Zhang, H., & Wang, Y. (2011). Molecular analysis of virulent determinants of Enterovirus 71. *PLoS One, 6* (10): e26237.

Li, Y. P., Liang, Z. L., Gao, Q., Huang, L. R., Mao, Q. Y., Wen, S. Q., Liu, Y., Yin, W. D., Li, R. C., & Wang, J. Z. (2012). Safety and immunogenicity of a novel human Enterovirus 71 (EV71) vaccine: A randomized, placebo-controlled, double-blind, Phase I clinical trial. *Vaccine, 30*(22): 3295-3303.

Liang, Z., & Wang, J. (2014). EV71 vaccine, an invaluable gift for children. *Clin Transl Immunology, 3*(10): e28.

Liao, C. C., Liou, A. T., Chang, Y. S., Wu, S. Y., Chang, C. S., Lee, C. K., Kung, J. T., Tu, P. H., Yu, Y. Y., Lin, C. Y., Lin, J. S., & Shiha, C. (2014). Immunodeficient mouse models with different disease profiles by in vivo infection with the same clinical isolate of Enterovirus 71. *J Virol, 88*: 12485-12499.

Lin, J. Y., & Shih, S. R. (2014). Cell and tissue tropism of enterovirus 71 and other enteroviruses infections. *J Biomed Sci, 21*(18).

Lin, T. Y., Twu, S. J., Ho, M. S., Chang, L. Y., & Lee, C. Y. (2003). Enterovirus 71 outbreaks, Taiwan: occurrence and recognition *Emerg Infect Dis, 9*(3): 291-293.

Lin, Y. W., Wang, S. W., Tung, Y. Y., & Chen, S. H. (2009). Enterovirus 71 infection of human dendritic cells. *Exp Biol Med (Maywood), 234*(10): 1166-1173.

Lin, Y. W., Yu, S. L., Shao, H. Y., Lin, H. Y., Liu, C. C., Hsiao, K. N., Chitra, E., Tsou, Y. L., Chang, H. W., Sia, C., Chong, P., & Chow, Y. H. (2013a). Human SCARB2 transgenic mice as an infectious animal model for enterovirus 71. *Plos One, 8*(2).

Lin, Y. W., Yu, S. L., Shao, H. Y., Lin, H. Y., Liu, C. C., Hsiao, K. N., Chitra, E., Tsou, Y. L., Chang, H. W., Sia, C., Chong, P., & Chow, Y. H. (2013b). Human SCARB2 transgenic mice as an infectious animal model for enterovirus 71. *PLoS One, 8*(2): e57591.

Linden, v. d. L., Wolthers, K. C., & Kuppeveld, v. F. J. (2015). Replication and Inhibitors of enteroviruses and parechoviruses. *Viruses, 7*(8): 4529-4562.

Linsuwanon, P., Poovorawan, Y., Li, L., Deng, X., Vongpunsawad, S., & Delwart, E. (2015). The fecal virome of children with hand, foot, and mouth disease that tested PCR negative for pathogenic enteroviruses. *PLoS One, 10*(8): e0135573.

Liou, A. T., Wu, S. Y., Liao, C. C., Chang, Y. S., Chang, C. S., & Shih, C. (2016). A new animal model containing human SCARB2 and lacking stat-1 is highly susceptible to EV71. *Sci Rep, 6*: 31151.

Liu, J., Dong, W., Quan, X., Ma, C., Qin, C., & Zhang, L. (2012). Transgenic expression of human P-selectin glycoprotein ligand-1 is not sufficient for enterovirus 71 infection in mice. *Arch Virol, 157*(3): 539-543.

Liu, L., Zhao, H., Zhang, Y., Wang, J., Che, Y., Dong, C., Zhang, X., Na, R., Shi, H., Jiang, L., Wang, L., Xie, Z., Cui, P., Xiong, X., Liao, Y., Zhao, S., Gao, J., Tang, D., & Li, Q. (2011a). Neonatal rhesus monkey is a potential animal model for studying pathogenesis of EV71 infection. *Virology, 412*(1): 91-100.

Liu, L. D., Zhao, H., Zhang, Y., Wang, J., Che, Y., Dong, C., Zhang, X., Na, R., Shi, H., Jiang, L., Wang, L., Xie, Z., Cui, P., Xiong, X., Liao, Y., Zhao, S., Gao, J., Tang, D., & Li, Q. (2011b). Neonatal rhesus monkey is a potential animal model for studying pathogenesis of EV71 infection. *Virology, 412*(1): 91-100.

Lu, S. (2014). EV71 vaccines: a milestone in the history of global vaccine development. *Emerg Microbes Infect, 3*(4): e27.

Lum, L. C. S., Wong, K. T., Lam, S. K., Chua, K. B., Goh, A. Y. T., Lim, W. L., Ong, B. B., Paul, G., AbuBakar, S., & Lambert, M. (1998). Fatal enterovirus 71 encephalomyelitis. *J Pediatr, 133*(795-798).

Maher, D. M., Zhang, Z. Q., Schacker, T. W., & Southern, P. J. (2005). Ex vivo modeling of oral HIV transmission in human palatine tonsil. *J Histochem Cytochem, 53*(5): 631-642.

McMinn, P., Lindsay, K., Perera, D., Chan, H. M., Chan, K. P., & Cardosa, M. J. (2001). Phylogenetic analysis of enterovirus 71 strains isolated during linked epidemics in Malaysia, Singapore, and Western Australia. *J Virol, 75*(16): 7732-7738.

Mcminn, P. C. (2003). Enterovirus 71 in the Asia-Pacific region: an emerging cause of acute neurological disease in young children. *Neurol J Southeast Asia, 8*: 57–63.

Muehlenbachs, A., Bhatnagar, J., & Zaki, S. R. (2015). Tissue tropism, pathology and pathogenesis of enterovirus infection. *J Pathol, 235*(2): 217-228.

Nagata, N., Iwasaki, T., Ami, Y., Tano, Y., Harashima, A., Suzaki, Y., Sato, Y., Hasegawa, H., Sata, T., Miyamura, T., & Shimizu, H. (2004a). Differential localization of neurons susceptible to enterovirus 71 and poliovirus type 1 in the central nervous system of cynomolgus monkeys after intravenous inoculation. *J Gen Virol, 85*(Pt 10): 2981-2989.

Nagata, N., Iwasaki, T., Ami, Y., Tano, Y., Harashima, A., Suzaki, Y., Sato, Y., Hasegawa, H., Sata, T., Miyamura, T., & Shimizu, H. (2004b). Differential localization of neurons susceptible to enterovirus 71 and poliovirus type 1 in the central nervous system of cynomolgus monkeys after intravenous inoculation. *J Gen Virol, 85*: 2981-2989.

Nagata, N., Shimizu, H., Ami, Y., Tano, Y., Harashima, A., Suzaki, Y., Sato, Y., Miyamura, T., Sata, T., & Iwasaki, T. (2002a). Pyramidal and extrapyramidal involvement in experimental infection of cynomolgus monkeys with enterovirus 71. *J Med Virol, 67*(2): 207-216.

Nagata, N., Shimizu, H., Ami, Y., Tano, Y., Harashima, A., Suzaki, Y., Sato, Y., Miyamura, T., Sata, T., & Iwasaki, T. (2002b). Pyramidal and extrapyramidal involvement in experimental infection of cynomolgus monkeys with enterovirus 71. *J Med Virol, 67*(2): 207-216.

Ohka, S., Matsuda, N., Tohyama, K., Oda, T., Morikawa, M., Kuge, S., & Nomoto, A. (2004). Receptor (CD155)-dependent endocytosis of poliovirus and retrograde axonal transport of the endosome. *J Virol, 78*(13): 7186-7198.

Ong, K. C., Badmanathan, M., Devi, S., Leong, K. L., Cardosa, M. J., & Wong, K. T. (2008a). Pathologic characterization of a murine model of human enterovirus 71 encephalomyelitis. *J Neuropatho Exp Neurol, 67*(6): 532-542.

Ong, K. C., Badmanathan, M., Devi, S., Leong, K. L., Cardosa, M. J., & Wong, K. T. (2008b). Pathologic characterization of a murine model of human enterovirus 71 encephalomyelitis. *J Neuropatho Exp Neurol 67*: 532-542.

Ong, K. C., Devi, S., Cardosa, M. J., & Wong, K. T. (2010). Formaldehyde-inactivated whole-virus vaccine protects a murine model of enterovirus 71 encephalomyelitis against disease. *J Virol, 84*(1): 661-665.

Ong, K. C., & Wong, K. T. (2015). Understanding enterovirus 71 neuropathogenesis and its impact on other neurotropic enteroviruses. *Brain Pathol, 25*(5): 614-624.

Ooi, M. H., Solomon, T., Podin, Y., Mohan, A., Akin, W., Yusuf, M. A., Sel, S. d., Kontol, K. M., Lai, B. F., Clear, D., Chieng, C. H., Blake, E., Perera, D., Wong, S. C., & Cardosa, J. (2007a). Evaluation of different clinical sample types in diagnosis of human enterovirus 71-associated hand-foot-and-mouth disease. *J Clin Microbiol, 45*(6): 1858-1866.

Ooi, M. H., Wong, S. C., Podin, Y., Akin, W., Sel, S., Mohan, A., Chieng, C. H., Perera, D., Clear, D., Wong, D., Blake, E., Cardosa, J., & Solomon, T. (2007b). Human enterovirus 71 disease in Sarawak, Malaysia: a prospective clinical, virological, and molecular epidemiological study. *Clin Infect Dis, 44*(5): 646-656.

Podin Y, Gias EL, Ong F, Leong YW, Yee SF, Yusof MA, Yao SC, Yao SK, & Cardosa, M. J. (2006). Sentinel surveillance for human enterovirus 71 in Sarawak, Malaysia: lessons from the first 7 years. *BMC Public Health*(6).

Podin, Y., Gias, E. L., Ong, F., Leong, Y. W., Yee, S. F., Yusof, M. A., Perera, D., Teo, B., Wee, T. Y., Yao, S. C., Yao, S. K., Kiyu, A., Arif, M. T., & Cardosa, M. J. (2006a). Sentinel surveillance for human enterovirus 71 in Sarawak, Malaysia: lessons from the first 7 years. *BMC Public Health., 6*(180): 1-10.

Podin, Y., Gias, E. L., Ong, F., Leong, Y. W., Yee, S. F., Yusof, M. A., Yao, S. C., Yao, S. K., & Cardosa, M. J. (2006b). Sentinel surveillance for human enterovirus 71 in Sarawak, Malaysia: lessons from the first 7 years. *BMC Public Health, 6*(180).

Rahn, E., Thier, K., Petermann, P., & Knebel-Morsdorf, D. (2015). Ex Vivo Infection of murine epidermis with herpes simplex virus type 1. *J Vis Exp, 102*: e53046.

Reed, L. J., & Muench, H. A. (1938). A simple method for estimating fifty percent endpoints. *Am J Trop Med Hyg, 27*: 493-497.

Ryu, W. S., Kang, B., Hong, J., Hwang, S., Kim, A., Kim, J., & Cheon, D. S. (2010). Enterovirus 71 infection with central nervous system involvement, South Korea. *Emerg Infect Dis, 16*(11): 1764-1766.

Santermans, E., Goeyvaerts, N., Melegaro, A., Edmunds, W. J., Faes, C., Aerts, M., Beutels, P., & Hens, N. (2015). The social contact hypothesis under the assumption of endemic equilibrium: elucidating the transmission potential of VZV in Europe. *Epidemics, 11*: 14-23.

Saxena, V. K., Sane, S., Nadkarni, S. S., Sharma, D. K., & Deshpande, J. M. (2015). Genetic diversity of enterovirus A71, India. *Emerg Infect Dis, 21*(1): 123-126.

Shi, W., Hou, X., Peng, H., Zhang, L., Li, Y., Gu, Z., Jiang, Q., Shi, M., Ji, Y., & Jiang, J. (2014). MEK/ERK signaling pathway is required for enterovirus 71 replication in immature dendritic cells. *Virol J, 11*: 227.

Shi, W., Li, X., Hou, X., Peng, H., Jiang, Q., Shi, M., Ji, Y., Liu, X., & Liu, J. (2012). Differential apoptosis gene expressions of rhabdomyosarcoma cells in response to enterovirus 71 infection. *BMC Infect Dis., 12*(327): 1-12.

Shieh, W. J., Jung, S. M., Hsueh, C., Kuo, T. T., Mounts, A., Parashar, U., Yang, C. F., Guarner, J., Ksiazek, T. G., Dawson, J., Goldsmith, C., Chang, G. J. J., Oberste, S. M., Pallansch, M. A., Anderson, L. J., Zaki, S. R., & Group., t. E. W. (2001). Pathologic studies of fatal cases in outbreak of hand, foot, and mouth disease, Taiwan. *Emerg Infect Dis, 7*(1): 146-148.

Solomon, T., Lewthwaite, P., Perera, D., Cardosa, M. J., McMinn, P., & Ooi, M. H. (2010). Virology, epidemiology, pathogenesis, and control of enterovirus 71. *Lancet Infect Dis, 10*(11): 778-790.

Sperling, T., Oldak, M., Ruckheim, W. B., Wickenhauser, C., Doorbar, J., Pfister, H., Malejczyk, M., Majewski, S., Keates, A. C., & Smola, S. (2012). Human papillomavirus type 8 interferes with a novel C/EBPbeta-mediated mechanism of keratinocyte CCL20 chemokine expression and langerhans cell migration. *PLoS Pathog, 8*(7): e1002833.

Tan, C. W., Poh, C. L., Sam, I. C., & Chan, Y. F. (2013). Enterovirus 71 uses cell surface heparan sulfate glycosaminoglycan as an attachment receptor. *J Virol, 87*(1): 611-620.

Tan, S. H., Ong, K. C., Perera, D., & Wong, K. T. (2016). A monoclonal antibody to ameliorate central nervous system infection and improve survival in a murine model of human Enterovirus-A71 encephalomyelitis. *Antiviral Res, 132*: 196-203.

Tan, S. H., Ong, K. C., & Wong, K. T. (2014a). Enterovirus 71 can directly infect the brainstem via cranial nerves and infection can be ameliorated by passive immunization. *J Neuropathol Exp Neurol, 73*(11): 999-1008.

Tan, S. H., Ong, K. C., & Wong, K. T. (2014b). Enterovirus 71 can directly infect the brainstem via cranial nerves and infection can be ameliorated by passive immunization. *J Neuropathol Exp Neurol, 73*: 999-1008.

Taylor, S. L., & Moffat, J. F. (2005a). Replication of varicella-zoster virus in human skin organ culture. *J Virol, 79*(17): 11501-11506.

Taylor, S. L., & Moffat, J. F. (2005b). Replication of varicella-zoster virus in human skin organ culture. *J Virol, 79*(17): 11501-11506.

Too, I. H., Yeo, H., Sessions, O. M., Yan, B., Libau, E. A., Howe, J. L., Lim, Z. Q., Suku-Maran, S., Ong, W. Y., Chua, K. B., Wong, B. S., Chow, V. T., & Alonso, S. (2016). Enterovirus 71 infection of motor neuron-like NSC-34 cells undergoes a non-lytic exit pathway. *Sci Rep, 6*: 36983.

Ueno, M. (2009). Mechanisms of the penetration of blood-borne substances into the brain. *Curr Neuropharmacol, 7*: 142-149.

Ventarola, D., Bordone, L., & Silverberg, N. (2015). Update on hand-foot-and-mouth disease. *Clin Dermatol, 33*(3): 340-346.

Victorio, C. B., Xu, Y., Ng, Q., Chua, B. H., Alonso, S., Chow, V. T., & Chua, K. B. (2016). A clinically authentic mouse model of enterovirus 71 (EV-A71)-induced neurogenic pulmonary oedema. *Sci Rep, 6*: 28876.

Wang, J., Cao, Z., Zeng, D. D., Wang, Q., Wang, X., & Qian, H. (2014). Epidemiological analysis, detection, and comparison of space-time patterns of Beijing hand-foot-mouth disease (2008-2012). *PLoS One, 9*(3): e92745.

Wang, Y. F., Chou, C. T., Lei, H. Y., Liu, C. C., Wang, S. M., Yan, J. J., Su, I. J., Wang, J. R., Yeh, T. M., Chen, S. H., & Yu, C. K. (2004a). A mouse-adapted enterovirus 71 strain causes neurological disease in mice after oral infection. *J Virol, 78*(15): 7916-7924.

Wang, Y. F., Chou, C. T., Lei, H. Y., Liu, C. C., Wang, S. M., Yan, J. J., Su, I. J., Wang, J. R., Yeh, T. M., Chen, S. H., & Yu, C. K. (2004b). A mouse-adapted enterovirus 71

strain causes neurological disease in mice after oral infection. *J Virol, 78*(15): 7916-7924.

Weng, K. F., Chen, L. L., Huang, P. N., & Shih, S. R. (2010). Neural pathogenesis of enterovirus 71 infection. *Microbes Infect, 12*(7): 505-510.

Wong, K. T., Munisamy, B., Ong, K. C., Kojima, H., Noriyo, N., Chua, K. B., Ong, B. B., & Nagashima, K. (2008a). The distribution of inflammation and virus in human enterovirus 71 encephalomyelitis suggests possible viral spread by neural pathways. *J Neuropathol Exp Neurol, 67*(2): 162-169.

Wong, K. T., Munisamy, B., Ong, K. C., Kojima, H., Noriyo, N., Chua, K. B., Ong, B. B., & Nagashima, K. (2008b). The distribution of inflammation and virus in human enterovirus 71 encephalomyelitis suggests possible viral spread by neural pathways. *J Neuropathol Exp Neurol, 67*(2): 162-169.

Wong, K. T., Ng, K. Y., Ong, K. C., Ng, W. F., Shankar, S. K., Mahadevan, A., Radotra, B., Su, I. J., Lau, G., Ling, A. E., Chan, K. P., Macorelles, P., Vallet, S., Cardosa, M. J., Desai, A., Ravi, V., Nagata, N., Shimizu, H., & Takasaki, T. (2012). Enterovirus 71 encephalomyelitis and Japanese encephalitis can be distinguished by topographic distribution of inflammation and specific intraneuronal detection of viral antigen and RNA. *Neuropathol Appl Neurobiol, 38*(5): 443-453.

Wong, S. S., Yip, C. C., Lau, S. K., & Yuen, K. Y. (2010). Human enterovirus 71 and hand, foot and mouth disease. *Epidemiol Infect, 138*(8): 1071-1089.

World Health Organization. (2004 Aug 31). Polio laboratory manual. from http://whqlibdoc.who.int/hq/2004/WHO_IVB_04.10.pdf

Xiu, J. H., Zhu, H., Xu, Y. F., Liu, J. N., Xia, X. Z., & Zhang, L. F. (2013). Necrotizing myositis causes restrictive hypoventilation in a mouse model for human enterovirus 71 infection. *Virol J, 10*(215).

Yamayoshi, S., Fujii, K., & Koike, S. (2014). Receptors for enterovirus 71. *Emerg Microbes Infect, 3*(7): e53.

Yamayoshi, S., Iizuka, S., Yamashita, T., Minagawa, H., Mizuta, K., Okamoto, M., Nishimura, H., Sanjoh, K., Katsushima, N., Itagaki, T., Nagai, Y., Fujii, K., & Koike, S. (2012). Human SCARB2-dependent infection by coxsackievirus A7, A14, and A16 and enterovirus 71. *J Virol, 86*(10): 5686-5696.

Yamayoshi, S., Yamashita, Y., Li, J., Hanagata, N., Minowa, T., Takemura, T., & Koike, S. (2009). Scavenger receptor B2 is a cellular receptor for enterovirus 71. *Nat Med, 15*(7): 798-801.

Yan, X., Zhang, Z. Z., Yang, Z. H., Zhu, C. M., Hu, Y. G., & Liu, Q. B. (2015). Clinical and etiological characteristics of atypical hand-foot-and-mouth disease in children

from chongqing, China: a retrospective study. *BioMed Research International, 2015*: 1-8.

Yang, S. L., Chou, Y. T., Wu, C. N., & Ho, M. S. (2011). Annexin II binds to capsid protein VP1 of enterovirus 71 and enhances viral infectivity. *J Virol, 85*(22): 11809-11820.

Yang, X., Li, G., Wen, K., Bui, T., Liu, F., Kocher, J., Jortner, B. S., Vonck, M., Pelzer, K., Deng, J., Zhu, R., Li, Y., Qian, Y., & Yuan, L. (2014). A neonatal gnotobiotic pig model of human enterovirus 71 infection and associated immune responses. *Emerg Microbes Infect, 3*(5): e35.

Yang, Y., Wang, H., Gong, E., Du, J., Zhao, X., McNutt, M. A., Wang, S., Zhong, Y., Gao, Z., & Zheng, J. (2009). Neuropathology in 2 cases of fatal enterovirus type 71 infection from a recent epidemic in the People's Republic of China: a histopathologic, immunohistochemical, and reverse transcription polymerase chain reaction study. *Hum Pathol, 40*(9): 1288-1295.

Yip, C. C. Y., Lau, S. K. P., Zhou, B., Zhang, M. X., Tsoi, H. W., Chan, K. H., Chen, X. C., Woo, P. C. Y., & Yuen, K. Y. (2010). Emergence of enterovirus 71 "double-recombinant" strains belonging to a novel genotype D originating from southern China: first evidence for combination of intratypic and intertypic recombination events in EV71. *Arch Virol, 155*(9): 1413-1424.

Yu, P., Gao, Z., Zong, Y., Bao, L., Xu, L., Deng, W., Li, F., Lv, Q., Gao, Z., Xu, Y., Yao, Y., & Qin, C. (2014a). Histopathological features and distribution of EV71 antigens and SCARB2 in human fatal cases and a mouse model of enterovirus 71 infection. *Virus Res., 189*: 121-132.

Yu, P., Gao, Z., Zong, Y., Bao, L., Xu, L., Deng, W., Li, F., Lv, Q., Gao, Z., Xu, Y., Yao, Y., & Qin, C. (2014b). Histopathological features and distribution of EV71 antigens and SCARB2 in human fatal cases and a mouse model of enterovirus 71 infection. *Virus Res, 189*: 121-132.

Zaoutis, T., & Klein, J. D. (1998). Enterovirus Infections. *Pediatr Rev, 19*(6): 183-191.

Zhang, W., Zhang, L., Wu, Z., & Tien, P. (2014). Differential interferon pathway gene expression patterns in rhabdomyosarcoma cells during enterovirus 71 or coxsackievirus A16 infection. *Biochem Biophys Res Commun., 447*(3): 550-555.

Zhang, Y., Cui, W., Liu, L., Wang, J., Zhao, H., Liao, Y., Na, R., Dong, C., Wang, L., Xie, Z., Gao, J., Cui, P., Zhang, X., & Li, Q. (2011). Pathogenesis study of enterovirus 71 infection in rhesus monkeys. *Lab. Invest, 91*(9): 1337-1350.

Zhou, S., Liu, Q., Wu, X., Chen, P., Wu, X., Guo, Y., Liu, S., Liang, Z., Fan, C., & Wang, Y. (2016). A safe and sensitive enterovirus A71 infection model based on human SCARB2 knock-in mice. *Vaccine, 34*(24): 2729-2736.

159

LIST OF PUBLICATIONS AND PAPERS PRESENTED

1. **Publications**

1. Win Kyaw Phyu, Kien Chai Ong, Kum Thong Wong: A Consistent Orally-Infected Hamster Model for Enterovirus A71 Encephalomyelitis Demonstrates Squamous Lesions in the Paws, Skin and Oral Cavity Reminiscent of Hand-Foot-and-Mouth Disease. PLoS ONE 01/2016; 11(1): e0147463. DOI:10.1371/journal.pone.0147463

2. Win Kyaw Phyu, Kien Chai Ong, Chee Kwan Kong, Tindivanam Muthurangam Ramanujam, Kum Thong Wong. Squamous epitheliotropism of Enterovirus A71 in human epidermis and oral mucosa. Sci Rep 2017; 7: 45069. DOI: 10.1038/srep45069

3. Win Kyaw Phyu, Kien Chai Ong, Kum Thong Wong. Modelling person-to-person viral transmission in an orally-infected hamster model of Enterovirus A71 hand-foot-and-mouth disease and encephalomyelitis. Emerging Microbes and Infections 2017; 6, e61; DOI:10.1038/emi.2017.49

2. **Presentations**

1. A consistently orally-infected enterovirus 71 encephalomyelitis hamster model demonstrates squamous lesions in the footpad, skin and oral cavity. 19th Biological Sciences Graduate Congress, 12-14th December 2014, National University of Singapore, Singapore. (International)

2. Keratinocytes in human epidermis are major targets of Enterovirus A71 infection. Hand, Foot & Mouth Disease International Conference, 25-26th July 2016, Matrix, Biopolis, Singapore. (International)